Colorimetric Detection of Pathogenic Bacteria Using Morphology-Controlled Gold Nanoparticles

by

Mohit Singh Verma

A thesis
presented to the University of Waterloo
in fulfillment of the
thesis requirement for the degree of
Doctor of Philosophy
in
Chemical Engineering (Nanotechnology)

Waterloo, Ontario, Canada, 2015

AUTHOR'S DECLARATION

I hereby declare that I am the sole author of this thesis. This is a true copy of the thesis, including any required final revisions, as accepted by my examiners.

I understand that my thesis may be made electronically available to the public.

Abstract

Simple and rapid detection of pathogens is crucial for preventing and treating infectious diseases. Conventional methods for pathogen detection are based on cell cultures and could require several days. The use of nanotechnology and specifically, gold nanoparticles has facilitated the development of biosensors that can potentially be used at the point-of-care because they provide a colorimetric output.

A systematic literature review demonstrates that most instances of gold nanoparticles are in the detection of amplified nucleic acids but these methods require specialized equipment. There is a growing drive for making the biosensors simpler and more sensitive such that they could be employed outside the laboratory.

This thesis focuses on the development of a gold nanoparticle-based biosensor that has the potential to rapidly detect and identify pathogens at the point-of-care. The biosensor consists of cationic gold nanoparticles that aggregate around target bacteria and produce a color change, which can be observed visually and quantified spectrophotometrically. Combining nanoparticles with various sizes and shapes creates a "chemical nose" biosensor, which uses a unique combination of responses to represent each target of interest, in a manner similar to the human sense of smell. This "chemical nose" biosensor can discriminate between bacterial species based on their cell wall components. This approach produces a versatile biosensor that can be deployed for a variety of applications as opposed to biofunctionalized nanoparticles, which are typically limited to a single target.

Development of the biosensor begins with the synthesis of gold nanostars because this shape allows control over size and degree of branching, both of which govern the optical properties of the solutions. Gold nanostars are synthesized by a surfactant-assisted seed-mediated growth method. Increasing the surfactant concentration increases the degree of branching while increasing the amount of seed decreases the particle size. The cationic surface facilitates electrostatic aggregation of the nanostars on the negatively charged bacterial cell wall. This aggregation allows a rapid visual detection of *Staphylococcus aureus*, a model Gram-positive pathogen. The colorimetric response of gold nanostars depends on the intrinsic size and morphology of particles.

Discriminating between bacteria of different species is important for accurate diagnosis. The ability of gold nanostars to identify the species of bacteria is explored by targeting ocular pathogens that are currently affecting contact lens wearers. Using two different degrees of branching of gold nanostars, a

"chemical nose" biosensor is developed, where colorimetric response from each type of nanostar is different for each bacterial species. The biosensor is able to discriminate between saline control and four species of bacteria at the same concentration with 99% accuracy. Transmission electron microscopy demonstrates that this discrimination in colorimetric responses is because of different degrees and patterns of aggregation of gold nanostars around bacteria.

In addition to identifying the species of bacteria, some applications require detection at various concentrations. Thus, the "chemical nose" was tested for the detection of eight species of bacteria at three different concentrations and an accuracy of 89% was obtained by analyzing the absorption spectra of the gold nanoparticles. Additionally, the potential of the "chemical nose" to detect polymicrobial infections was demonstrated by measuring the colorimetric response of mixtures of bacteria. The "chemical nose" was able to discriminate between *Staphylococcus aureus, Escherichia coli, Pseudomonas aeruginosa,* and their binary and tertiary mixtures with 100% accuracy.

Implementation of the "chemical nose" biosensor at the point-of-care requires a rapid response. This is possible by acquiring absorption spectra at a faster rate. Using a portable charge-coupled device spectrophotometer, the "chemical nose" was able to distinguish between mixtures of bacteria within two minutes of data acquisition. This was possible by exploiting the kinetics of color change, which is unique for each bacterial species and their mixtures. Additionally, within each mixture, the bacteria seem to maintain their patterns and extent of aggregation of gold nanoparticles as confirmed by transmission electron microscopy.

Finally, the effect of morphology was further studied using two Gram-positive and two Gram-negative bacteria. Gold nanoparticles with different shapes – nanospheres, nanostars, nanocubes, and nanorods – were incubated with the bacteria to obtain a concentration dependent response. While the responses were similar for Gram-positive bacteria, there were significant differences for Gram-negative ones with the order of decreasing response being: nanostars> nanocubes> nanospheres > nanorods. Additionally, the concentration of gold nanoparticles determines the range of concentration of bacteria that can be detected.

This thesis demonstrates that detection, identification, and quantification of bacteria could be possible using gold nanoparticles for applications in food, water, and environmental contamination. In these applications, gold nanoparticles have exploited intrinsic properties of the nanoparticles and analytes to provide specific responses. Thus, gold nanoparticles exemplify the tremendous potential offered by nanotechnology.

Acknowledgements

First and foremost, I express my heartfelt gratitude to my supervisor, Professor Frank Gu, for his guidance, mentorship, advice, and recommendations throughout my research. He has been an excellent advisor while providing invaluable input to my research projects. He has constantly motivated me to perform at my full potential and always provided critical feedback when faced with roadblocks. The training in his laboratory has honed me into an independent researcher and thereby shaped my career path. I also extend my deepest gratitude to my external mentor and collaborator Professor Lyndon Jones who has guided the research project and provided critical comments on the project's direction.

I deeply appreciate the constructive comments from my thesis committee members, Professor Juewen Liu, Professor Perry Chou, and Professor Neil McManus. I am also extremely grateful to my external committee member Professor Aristides Docoslis for his participation in my thesis defense and for providing critical comments.

I would like to acknowledge the help from various research groups and individuals who have been instrumental to the execution of this research project. I am thankful to Dr. David McCanna and Dr. Brad Hall from Professor Lyndon Jones' laboratory for their advice on microbiological techniques and portable spectrophotometer respectively. I am also thankful to Dr. Parisa Sadatmousavi from Professor Pu Chen's group for her help with zeta potential measurements. I acknowledge the valuable input provided by Dr. Mohammadreza Khorasaninejad from Professor Simarjeet Saini's group on image processing and analysis. I am grateful to Professor James Forrest for his guidance in the rapid detection of pathogens. I also appreciate the critical advice provided by Professor Byron Gates from Simon Fraser University on the synthesis of gold nanoparticles. I am also extremely grateful to Shih-Chung Wei and Professor Chii-Wann Lin for their assistance with modeling of gold nanoparticles. I would also like to acknowledge Dr. Hsueh-Liang Chu and Professor Chia-Ching Chang for their advice on lipid blot assays.

Within our research group, I am indebted to the support from all lab members who have helped me with my experiments on numerous occasions. I am especially grateful to the co-op students Paul Chen, Jackson Tsuji, Matthew Dozois, Mostafa Saquib, and Yih Yang Chen; the current graduate students Jacob Rogowski, Shengyan (Sandy) Liu, Sarah LeBlanc, Peter Lin, Drew Davidson,

Timothy Leshuk, and Erin Bedford; and the graduated lab members Terence Chan, Benjamin Lehtovaara, Serge Yoffe, Joshua Rosen, and Ameena Meerasa.

I am extremely grateful to my friends and family for their constant support. I would like to thank both my parents and my brother Rohit for their endless encouragement and compassion.

Finally, I am extremely appreciative of the financial support provided by the Natural Sciences and Engineering Research Council of Canada (NSERC) Vanier Canada Graduate Scholarship, 20/20 NSERC – Ophthalmic Materials Network, University of Waterloo (UW) Faculty of Engineering Graduate Scholarship, UW Graduate Research Studentship, and M. Moo-Young Biochemical Engineering Scholarship. Additionally, I am also grateful for the Waterloo Institute for Nanotechnology (WIN) Nanofellowship, UW President's Graduate Scholarship, NSERC Julie Payette Master's Postgraduate Scholarship, and the NSERC Canada Graduate Scholarships – Michael Smith Foreign Study Supplements.

Dedication

To my spiritual guru H. H. Shri Mataji Nirmala Devi

and

my mother, father, and brother.

Table of Contents

List of Figures

List of Tables

List of Abbreviations

BSA	Bovine serum albumin
CCD	Charge-coupled device
CFU	Colony forming unit
CL	Cardiolipin
CTAB	Cetyltrimethylammonium bromide
DAB	3,3'-diaminobenzidine
DLS	Dynamic light scattering
DMPC	1,2-dimyristoyl-*sn*-glycero-3-phosphocholine
DMPE	1,2-dimyristoyl-*sn*-glycero-3-phosphoethanolamine
DMPG	1,2-dimyristoyl-*sn*-glycero-3-phospho-(1'-*rac*-glycerol)
DNA	Deoxyribonucleic acid
DNAzymes	Deoxyribonucleic acid enzymes
dNTPs	Deoxyribonucleotide triphosphates
dsDNA	Double-stranded deoxyribonucleic acid
ELISA	Enzyme linked immunosorbent assay
EPA	United States Environmental Protection Agency
EPS	Extracellular polymeric substances
FDA	United States Food and Drug Administration
FWHM	Full width half maximum
HBV	Hepatitis B virus
HCA	Hierarchical clustering analysis
HIV-1	Human immunodeficiency virus type-1
HPV	Human papillomavirus

HPV-16	Human papillomavirus type 16
HPV-18	Human papillomavirus type 18
HRP	Horseradish peroxidase
ICS	Immunochromatographic strip
IgA1P	Immunoglobulin A1 protease
KSHV	Karposi's sarcoma-associated herpesvirus
LDA	Linear discriminant analysis
LPS-R	Rough strain (Rd) lipopolysaccharides
LPS-S	Smooth lipopolysaccharides
LTA	Lipoteichoic acids
MNAzyme	Multicomponent nucleic acid enzyme
mRNA	Messenger ribonucleic acid
MRSA	Methicillin-resistant *Staphylococcus aureus*
NASBA	Nucleic acid sequence-based amplification
NC	Nitrocellulose
PAGE	Polyacrylamide gel electrophoresis
PCA	Principal components analysis
PCR	Polymerase chain reaction
PE	Phosphatidylethanolamine
PepG	Peptidoglycan
PG	Phosphatidylglycerol
PVDF	Polyvinylidene difluoride
RCA	Rolling circle amplification
RGB	Red, green, blue

RNA	Ribonucleic acid
rRNA	Ribosomal ribonucleic acid
RT-PCR	Reverse transcription polymerase chain reaction
ssDNA	Single-stranded deoxyribonucleic acid
TEM	Transmission electron microscopy
TMB	3,3’,5,5’-tetramethylbenzidine
TSA	Trypticase soy agar
TSA II	Trypticase soy agar with 5% sheep blood
UV-Vis	Ultraviolet-Visible

Chapter 1
Introduction

1.1 Overview

Pathogens cause infections in a variety of forms and can have consequences ranging from blindness to death [1, 2]. In order to treat such infections, it is necessary to first diagnose them rapidly and accurately. Detection of pathogens has conventionally been performed using culture-based methods which tend to be slow, tedious, and insensitive [2, 3]. These drawbacks have inspired the development of biosensors that could be used for faster and more sensitive detection of pathogens. While these biosensors have demonstrated significant advancements to provide even subcellular characterization [4], they are mostly limited to be used in a laboratory environment because they require specialized equipment and technical expertise. There is a growing need for simple methods of detection that could be used by the general public or at the point-of-care [5, 6].

Nanotechnology plays an important role in facilitating sensors that could be used in simple assays. Nanoparticles exhibit unique physical, chemical, and optical properties in comparison to their bulk counterparts [7]. Some of these properties are a result of the high surface area to volume ratio while others are due to confinement of electrons at the nanometer scale. Specifically, gold nanoparticles have generated tremendous interest for use as biosensors because of their strong color, aggregation dependent optical properties, and thiol-reactivity [8-10]. The optical properties of gold nanoparticles depend on their particle size, shape, and environmental conditions. This dependence has been exploited to produce a variety of different colors of gold nanoparticles by using shapes such as spheres, shells, rods, prisms, hexagonal plates, cubes, and stars [11]. In the context of pathogens, gold nanoparticles have been used for the detection of nucleic acids, proteins, lipopolysaccharides as well as whole cells. Functionalizing the gold nanoparticles with small molecules, proteins, and nucleic acids enables their wide range of applications but yet, most studies focus on the detection of a single pathogen.

A variety of pathogens are often responsible for contaminating food, water, or hospitals [2]. Thus, an ideal biosensor would be able to detect many different pathogens specific to an application of interest. Using typical “lock and key” recognition strategies, where the target analyte is detected using

specific biomolecules like aptamers or antibodies, can limit the number of pathogens that can be detected because each biomolecule is usually specific to a single analyte [12]. This limitation is currently being overcome by a new class of biosensors, which can identify the analytes based on a set of unique responses rather than depending on a single response [12-14]. Since these biosensors function in a manner similar to our sense of smell, where a set of specific receptors are activated in the presence of an odor molecule, they are often called "chemical nose" biosensors. Such a "chemical nose" biosensor has been designed for detecting bacteria but it requires the modification of gold nanoparticles with a variety of small molecules and it also employs a fluorescence spectrophotometer [15, 16], which can limit its use at the point-of-care. Existing "chemical nose" biosensors have not demonstrated the ability to detect mixtures of bacteria and hence there is a need for simpler and more versatile system.

This research project exploits the unique tools provided by nanotechnology to produce a simple colorimetric biosensor using the intrinsic properties of gold nanoparticles and bacteria and the interactions between the two. The synthesis of gold nanoparticles has been studied here to gain an understanding of the parameters that can change the size and morphology of nanoparticles. Additionally, the impact of these physical properties of gold nanoparticles on their ability to detect bacteria is explored. Then, the gold nanoparticles are deployed as a "chemical nose" platform to differentiate between various pathogenic bacteria that can contaminate contact lenses, food, water, and hospitals. In order to bring the biosensor closer to point-of-care, the speed of detection has been increased by incorporating the kinetics of the colorimetric response. Some of the avenues that will be pursued in future studies are improved sensitivity, detection in complex media, and specific understanding of the components of bacteria causing the colorimetric response.

1.2 Research Objectives

Developing a biosensor for use at the point-of-care requires that it is simple, versatile, cost-effective, rapid, and portable. This research focuses on developing a biosensor based on gold nanoparticles such that a simple colorimetric output is provided. Controlling the size and shape of nanoparticles can determine the colorimetric response and hence provide versatility to the biosensor. Cost-effectiveness is achieved by avoiding the use of biomolecules such as aptamers and antibodies and instead, using intrinsic properties of gold nanoparticles for obtaining unique responses. A rapid and portable system

is designed by coupling the biosensor with a portable spectrophotometer. The specific objectives for the project are as follows:

1. Demonstrate the capabilities of gold nanoparticles to act as colorimetric biosensors for detection of bacteria
    - Determine the effect of size and branching on the colorimetric properties of gold nanostars
    - Study the effect of size and morphology of gold nanostars on the biosensing ability in the presence of model Gram-positive bacterium *Staphylococcus aureus*
2. Develop a "chemical nose" biosensor for detection and identification of ocular pathogens
    - Select optimal formulations from the library of nanostars to obtain a set of unique responses for each ocular pathogen
    - Test the ability of "chemical nose" to distinguish between bacteria using emerging contaminants affecting contact lens wearers
3. Enhance the "chemical nose" biosensor for quantification of bacteria and detection of polymicrobial mixtures
    - Determine the effect of concentration of bacteria on the detection capabilities of the "chemical nose" by including pathogens that contaminate food, water, and hospitals
    - Determine the possibility of detecting and discriminating between mixtures of bacteria
4. Exploit the kinetics of color change for rapid detection of bacteria using "chemical nose"
    - Determine if the rate of color change of nanoparticles is unique for each bacterial species and for mixtures
    - Characterize the color change using a portable spectrophotometer to enable the possibility of point-of-care diagnosis
5. Explore the effects of other shapes on the interactions between gold nanoparticles and bacteria surface

- Synthesize gold nanoparticles with various shapes: nanospheres, nanostars, nanorods, and nanocubes
- Determine the performance of each shape as a "chemical nose" biosensor by characterizing the colorimetric response in the presence of various Gram-positive and Gram-negative bacteria.

1.3 Thesis Outline

The thesis consists of one chapter on literature review followed by five research-based chapters. Additionally, the final chapter presents the conclusions and recommendations for future work. Chapter 1 is an introduction to the thesis, where the research problem is presented and specific objectives are outlined.

Chapter 2 reviews current literature specific to the use of gold nanoparticles as biosensors for detection of pathogens affecting food, water, and hospitals. The review highlights that previously the focus of gold nanoparticles has been on improving existing nucleic acid based technologies, while emerging biosensors are focusing on the detection of proteins, small molecules, and also whole cells to minimize detection time and enhance detection limits. The review demonstrates that versatile biosensors for detecting multiple species of bacteria are lacking.

Chapter 3 explores the synthesis of gold nanostars and the control of morphological parameters using synthesis conditions. The effects of nanoparticle features are also related to their colorimetric response in the presence of model Gram-positive bacterium *Staphylococcus aureus*. This chapter lays the foundation for the "chemical nose" biosensor since it demonstrates that the size and branching of gold nanostars determine the colorimetric response obtained in the presence of bacteria.

Chapter 4 utilizes the knowledge of differential response from Chapter 3 and uses it to build a "chemical nose" biosensor, where a set of responses is obtained by using a mixture of gold nanoparticles with varying morphologies. This chapter provides proof-of-concept for implementing cationic gold nanoparticles for differentiating between four different species of ocular pathogens without the use of biomolecules such as antibodies or aptamers.

Chapter 5 enhances the “chemical nose” developed in Chapter 4 by extracting additional responses from the nanoparticle solutions and detecting eight different species of pathogenic bacteria affecting food, water, contact lenses, and hospitals. This chapter exemplifies the versatility of the “chemical nose” by differentiating between bacteria at three different concentrations and by detecting polymicrobial mixtures containing two or three different species of bacteria mixed together.

Chapter 6 highlights how the “chemical nose” biosensor could be translated to point-of-care use by coupling the biosensor with a portable spectrophotometer for rapid acquisition of absorption spectra. Using the kinetics of color change, rapid detection of bacteria is possible within two minutes. This design brings the gold nanoparticle-based biosensor a step closer to deployment with the end user.

Chapter 7 revisits the question of the effect of shapes on the response of “chemical nose” biosensors by using nanospheres, nanostars, nanocubes, and nanorods. The chapter provides design guidelines for selecting the concentration of nanoparticle depending on the desired range of bacteria to be detected. This chapter paves the way for expanding the applications of the “chemical nose” biosensor by suggesting that using additional shapes could help discriminate between more species of bacteria.

Finally, chapter 8 presents the conclusions drawn from this research project and based on these conclusions, provides recommendations for future research avenues. One of the key avenues of research is exploring methods of enhancing the response such that the sensitivity of the biosensor can be increased. Another important area is the testing of the “chemical nose” biosensor in complex media such as food products or blood samples. Additionally, to expand the application of “chemical nose” to a variety of other pathogens, an understanding of the interactions between nanoparticles and cell wall components needs to be established.

Chapter 2
Literature Review

2.1 Summary

Rapid detection of pathogens is crucial to minimize adverse health impacts of nosocomial, foodborne and waterborne diseases. Gold nanoparticles are extremely successful at detecting pathogens due to their ability to provide a simple and rapid color change when their environment is altered. Here, we review general strategies of implementing gold nanoparticles in colorimetric biosensors. First, we highlight how gold nanoparticles have improved conventional genomic analysis methods by lowering detection limits while reducing assay times. Then, we focus on emerging point-of-care technologies that aim at pathogen detection using simpler assays. These advances will facilitate the implementation of gold nanoparticle-based biosensors in diverse environments throughout the world and help prevent the spread of infectious diseases.

2.2 Introduction

Mankind has been fascinated by gold nanoparticles for centuries and the Lycurgus cup is a prime example of their unique optical properties. In the 21st century, research involving gold nanoparticles has witnessed significant growth with applications in drug delivery [17-19], photothermal therapy [20-22], diagnostic imaging [23-25], and biosensors [26-28]. Along with being the most stable metallic nanoparticles [29], gold nanoparticles flaunt several outstanding features, including facile reactivity with biomolecules, high surface area to volume ratios, and environment dependent optical properties, which make them the ideal candidate for use in colorimetric biosensors [7].

Pathogens—including bacteria, viruses, fungi, and protozoa—are a leading cause for loss of lives in the developing world, as well as rural areas of developed countries, due to lack of infrastructure and resources [2]. Since pathogens can be transmitted via plants, animals, and humans, infectious diseases can spread exponentially and lead to a pandemic if left unchecked [30]. The most effective method for preventing the spread of infectious diseases is early diagnosis, which is challenging using conventional methods because of expensive equipment, specialized sample preparation, and slow data

output [2]. Modern biosensors have overcome these obstacles by miniaturizing devices and providing simple rapid output that can be analyzed at the point-of-care without specialized training [31-33].

In addition to point-of-care diagnostics and early treatment of infectious diseases in humans, microbial pathogens are also a concern at various levels of the food industry. Many bacterial genera are associated with food-borne illness such as *Salmonella*, *Listeria*, and *Escherichia*. Infections are typically caused by consumption of food or drink contaminated with these pathogens, and may lead to various inflammatory conditions including gastroenteritis, meningitis, and sepsis. Serious infections may require hospitalization and can be fatal for more vulnerable segments of the population (e.g. immunocompromised patients) [34]. While low levels of bacteria and other microbial life are sometimes tolerable, high concentrations are frequently associated with food-borne illnesses [35]. Various agencies have implemented guidelines for food production, preparation, and distribution, which aim to keep pathogen loads at acceptable levels. Often these guidelines have stringent concentration requirements and hence, screening assays require excellent detection limits.

Gold nanoparticles have been implemented for the detection of pathogens, which contaminate food, water, and hospital surfaces [2, 7, 8, 10, 13, 36, 37]. A major focus of research is to improve conventional genomic analysis methods using gold nanoparticles such that the assays have lower detection limits and faster response times (Figure 1). Concurrently, novel methods of detection have been developed independent of gene amplification and the most popular strategy is based on the surface modification of gold nanoparticles with antibodies, which has led to several commercially available products for easy and timely testing of pathogens in complex samples such as plant extracts, foods, and bodily fluids. An emerging strategy is to exploit the intrinsic surface properties of gold nanoparticles and pathogens which leads to electrostatic interactions and a color change.

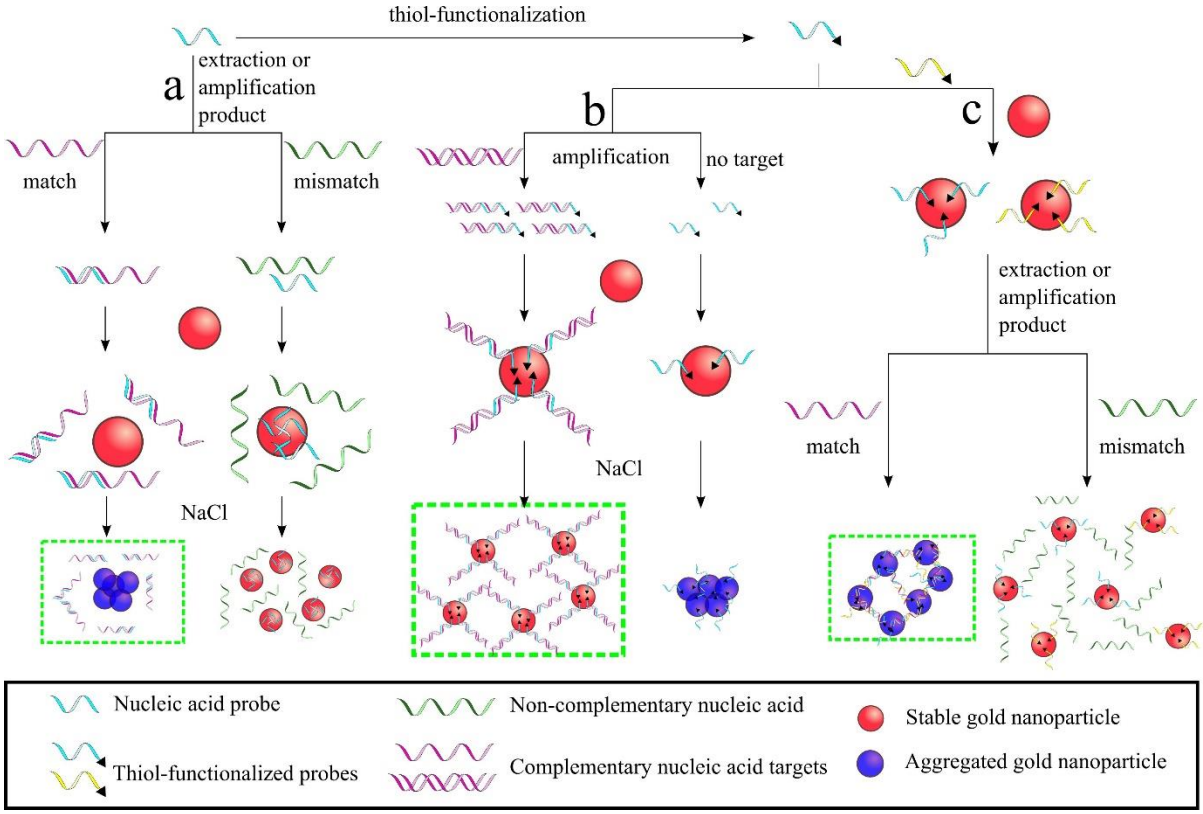

Figure 1: Colorimetric detection of nucleic acids using non-functionalized and functionalized gold nanoparticles, adapted from [38, 39]**; a) the use of a single non-thiolated probe with non-functionalized gold nanoparticles, b) use of single thiolated probe with non-functionalized nanoparticles, c) use of a pair of thiolated probes for functionalizing gold nanoparticles.**

2.3 Conventional methods for pathogen detection

The importance of pathogen detection in several sectors has led to continuous improvement in detection technologies. Currently, conventional methods for pathogen detection can be roughly divided into three categories: culture and colony counting, immunological assays, and polymerase chain reaction (PCR)-based methods [35]. These methods offer high sensitivity and specificity, providing both quantitative and qualitative information, which is often a necessity. However, some key drawbacks, chief of which being required processing times, clearly indicate a need for better solutions.

Colony counting is widely considered to be the gold standard for pathogen detection in settings ranging from clinical diagnosis to food pathogen measurement [31, 35, 40]. This process involves isolation and growth of a suspect pathogen, followed by visual inspection. Due to the inherent amplification during colony growth, this method is good for identifying very low levels of organisms (i.e. single cells). Unfortunately, turn-around times for results are very slow using this technique due to long incubation periods and the need for intensive labor. Depending on the pathogen, initial results often require at least 2 days, with conformation after 7-10 days [35, 40]. Furthermore, colony counting methods require a pathogen to be culturable, which may not always be the case given stringent environmental or nutritional requirements.

Immunological assays are very common for pathogen detection due to their adaptability for a wide variety of pathogens including bacteria and viruses. The enzyme-linked immunosorbent assay (ELISA) method is an example of a well-known immunological assay. These assays rely on antibody recognition of antigens and other biomolecules specific to the target. Once antibodies are identified and available, the primary advantage of immunological assays over colony counting is reduced assay time while maintaining high specificity. ELISA has the ability to provide an optical response and hence is widely deployed in clinical laboratories with the use of commercially available ELISA kits. The technique still suffers from the drawbacks of requiring multiple steps, specialized training, and several hours of runtime [31, 41]. Antibody-labelled gold nanoparticles have been able to overcome these challenges by using an immunochromatographic strip (ICS) format and unique products are available for testing of foods and clinical samples. The testing of food products is facilitated by Merck Millipore's Singlepath® and Duopath® products (Billerica, MA, USA), but these products require selective enrichment of bacteria before the sample is analyzed, which is necessary because of low sensitivity and the need to detect low concentration of pathogens in food. Thus, the assay requires several hours for completion even though the ICS can respond within 20 minutes. In a clinical diagnostic setting, ICS-based assays have been developed by Coris Bioconcept (Gembloux, Belgium) for the detection of viruses and bacteria in stool, urine, and blood samples [42]. Current challenges faced by ICS-based assays include the variability caused by user sample preparation and cross-reactivity of analytes, yet ICS has been the biggest commercially available success of colloidal gold nanoparticles because of their ability to analyze samples in a complex media with minimal

purification. We will highlight how emerging technologies have adopted the success of antibody-labeled gold nanoparticles in later sections of this chapter.

PCR-based methods constitute a wide variety of detection schemes relying on nucleic acid amplification to increase the concentration of the detection target. Amplification of target deoxyribonucleic acid (DNA) sequences lends PCR-based conventional methods a high degree of sensitivity, even capable of detecting single gene copies. It is important to note that unlike colony counting, this sensitivity is achieved without a prolonged incubation time since bacteria do not need to be grown [41]. Specificity is achieved through the design of primers and probes that target sequences that are unique to the pathogen of interest. However, interference from non-pathogenic genetic material may lead to misleading results due to mismatch or non-specific amplification [35, 41]. Precise genetic information is therefore required for confidence in results. Following target amplification, samples are traditionally separated by gel electrophoresis but complex sample preparations and manipulations increase labor cost and processing times [31]. Newer technologies such as real-time PCR and fluorescent molecular probes aim to reduce these factors. Perhaps the main drawback of traditional PCR-based methods for pathogen detection is the inability to distinguish viable and non-viable cells, since both contain the amplification target [35]. To address this issue, assays have been developed that employ reverse trascription PCR (RT-PCR) to target rapidly degrading messenger ribonucleic acid (mRNA) strands present during the cell's growth cycle [35, 43].

2.4 Principles of gold nanoparticle sensing

The unique optical properties of gold nanoparticles make them very popular for pathogen detection. Most of these assays rely on the basic principle of surface plasmon resonance to detect changes in nanoparticle aggregation states [29]. The peak absorbance of gold nanoparticles depends on their size and shape. Spherical nanoparticles with mean particle sizes ranging from 9 – 99 nm have been observed with absorbance peaks from 517 – 575 nm, respectively [29]. Gold nanorods exhibit two absorbance peaks: one corresponding to transverse band (about 520 nm) and another corresponding to the longitudinal band (in the infrared region). The longitudinal band is typically more sensitive when gold nanorods are used in biosensors [44]. Star-shaped gold nanoparticles have also been used for the colorimetric detection of pathogens, where the absorption peak is governed by the particle size and

degree of branching [9]. Smaller particles are more colloidally stable but bigger particles can be more sensitive. Thus, optimization of particle size is important but rarely explored for pathogen detection [9, 45]. Most commonly, spherical gold nanoparticles in the size range of 13 – 20 nm with absorbance peak around 520 nm have been employed in biosensors due to ease of synthesis.

The peak absorbance wavelength is sensitive to the distance between particles. Upon aggregation, the surface plasmon resonance of individual particles become coupled and shifts the absorbance spectrum [46]. This shift can be large enough to produce a visible color change, which makes the techniques favorable for rapid point-of-care diagnostics. Peak absorbance wavelengths exhibit a red-shift with increases in size, typically giving stable (non-aggregated) nanoparticles a red color, while aggregated nanoparticles appear blue (Figure 2) [47]. Use of an ultraviolet-visible spectrophotometer can help quantify the shift in the surface plasmon resonance peak.

Figure 2: Typical colors of gold nanoparticles. Aggregation of nanoparticles causes a shift from red to blue, adapted from [47]

Gold nanoparticles are typically stabilized electrostatically, where citrate-capped nanoparticles are negatively charged and cetyltrimetylammonium bromide (CTAB)-coated nanoparticles are positively charged. The electrostatic repulsion between nanoparticles can be shielded by the addition of salts (most commonly sodium chloride), which then leads to the aggregation of nanoparticles and hence, a color change [48].

Optical effects of surface plasmon resonance have been implemented for pathogen detection by either inducing particle aggregation or stabilization. These effects are governed by target ligands, nanoparticle functionalization, competitive binding sites, or salts. The specific combinations of these factors make up the wide variety of applications investigated in this chapter.

2.5 Gold nanoparticles for amplified nucleic acids

2.5.1 Techniques for amplification of nucleic acids

DNA amplification refers to the process of increasing the copy number of a particular DNA sequence. Amplification is a common strategy in molecular diagnostics in order to increase signal strength. While other signal amplification strategies amplify by manipulating reporter molecules, DNA amplification increases the concentration of the target analyte directly, thereby increasing the response.

Ribonucleic acid (RNA) amplification can be used instead of DNA amplification when transcriptional information is of particular interest. While less chemically stable than DNA, RNA transcripts are commonly used in the area of functional genomics since they provide information on cellular activities and can change in response to life-cycle or stimulus events. RNA amplification of transcripts exclusive to cell growth phases have been used to differentiate between viable and dead cells [43].

Various methods used for the amplification of nucleic acids have been highlighted in molecular diagnostic reviews [49-51]. Here, we briefly describe the methods that are used in combination with gold nanoparticles for detection of pathogens. One of the most common techniques for nucleic acid amplification is PCR. The general principle behind PCR is the extension of nucleic acid primers using deoxyribonucleotide triphosphates (dNTPs) and polymerase enzymes. The entire process can be separated into three stages. During the denaturation phase, high temperatures are used to break apart double-stranded structures of DNA. Lower temperatures during the annealing phase allow short nucleotide sequences known as primers to attach to the separated strands. Polymerase enzymes can then reconstruct the complementary strand using dNTPs in solution, reforming double stranded DNA. The process is then repeated, increasing the DNA copy number exponentially each cycle. A common

way to visualize the final product is by polyacrylamide gel electrophoresis (PAGE), whereby DNA strands are separated by size and stained for observation.

Real-time (a.k.a. quantitative) PCR is an alternative to PCR followed by PAGE, where DNA is amplified and copy numbers simultaneously quantified. A common method for DNA quantification is the use of fluorescent probes. Complementary nucleotide probes can be designed with fluorophores and quencher dyes so as to produce a fluorescent signal upon binding to target DNA (i.e. molecular beacon probes) or upon degradation by polymerase enzymes (i.e. TaqMan probes). As copy number increases, so does the availability of binding regions for probes, thereby increasing the fluorescent signal.

Many variations of traditional PCR and real-time PCR exist for specific targets and amplification conditions. RT-PCR is used to amplify RNA targets into complementary DNA sequences, such as when studying transcriptional levels. This technique is similar to PCR but incorporates a reverse transcription step at the beginning to obtain complimentary DNA. Asymmetric PCR can be used when amplifying a target for sequencing. In order to amplify the coding strand preferentially over the non-coding strand, one primer is used in excess. This arithmetic amplification is slower than traditional PCR, but ensures a higher copy number for the coding strand. Rolling circle amplification (RCA) is an isothermal amplification technique commonly used for circular DNA sequences such as plasmids and bacterial chromosomes. Nucleic acid sequence-based amplification (NASBA) is another isothermal method used to amplify RNA which combines reverse transcriptase and RNase digestion of the RNA template to generate RNA amplicon [52]. NASBA has the advantage of being isothermal as compared to RT-PCR and hence can be more versatile for out-of-laboratory field applications.

2.5.2 Non-functionalized gold nanoparticles

Non-functionalized gold nanoparticles are usually used for the detection of amplified products by the addition of salt. In the presence of salt, typically gold nanoparticles will aggregate and change color from red to blue unless they can be stabilized by nucleic acids. Two primary strategies can be utilized for stabilizing the gold nanoparticles: adsorption of nucleic acids on the surface or reaction with thiol probe, which has been hybridized with the target nucleic acids (Figure 1 a, b). Another approach involves the use of cationic gold nanoparticles, where the interactions between nucleic acids and the surface of gold nanoparticles lead to aggregation of the nanoparticles. This approach is similar to the

one explained in Figure 1 c, except the gold nanoparticles are not functionalized with a thiol-probe but rather coated with the probe using electrostatic interactions.

DNA from bacteria and viruses has been used for detection by adsorption on the surface of gold nanoparticles. *Salmonella spp.* are troublesome for causing foodborne illnesses. Regulatory levels published by the United States Food and Drug Administration (FDA) and United States Environmental Protection Agency (EPA) for food safety require complete absence of *Salmonella spp.* in a 25 gram sample [53] It is therefore important for detection assays to have high sensitivity to very low (individual) pathogen levels. *Salmonella* spp. has been detected by targeting the *stn* gene where a oligonucleotide probe was designed to be complementary to the PCR product [54]. Here, 23 nm gold nanoparticles were able to produce a detection limit 10x more sensitive than gel electrophoresis. Also, a sensitivity (true positive rate) of 89.15% and specificity (true negative rate) of 99.04% was obtained for various food samples as compared to conventional culture methods. Detection of *Bacillus anthracis,* the causative agent of anthrax, is possible by using a similar strategy. Here, it was demonstrated that when the DNA is longer than about 100 nt (single-stranded DNA, ssDNA) or 100 bp (double-stranded DNA, dsDNA), it can prevent salt-induced aggregation of 15 nm gold nanoparticles [55] and the colorimetric response is visible by the naked eye. When considering viruses, Hepatitis B virus (HBV) is notorious for causing acute and chronic liver diseases worldwide. HBV has been detected by designing a probe targeting the *rtM204M* wild type gene [56]. A colorimetric response from 13 nm gold nanoparticles was able to distinguish between target DNA and single base pair mismatched DNA. On the other hand, RCA has been used for the detection of H1N1 viral DNA, where long ssDNA curled into balls and could not stabilize 13 nm gold nanoparticles [57].

The use of thiol-modified probes coupled with non-functionalized nanoparticles has primarily been used for detection of bacterial DNA. *Chlamydia trachomatis* is responsible for most of the bacterial sexually transmitted diseases worldwide. The gene encoding virulence proteins was targeted with thiolated probes and detected in human urine samples using 13 nm gold nanoparticles [38]. *Listeria monocytogenes* and *Salmonella enterica* are notorious for contaminating foods and causing fatalities. FDA regulations have a “zero-tolerance” policy of no detectable *L. monocytogenes* in two 25 g samples of food or beverage [58]. The detection of these food-borne bacteria has been possible by

designing thiolated probes to target the *hly* and *hut* genes for *L. monocytogenes* and *S. enterica* respectively. This assay was able to detect bacteria in contaminated milk samples using 13 nm gold nanoparticles and the specificity was confirmed by a lack of response from *Escherichia coli* [59].

The detection of DNA from human immunodeficiency virus type 1 (HIV-1) has been possible using cationic gold nanorods. The probe is designed to target sections of the *HB-hp3-LTR1.8* DNA and in the presence of the target, aggregation is induced [60]. The specificity of this assay was confirmed by comparing results against genes from *Mycobacterium tuberculosis* and genes encoding for *Bacillus* glucanase. It was possible to perform detection under physiological conditions because the assay is tolerant to high salt concentrations. Another use of gold nanorods is for the detection of *Leishmania major,* a protozoan parasite that has led to 1.5 million cases of cutaneous leishmaniasis annually worldwide. The disease can lead to disabilities and even death. The detection of the parasite using culture-based methods is extremely slow and insensitive. Thus, molecular diagnostics can offer an improved method for detection. NASBA has been employed for the detection of 18S ribosomal RNA (rRNA) of *L. major* by designing the appropriate primer [61]. After amplification, the NASBA amplicons are incubated with gold nanorods leading to aggregation. Clinical skin biopsies were tested using this method and a sensitivity of 100% and specificity of 80% was obtained as compared to RT-PCR and gel electrophoresis.

Non-functionalized gold nanoparticles have the advantage of providing rapid response as compared to gel electrophoresis. Additionally, the equipment necessary for gel electrophoresis is not needed since a simple colorimetric response is obtained, which can be visually observed with minimal training. The synthesis of non-functionalized nanoparticles can often be executed in a single step, which simplifies the assay. The main limitation to this approach is that the conditions for detection often need to be optimized such that the appropriate concentrations of salts and reagents are used to avoid unnecessary aggregation of gold nanoparticles. The optimization of assay conditions demands extra efforts for each target in question. The studies using non-functionalized gold nanoparticles for amplified nucleic acids have been summarized in Table 1. They are divided by pathogen type: bacteria, viruses, and protozoa, and then sorted chronologically.

Table 1: Nucleic acid amplification followed by interaction with non-functionalized gold nanoparticles

Pathogens of interest	Sample type	Analysis time	Detection limit (copies/µL DNA)	Working range (copies/µL DNA)	References
Chlamydia trachomatis	Urine	1 hr post-amplification	20	20-20,000	[38]
Salmonella spp.	Culture	<8 hr	2×10^9	$2x10^9 – 2x10^{11}$	[54]
Listeria monocytogenes and *Salmonella enterica*	Food	3 – 4 hr	2.1×10^4 (*L. monocytogenes*) 2.6 x 10^4 (*S. enterica*)	$2.1 \times 10^4 – 2.1 \times 10^{11}$ (*L. monocytogenes)* 2.6 x $10^4 – 2.6 \times 10^{11}$ (*S. enterica)*	[59]
Bacillus anthracis	Nucleic acids	-	~3.9×10^{6a}	~$3.9 \times 10^6 – 3.9 \times 10^{8a}$	[55]
HIV-1	Nucleic acids	<5 min post-amplification	4.8×10^7	$1.0 \times 10^8 – 7.0 \times 10^9$	[60]
Hepatitis B virus	Serum	-	3×10^9	$3 \times 10^9 – 3x\ 10^{11}$	[56]
H1N1 virus	Nucleic acids	3 h	6.02×10^5	$6.02 \times 10^5 – 6.02 \times 10^{10}$	[57]
Leishmania major	Skin biopsy	-	-	-	[61]

[a]a mixture of ssDNA and ds DNA was used, molecular weight of ssDNA was used for calculations.

2.5.3 Functionalized gold nanoparticles

Gold nanoparticles can be easily functionalized with nucleic acid probes by using thiol-gold chemistry. There are two primary approaches to detection, which are governed by the number of probes used. In one scenario, salt is used to induce aggregation of probe-conjugated gold nanoparticles. Only one type of probe is used for binding to the target sequence. This approach is similar to the illustration in Figure 1 b, except the gold nanoparticles are conjugated to the thiolated probe before hybridization. In this situation, binding of the target to the probe results in double helix formation and particles can remain stable under higher salt conditions. Consequently, absence of the target would lead to particle aggregation at similar salinity. In another scenario, two probes are used such that each probe can bind to the same nucleic acid strand. There are two main methods within the two-probe approach. In one method, gold nanoparticles are functionalized with each of the two probes separately and then mixed together. The presence of the target causes particle aggregation by cross-linking gold nanoparticles together. In the absence of the target sequence or the presence of a mismatched sequence, aggregation does not occur and particles remain stable in suspension (Figure 1

c). Another method using two probes is called gold label silver stain. Here, one probe is immobilized on a glass slide and another on the gold nanoparticles. The target nucleic acid binds to the glass slide first, followed by the addition of the gold nanoparticles and then silver for signal enhancement [62]. In recent studies, the probe immobilized on gold nanoparticle has been replaced by streptavidin and the PCR product has been functionalized with biotin for facilitating binding *via* streptavidin-biotin interactions instead of hybridization.

Using the one-probe approach, *Mycobacterium tuberculosis* has been detected by designing probes targeting the *rpoB* gene and immobilizing them on 14 nm gold nanoparticles [63]. The design is able to discriminate against the non-tuberculosis causing *Mycobacterium kansasii*. This design has also been implemented in a paper format, by using wax-based ink for making a 384-well paper microplate [64]. The assay has been adapted for differentiating between *Mycobacterium bovis* and *M. tuberculosis* by targeting the *gyrB* gene [65]. Three probes were designed to target specific segments of the *gyrB* gene and immobilized on gold nanoparticles. Each strain of *Mycobacterium* interacted differently with the probes and hence allowed accurate identification. Another notorious pathogen methicillin-resistant *Staphylococcus aureus* (MRSA) has been responsible for numerous persistent infections. It has been possible to detect MRSA by using probes towards 23S rRNA and *mecA* genes [66]. In this study, the sensitivity and specificity were comparable to real-time PCR assays but with a lower cost per reaction. RNA has also been targeted using the one-probe approach. One example is the detection of *dnaK* messenger RNA of *Salmonella enterica* serovar Typhimurium after amplification by NASBA [67]. The probe was immobilized on 17 to 23 nm gold nanoparticles and the assay was able to distinguish between RNA from *S.* Typhimurium and *Bacillus firmus.*

The two-probe approach has also gained popularity for a variety of bacterial and viral targets. *Helicobacter pylori* is responsible for several gastric conditions such as chronic gastritis, gastric adenocarcinoma and gastric ulcers. Detection of *H. pylori* is possible by designing probes towards the *ureC* gene and immobilizing them on gold nanoparticles. Target DNA was amplified using thermophilic helicase-dependent isothermal amplification and the assay was able to distinguish between *H. pylori*, *E. coli*, and human DNA [68]. While some strains of *E. coli* can be harmless, Shiga toxin producing *E. coli* O157:H7 can cause disease outbreaks when it gets transmitted *via* food or water. FDA and EPA regulations for clams, mussels, oysters, and scallops require *E. coli* levels to

be below 330/100g as determined by the Most Probable Number method, which translates to approximately 3.3 colony forming unit (CFU)/g [53]. The detection of *E. coli* O157:H7 has been achieved by designing a pair of probes targeting the *stx2* gene and immobilizing them on gold nanoparticles for a visible color change [69]. Another food-borne pathogen is *S.* Typhimurium, which can be detected by targeting the invasion (*inv* A) gene. [70]. The specificity of this assay was confirmed by comparing response to PCR products of other non-*Salmonella* spp. bacteria. The assay can provide better sensitivity compared to gel electrophoresis [70]. While most studies have focused on detection of a single species of bacteria, it is also possible to design gold nanoparticles for the detection of multiple bacteria, including the non-pathogenic ones. This is especially important in blood components because of the zero-tolerance policy. The 16S rDNA sequence is present in most bacteria and hence can be used as a target for detection [71]. A pair of 12-mer probes have been designed to target the 16S rDNA sequence and immobilized on gold nanorods. This method was tested for detection of the following species of bacteria in platelet concentrates: *Pseudomonas aeruginosa, Staphylococcus aureus, Staphylococcus epidermidis, Klebsiella pneumoniae, Serratia marcescens* and *Bacillus cereus*. It was found that the assay was most sensitive for the detection of *S. marcescens*. The assay provides a simple method for giving a yes/no result in contamination of blood components, but it does not identify the species of contamination.

A slightly different two-probe approach has been adapted for the detection of human papillomavirus (HPV) type 16 (HPV-16) and type 18 (HPV-18). These viruses are responsible for over 70% of cervical cancer cases and hence fall under the “high risk” category. Two pairs of thiolated oligonucleotide probes have been designed to target the L1 gene of HPV-16 and HPV-18. These probes were immobilized on 13 nm gold nanoparticles, which aggregate in the presence of asymmetric PCR products. In the presence of the target, gold nanoparticles remain stable under high salt conditions because they are spaced apart by the target DNA [72].

Modifications of gold label silver stain method have been implemented for detection of viruses and bacteria. HIV-1 and *Treponema pallidum* are prominent causes of sexually transmitted diseases and their prevalence has been rising. Amino-terminated oligonucleotide probes have been designed to target the *gag* gene for HIV-1 and 47k Ag gene for *T. pallidum* and immobilized on glass surfaces. The target genes were amplified and biotinylated by multiplex asymmetric PCR and then detected

[73]. A similar approach has been deployed for the detection of *Acinobacter baumannii*, which is responsible for a high incidence of bacteremia in hospitals. The specificity of the assay has been determined by comparing the response to other strains within the species (positive control), other species within the same genus (negative control), and bacteria from other genera (negative control) [74]. In order to test a large number of samples simultaneously, the assay has been incorporated in microarrays. Typical biotin-tyramine microarray designs do not provide sufficient accumulation of gold nanoparticles and hence 1.4 nm gold nanoparticles have been modified with 3,3'-diaminobenzidine (DAB), which is a substrate for horseradish peroxidase (HRP) [75]. Here, the HRP is modified with streptavidin, which binds to biotinylated PCR products that are immobilized on the glass surface via a probe. The presence of DAB promotes the accumulation of gold nanoparticles and simplifies the assay by reducing an incubation step compared to biotin-tyramine based microarrays. This approach was deployed for the detection of *Salmonella enterica* serovar Typhi, which is responsible for causing typhoid fever (a life-threatening infection, especially in developing countries) [75].

Finally, biotin-streptavidin interactions have also been exploited for implementing gold nanoparticles in an ICS format for the detection of influenza H1N1 virus. An ICS format is ideal for detection because of its portability and easy readout. In this design, gold nanoparticles were functionalized with anti-hapten antibodies and added to the conjugate pad. RT-PCR products labelled with biotin and Texas Red (a hapten) are added to the conjugate pad, where they attach to the gold nanoparticles. The test line contains streptavidin while the control line contains anti-mouse IgG and thus, the gold nanoparticles attach to test line only if the biotin labelled RT-PCR products are present [76].

Functionalized gold nanoparticles share the advantage of eliminating the need for gel electrophoresis as was the case with non-functionalized nanoparticles. Additionally, functionalization widens the scope of formats in which the assays are implemented ranging from solution-based methods to strip-based methods. The major limitation of functionalization is that the gold nanoparticles need to be modified for each analyte of interest and then purified before use. These additional processing steps can require additional time and technical expertise and also lead to loss of

nanoparticle yield. The studies employing functionalized gold nanoparticles for amplified nucleic acids have been summarized in Table 2.

Table 2: Nucleic acid amplification followed by interaction with functionalized gold nanoparticles

Pathogens of interest	Sample type	Analysis time	Detection limit	Working range	Sensitivity	Specificity	References
Helicobacter pylori	Gastric biopsy	<1 h	10 CFU/mL	10-10,000 CFU/mL	92.5% (culture) 100% (histology)	95.4% (culture) 98.8% (histology)	[68]
Escherichia coli O157:H7	Culture	-	2.2 x 10^5 copies/µL DNA	2.2 x 10^5 – 2.2 x 10^7 copies/µL	-	-	[69]
Mycobacterium tuberculosis	Respiratory samples	15 min post-amplification	4.5 x 10^{10} copies/µL DNA	-	84.7% (*AccuProbe®)*	100% (*AccuProbe®)*	[63-65]
Acinetobacter baumannii	Culture	~ 4 h post-amplification	1.07 x 10^7 copies/µL DNA	1.07 x 10^7 – 3.57x10^{10} copies/µL	-	-	[74]
Salmonella enterica serovar Typhi	Culture	~ 1 hr post-amplification	10^3 CFU/mL	10^3-10^5 CFU/ml	-	-	[75]
Pseudomonas aeruginosa, Staphylococcus aureus, Staphylococcus epidermidis, Kelbsiella pneumoniae, Serratia marcescens and *Bacillus cereus*	Spiked platelet concentrates	0.8 hr post-amplification	~3 x 10^6 copies/µL DNA	~3 x 10^6 – 6 x 10^9 copies/µL	-	-	[71]

Pathogens of interest	Sample type	Analysis time	Detection limit	Working range	Sensitivity	Specificity	References
Salmonella enterica serovar Typhimurium	Culture	~8 h	~3.6 x 10^{11} copies/µL	-	-	-	[67, 70]
Staphylococcus aureus (methicillin-resistant)	Blood culture, urine, respiratory samples, wound swabs, pus and body fluids	~ 20 min post-amplification	~8 x 10^{10} copies/µL DNA	-	97.14% (Culture)	91.89% (Culture)	[66]
HIV-1 and *Treponema pallidum*	Serum	~5h post-amplification	10 copies/µL DNA	-	100% (ELISA & real-time PCR)	100% (ELISA & real-time PCR)	[73]
HPV-16 and HPV-18	Ectocervical/endocervical cell samples	20 min post-amplification	8.4 x 10^{7} copies/µL DNA	8.4 x 10^{7} – 8.4 x 10^{11} copies/µL	95% (real-time PCR)	90% (real-time PCR)	[72]
Influenza H1N1 virus	Nucleic acids	2.5 hr	2.58 x 10^{8} copies/µL RNA	2.58 x 10^{8} – 2.58 x 10^{9} copies/µL	-	-	[76, 77]

2.6 Emerging biosensors without nucleic acid amplification

While several strategies have been presented for the detection of nucleic acid amplification products, it is possible to detect pathogens without the use of these amplification processes. Non-functionalized gold nanoparticles can use the native surface charges of nanoparticles and bacteria for producing a color change. Functionalizing gold nanoparticles with nucleic acids, proteins, or small molecules can facilitate the detection of unamplified nucleic acids, lipopolysaccharides, or even whole cells.

2.6.1 Non-functionalized gold nanoparticles for pathogen detection

As-synthesized gold nanoparticles can exert surface charges and hence be used directly for detection without specific functionalization. Most of the studies that incorporate this strategy depend on the color change of gold nanoparticles from red to blue due to their electrostatic aggregation behavior.

Two common coatings are present on as-synthesized nanoparticles: citrate for providing a net negative charge and CTAB for providing a net positive charge. Another approach is to modulate the growth conditions of nanoparticles, which controls the size and morphology of the nanoparticles and hence their color.

Citrate capped nanoparticles have been used for the detection of nucleic acids in a manner similar to the illustration in Figure 1 a, where nanoparticles aggregate when the target is present. This approach has been implemented in the detection of hepatitis C virus RNA by designing probes targeting the 5'UTR region and using them with 15 nm gold nanoparticles [78]. Another approach is to design aptamers for specific targets and allow them to adsorb on the surface of gold nanoparticles. In the presence of the target, the aptamers get stripped from the surface of gold nanoparticles and bind to the target, which destabilizes the gold nanoparticles in high salt conditions. This strategy has been applied for the detection of *E. coli* O157:H7 and *S.* Typhimurium, where aptamers were selected against these bacteria and adsorbed on 15 nm gold nanoparticles. The specificity of the assay was confirmed by testing the interaction with seven other species of bacteria and a significant response was observed only when the desired target was present [79].

In addition to nucleic acids and whole cells, citrate-capped nanoparticles have also been used to detect proteins. β-Lactamases are bacterial enzymes that cleave β-lactam antibiotics and hence render them ineffective towards bacterial infections. The detection of β-lactamase activity can assist in designing better antibiotics. *Enterobacter cloacae* is a pathogen responsible for producing class C P99 β-lactamase, which can cleave cephalosporin derivatives and produce products with free thiols and positively charged amino groups. These products can replace some citrate ions on the surface of gold nanoparticles and then lead to their aggregation due to electrostatic interactions. With the help of 16 nm citrate capped gold nanoparticles, P99 β-lactamase could be detected [80]. The same method has also been used for detection of class A β-lactamases as well, which are produced by *E. coli*, *B. cereus* and *K. pneumoniae* [81]. Another notorious enzyme is the immunoglobulin A1 protease (IgA1P) produced by *Streptococcus pneumoniae,* which allows the bacterium to infect the lower respiratory tract, ear, or bloodstream and lead to diseases such as pneumonia, otitis media, sepsis, and meningitis. The protease cleaves human IgA1 and coats the bacterium with Fab fragments to act as a shield against the immune response and also to assist invasion into epithelial cells. Thus, IgA1P

serves as a promising antibacterial target to curb the infection. The detection of IgA1P has been achieved using IgA1 and 20 nm citrate-adsorbed gold nanoparticles. In the presence of IgA1P, the IgA1 is cleaved to produce positively charged Fab regions, which is detected by the aggregation of the anionic nanoparticles. The specificity of the assay was confirmed by the lack of response in the presence of IgA2, which is not cleaved by IgA1P [82].

CTAB-coated gold nanoparticles have been used for the detection of DNA as well as whole cells. When detecting DNA, the idea is similar to Figure 1 c, except instead of using thiolated probes, the probes are electrostatically adsorbed. Detection of HIV-1 and *B. antharcis* has been possible by designing probes to target the U5 long terminal repeat sequence of HIV-1 and cryptic protein and protective antigen precursor genes of *B. anthracis.* The probes were adsorbed on 16-30 nm gold nanoparticles for obtaining a color change from red to purple [83]. Whole cell detection has been achieved using CTAB-coated gold nanostars with a size range of 31 nm to 113 nm [9]. Here, the positive charges on gold nanostars interact with the negative charges on bacterial cell walls presented by teichoic acids, lipopolysaccharides, and phospholipids. This strategy produced a unique degree of color change for different species of bacteria when testing the ocular pathogens: *S. aureus*, *Achromobacter xylosoxidans*, *Delftia acidovorans*, and *Stenotrophomonas maltophilia*. An accuracy of 99% was obtained for identifying randomized samples of the four bacteria [84].

ELISA has been used in a variety of applications for highly specific and sensitive detection of target molecules. Typically, a color change is obtained at the end of the assay because of enzymatic conversion of the substrate into a colored molecule, which is then detected by a spectrophotometer. The color change could also be obtained using growth of gold nanoparticles such that it would be visually detectable. In the absence of target molecules, a high concentration of hydrogen peroxide is present, which rapidly reduces gold ions and forms spherical non-aggregated nanoparticles, producing a red color. In the presence of target molecules, hydrogen peroxide is consumed by the enzyme and hence growth of the gold nanoparticles is slower, which results in aggregated particles with a blue color. This approach has been used for detection of HIV-1 capsid antigen p24 with the naked eye. This method presents an extremely sensitive assay, which performs better than existing established methods based on nucleic acid detection. [85].

Eliminating nucleic acid amplification provides major advantages in the required analysis time and equipment. Specifically, the use of non-functionalized nanoparticles simplifies the synthesis of gold nanoparticles and thus the entire assay. As compared to conventional methods for pathogen detection, the non-functionalized gold nanoparticles provide a dramatic colorimetric output, which can often be visualized by the naked eye. The most important limitation of this strategy is that various interferents from the environment can cause aggregation of nanoparticles and hence a false positive response, since the target analyte is often very general. The studies using non-functionalized gold nanoparticles for detection have been summarized in Table 3.

Table 3: Non-functionalized gold nanoparticles for detection without nucleic acid amplification

Pathogens of interest	**Sample type**	**Analysis time**	**Detection limit**	**Working range**	**References**
Escherichia coli, Bacillus cereus and *Klebsiella pneumoniae*	Culture	~ 1 hr	~ 10^8 CFU/mL	-	[81]
Enterobacter cloacae	β-lactamase	~ 35 min	16 fmol/mL of P99 β-lactamase	15 – 80 fmol/mL	[80]
Escherichia coli O157:H7 and *Salmonella enterica* serovar Typhimurium	Culture	20 min	10^5 CFU/mL	10^5 – 10^8 CFU/mL	[79]
Streptococcus pneumoniae	Culture	~ 20 hr	-	-	[82]
Staphylococcus aureus, Achromobacter xylosoxidans, Delftia acidovorans, Stenotrophomonas maltophilia	Culture	~ 5 min	~ 1.5 x 10^6 CFU/mL	-	[9, 84]
Hepatitis C virus[a]	Serum	30 min	2.5 copies/µL RNA	~ 2.5 – 100 copies/µL	[78]
HIV-1 and *Bacillus anthracis*	Nucleic acids	~ 30 min	6 x 10^7 copies/µL DNA	6 x 10^7 – 3 x 10^9 copies/µL	[83]
HIV-1	Serum	~ 21 hr	10^{-15} g/µL capsid antigen p24	10^{-15} – 10^{-18} g/µL	[85]

[a]Sensitivity 92% and specificity 88.9% compared to RT-PCR

2.6.2 Gold nanoparticles functionalized with nucleic acids

Unamplified nucleic acids can be detected by functionalizing gold nanoparticles with specific thiolated probes. Three main strategies have been employed for implementing this method: functionalizing with a single probe (Figure 1 b), functionalizing with two probes (Figure 1 c), and the use of DNA enzymes (DNAzymes). As compared to amplification-based methods, these assays are simpler and faster.

A thiolated nucleic acid probe has been designed for the detection of *Mycobacterium* spp. by targeting the 16s-23s DNA region of mycobacterial species. The probe was immobilized on 15-20 nm gold nanoparticles and the presence of target DNA stabilized the nanoparticles upon addition of HCl (Figure 1 a). Specificity of the assay was confirmed by comparing the response from non-mycobacterial species [86]. Detection of *E. coli* genomic DNA has been possible by targeting the *malB* gene and immobilizing the obtained probe on 20 nm gold nanoparticles. In this assay, the enzymatic degradation of DNA before hybridization improved the detection limit of the assay by 5 times. Specificity was confirmed by comparing the response to other pathogenic bacteria [87].

Aggregation of nanoparticles by target DNA can also be used for the colorimetric detection if a pair of appropriate probes is designed (Figure 1 c). One example of this approach is the detection of Kaposi's sarcoma-associated herpesvirus (KSHV). KSHV is responsible for Karposi's sarcoma, an infectious cancer most commonly occurring in HIV positive patients. The detection of KSHV is challenging because several other diseases present similar symptoms and histopathological features. One such confounding disease is bacillary angiomatosis, which can be caused by *Bartonella quintana* and *Bartonella henselae.* Thus, distinction between these pathogens is necessary and has been achieved by designing pairs of thiolated oligonucleotide probes targeting the DNA that codes for vCyclin in KSHV and conserved regions of *Bartonella* strains. The probes for KSHV and *Bartonella* were then immobilized on 15 nm gold and 20 nm silver nanoparticles respectively to obtain different color changes [88]. Another study has demonstrated the detection of genomic DNA of *Salmonella enterica* by the use of probes targeting the *invA* gene. Here, the mechanism of detection was unclear because detection of genomic DNA was possible using both one-probe and two-probe approaches. Additionally, the thiolated probes were first incubated with the genomic DNA and then incubated

with 15 nm gold nanoparticles. In this study, the absence of target DNA allows gold nanoparticles to maintain stability, which is most likely because of high coverage of the probe molecules on the surface of the nanoparticles. In the presence of the target, the probes hybridize with the target DNA and hence, are probably unable to cover the gold nanoparticles sufficiently to stabilize them. This leads to the aggregation of gold nanoparticles and hence detection of the target DNA. This assay allowed the detection of dsDNA at room temperature [89].

DNAzymes are nucleic acids that can catalyze the cleavage of other nucleic acids with multiple turnovers and hence are capable of providing amplification in an assay. Multicomponent nucleic acid enzyme (MNAzyme) is a type of DNAzyme that can be designed to perform catalysis specifically in the presence of the target DNA. Gold nanoparticle cross-linkers can be used as MNAzyme substrates such that aggregation of gold nanoparticles can be modulated by the presence of target DNA. This approach has been applied for the detection of AF-1 and genetic sequences from *Neisseria gonorrhoeae, Treponema pallidum, Plasmodium falciparum,* and HBV. In the absence of target DNA, the cross-linker remained intact and led to aggregation of 13 nm gold nanoparticles. Designing the appropriate MNAzymes allows this method to detect multiple targets, which is useful for diagnosing co-infections [90]. Another example of DNAzymes is the detection of dengue viruses. Dengue viruses cause periodic explosive epidemics and can lead to 50-100 million infections annually. These viruses are typically carried by mosquitoes and can lead to dengue fever or potentially fatal dengue hemorrhagic fever. DNAzymes have been designed and immobilized on 15 nm gold nanoparticles to cleave dengue virus RNA in the presence of magnesium ions. The cleaved RNA leads to aggregation of gold nanoparticles in the presence of salt and heat [91].

Functionalizing gold nanoparticles with DNAzymes has allowed the incorporation of signal amplification during detection and hence provided excellent detection limits. The major limitation of this approach has been the requirement of nucleic acid extraction, since it can increase the assay time by several hours. The studies employing gold nanoparticles functionalized with nucleic acids are summarized in Table 4.

Table 4: Gold nanoparticles functionalized with nucleic acids

Pathogens of interest	Sample type	Analysis time	Detection limit	Working range	References
Mycobacterium spp.[a]	Goat faeces	~ 15 min post-extraction	18.8 ng/µL mycobacterial DNA	18.8 – 1,200 ng/µL	[86]
Escherichia coli[b]	Spiked urine	< 30 min post-extraction	5.4 ng/µL genomic DNA	5.4 – 43 ng/µL	[87]
Kaposi's sarcoma-associated herpesvirus and *Bartonella*	Nucleic acids	2 h post-extraction	1 x 10^9 copies/µL DNA	1-10 x 10^9 copies/µL	[88]
Neisseria gonorrhoeae, Treponema pallidum, Plasmodium falciparum and hepatitis B virus	Nucleic acids	~ 1.5 h post-extraction	3 x 10^7 copies/µL model DNA	3 x 10^7 – 6 x 10^8 copies/µL	[90]
Salmonella enterica	Nucleic acids	~ 15 min post-extraction	2.2 x 10^4 copies/µL genomic DNA	2.2 x 10^4 – 3.8 x 10^5 copies/µL	[89]
Dengue virus	Culture	5 min post-extraction	4 x 10^7 copies/µL RNA	4 x 10^7 – 4 x 10^{12} copies/µL	[91]

[a]Sensitivity 87.5%, specificity 100% (real-time PCR). [b]specificity 100% (PCR)

2.6.3 Gold nanoparticles functionalized with proteins

Gold nanoparticles are often functionalized with antibodies that can target specific sites on the surface of pathogens. This antibody-antigen association leads to aggregation of gold nanoparticles around the pathogen of interest and can thus generate a colorimetric response (Figure 3). Another common approach is to use aggregation of antibody-functionalized gold nanoparticles as a labelling method followed by amplification of the signal using the growth of silver or gold around the initial seeds. Finally, these nanoparticles have been widely implemented in an ICS format as a replacement for ELISA.

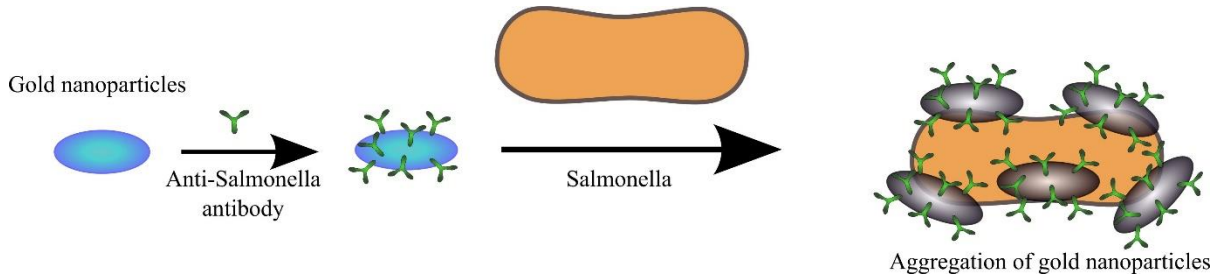

Figure 3: Gold nanoparticle functionalized with antibodies aggregate around bacteria and lead to color change, adapted from [92]**.**

The aggregation of gold nanoparticles around bacteria has been used for the detection of multi-drug resistant *S.* Typhimurium DT104. The bacterium presents a great challenge in health care because of its persistent survival. The detection was possible by functionalizing 30 nm popcorn-shaped gold nanoparticles with monoclonal M3038 antibody against *S.* Typhimurium DT104. The response was specific to the drug resistant *S.* Typhimurium as compared to other *Salmonella* or *E. coli* strains. [93].

Colorimetric response from the aggregation of nanoparticles can often have insufficient sensitivity. Thus, the growth of gold or silver is used for signal amplification. This strategy has been deployed for the detection of protozoa and bacteria. The detection of intestinal protozoan *Giardia lamblia* is possible by first separating it from solution using centrifuge filtration (0.45 µm pore size) and then incubating it with a solution of anti-*G. lamblia* antibody-coated 15 nm gold nanoparticles. The unbound gold nanoparticles are removed by centrifuge filtration followed by the addition of a gold growth solution, which changes color depending on the concentration of gold nanoparticles. Since the assay uses centrifugation for concentration, it is possible to implement this assay in large sample volumes [94]. The filtration approach can be combined with magnetic nanoparticles to allow detection in complex media. This approach has been used for the detection of *S. aureus* in milk. Magnetic nanoparticles were first coated with bovine serum albumin (BSA) and then with 10 nm gold nanoparticles. Anti-*S. aureus* antibodies were then adsorbed on the surface of gold nanoparticles. This hybrid system of nanoparticles was incubated with the sample contaminated with bacteria, magnetically separated, and then filtered through a 0.8 µm cellulose acetate membrane. The magnetic separation retained all the nanoparticles and bacteria that were attached to the nanoparticles. The filter retained bacteria and attached nanoparticles while allowing free nanoparticles to pass through.

Finally, the color of nanoparticles on the filter was enhanced by a gold growth solution. The specificity of the assay was confirmed by comparing the response to samples contaminated with other pathogenic bacteria [95].

In addition to nucleic acid detection, gold label silver staining has also been implemented for antibody-functionalized nanoparticles. This method has been used for the detection of *Campylobacter jejuni* by using monoclonal antibodies against the bacterium and coating them on 18 nm gold nanoparticles. In order to implement this method, a glass slide functionalized with streptavidin is first conjugated with biotinylated polyclonal antibodies against *C. jejuni*. This is followed by the addition of the bacteria and then the functionalized gold nanoparticles. Then, the gold growth solution is added followed by silver enhancement. The silver enhancement is stopped by immersing the slide in deionized water. Using this method, specificity was confirmed by comparing the response obtained from *C. jejuni* to that of *Salmonella enteritidis* and *E. coli* [96].

Immobilization of antibodies has also been extended to nitrocellulose paper, which is followed by the addition of the target and then the protein-functionalized gold nanoparticles. This has been used for the detection of Vi antigen of *S.* Typhi by adsorbing anti-*Salmonella* antibodies on 30 nm gold nanoparticles. This assay has a potential of detecting typhoid early because it can not only detect the whole bacterial cell, but also just the Vi antigen [97]. Similarly, ICS-based assays have been developed for the detection of *P. aeruginosa* and *S. aureus* by using polyclonal antibodies against the bacteria and conjugating them to ~20 nm gold nanoparticles. The test line in these assays had monoclonal antibodies against the bacteria and produced a red color in the presence of the target bacteria [98]. Another example of ICS is the detection of toxic metabolites produced by the microscopic fungi *Aspergillus*. These metabolites, such as ochratoxin A, can lead to nephrotoxicity, hepatotoxicity, and carcinogenicity in humans. In this scenario, a competitive assay was developed by immobilizing a BSA conjugate of ochratoxin A on the test zone and immobilizing monoclonal antibodies against ochratoxin A on 27 nm gold nanoparticles. In the presence of target ochratoxin A, gold nanoparticles do not bind to the test line and hence there is no color [99].

A unique strategy using switchable linkers has been deployed for detection by functionalizing gold nanoparticles with streptavidin. The switchable linker specifically binds to the target of interest and also contains biotin, which would lead to aggregation of streptavidin-coated gold nanoparticles.

Changing the concentration of the target will change the number of free switchable linkers available and hence change the degree of aggregation of gold nanoparticles. If there is a high concentration of the switchable crosslinker, they occupy all the binding sites on the gold nanoparticles and prevent crosslinking. Therefore, there is a specific concentration of crosslinker and target within which the color changes. When biotinylated anti-*E. coli* polyclonal antibodies are used as the switchable crosslinker, *E. coli* can be easily detected at low concentrations [100].

Antibody-labeled gold nanoparticles have facilitated the detection of whole cells, which minimizes the efforts required for sample preparation and yet provides faster response compared to culture-based methods. As compared to ELISA, methods employing functionalized gold nanoparticles immobilized on paper substrates (eg. ICS) are simpler to deploy in the field since the strips can be easily transported and require minimal training. Two major limitations exist for gold nanoparticles functionalized by proteins: the assays often require antibodies for specific targets, which can increase the cost of the assay, and many assays require centrifugation or filtration, which is often only available in laboratories. The studies that utilize gold nanoparticles functionalized with proteins have been summarized in Table 5.

Table 5: Gold nanoparticles functionalized with proteins

Pathogens of interest	Sample type	Analysis time	Detection limit	Working range	References
Campylobacter jejuni	Culture	Overnight	10^6 CFU/mL	$10^6 – 10^9$ CFU/mL	[96]
Salmonella enterica serovar Typhimurium DT104	Culture	< 5 min	10^3 CFU/mL	$10^3 – 10^4$ CFU/mL	[93]
Pseudomonas aeruginosa and *Staphylococcus aureus*	Culture	3 min	5×10^2 CFU/mL	$5 \times 10^2 – 5 \times 10^3$ CFU/mL	[98]
Salmonella enterica serovar Typhi	Spiked blood	~ 1 h	10^2 CFU/mL	$10^2 – 10^7$ CFU/mL	[97]
Escherichia coli	Culture	-	10^2 CFU/mL	$10^2 – 10^6$ CFU/mL	[100]
Staphylococcus aureus	Spiked milk	40 min	1.5×10^7 CFU/mL (milk) 1.5×10^5 CFU/mL (PBS)	$1.5 \times 10^7 – 1.5 \times 10^8$ CFU/mL (milk) $1.5 \times 10^5 – 1.5 \times 10^8$ CFU/mL (PBS)	[95]
Aspergillus	Plant extracts	10 min	5 ng/mL ochratoxin A	5 – 50 ng/mL	[99]
Giardia lamblia cysts	Culture	-	1.088×10^3 cells/mL	$10^3 – 10^4$ cells/mL	[94]

Sensitivity and specificity were not reported for any of the studies

2.6.4 Gold nanoparticles functionalized with small molecules

Besides proteins and nucleic acids, small molecules can also be used for detection of pathogens by exploiting the electrostatic, covalent, or receptor-mediated interactions. In a typical case, the small molecule is immobilized on gold nanoparticles, which allows their aggregation around the pathogen of interest and hence leads to a color change. Electrostatic interactions have been possible by modifying the surface of nanoparticles to make them cationic. Covalent interactions have been exploited by using phenylboronic acid and its ability to bind to diol groups in bacterial polysaccharides. Receptor-mediated interactions are possible by functionalizing gold nanoparticles with sialic acids, which exhibit binding to haemagglutinin present on the surface of viruses.

Cationic nanoparticles have been used for the detection of lipopolysaccharides and whole cells. Lipopolysaccharides are present on the surface of Gram-negative bacteria and provide a high negative charge to these surfaces. The detection of lipopolysaccharides is important because they can lead to sepsis or septic shock. When gold nanoparticles are modified with cysteamine, they aggregate in the presence of lipopolysaccharides and hence allow their detection as compared to other biological anions. These nanoparticles could also interact with lipopolysaccharides on the surface of *E. coli* 055:B5, which was confirmed by observing their aggregation using transmission electron microscopy [101]. This modification has also been used for colorimetric detection of *E. coli* O157:H7 [102]. Whole cells can be detected by using cationic gold nanoparticles obtained by using a variety of small molecules with varying alkyl chain lengths and hydrophobicity. This approach was used for detecting *E. coli* XL1. An enzyme (β-galactosidase) is first adsorbed on the gold nanoparticles by electrostatic interactions. Then, in the presence of *E. coli*, gold nanoparticles aggregate around the bacteria and release the enzyme, which catalyzes the hydrolysis of chlorophenol red β-D-galactopyranoside and causes a color change [103].

Covalent interactions have been used for the detection of a variety of bacteria. In one of the studies involving *E. coli* O157:H7, gold nanoparticles were first coated with platinum and then functionalized using 4-mercaptophenylboronic acid. The platinum on the surface of gold nanoparticles acts as a peroxidase mimic and can catalyze oxidation of 3,3’,5,5’-tetramethylbenzidine (TMB) by hydrogen peroxide. Thus, when functionalized gold nanoparticles are mixed with *E. coli* O157:H7, they aggregate around the bacteria. After purification by centrifugation, the bound nanoparticles were

mixed with hydrogen peroxide and TMB, which led to a color change depending on the concentration of bacteria present. The specificity of this method was shown by demonstrating the lack of response from *S. aureus* [104]. In contrast to this study [104], another group functionalized 13 nm gold nanoparticles with dithiodialiphatic acid-3-aminophenylboronic acid and achieved the detection of *S. aureus.* In this case, the functionalized gold nanoparticles were allowed to interact with *S. aureus* and then the bacteria were separated by centrifugation. The separated bacteria had a red color characteristic of the gold nanoparticles. The specificity was confirmed by comparing the response from *S. aureus* to that from *E. coli*, *Bacilus subtilis*, and *Enterobacter cloacae.* The difference between the two studies is most likely because of the different configurations of phenylboronic acid used and also because of additional functionalization of gold nanoparticle with a pentapeptide for stabilization in the detection of *S. aureus* [105].

In addition to bacteria, influenza viruses can be detected using gold nanoparticles functionalized with sialic acids. Influenza viruses present haemagglutinin on the surface, which recognizes sialic acids on host cells for infecting the cells. Haemagglutinin has been used as a target for detecting viruses because they can facilitate aggregation of functionalized gold nanoparticles. To achieve detection, 16 nm gold nanoparticles were functionalized with trivalent α2,6-thio-linked sialic acid and mixed with human influenza virus X31 (H3N2) to observe a color change. This method was able to distinguish between human influenza virus and avian influenza virus (H5N1) because the human strain binds to α2,6 residues, whereas the avian strain binds to α2,3 residues. Detection was also possible in influenza allantoic fluid, which demonstrates the possibility of detection in clinical samples [106]. A similar method has been employed for the detection of influenza B/Victoria and influenza B/Yamagata, where 20 nm gold nanoparticles were synthesized and stabilized using sialic acid using a one-pot method [107].

Gold nanoparticles modified with small molecules have typically provided some of the fastest response times while maintaining excellent detection limits. Small molecules are typically cheaper than proteins or nucleic acids and hence the overall cost of the assay is lower. The major limitation of this approach is that small molecules target general components of the pathogens and hence cross-reactivity is likely. Thus, the assay might provide a false positive response if a closely related

pathogen was present instead of the targeted one. All the studies using gold nanoparticles functionalized with small molecules have been summarized in Table 6.

Table 6: Gold nanoparticles functionalized with small molecules

Pathogens of interest	Sample type	Analysis time	Detection limit	Working range	Small molecule used	References
Escherichia coli XL1	Culture	~ 10 min	10^2 CFU/mL (solution) 10^4 CFU/mL (test strip)	10^2 – 10^7 CFU/mL (solution) 10^4 – 10^8 CFU/mL (test strip)	Several different cationic molecules	[103]
Staphylococcus aureus	Spiked milk, urine, lung fluid	~ 2 h	50 CFU/mL	5 x 10^2 – 5 x 10^6 CFU/mL	dithiodialiphatic acid-3-aminophenylboronic acid	[105]
Escherichia coli O157:H7	Culture	< 40 min	7 CFU/mL	7 – 6 x 10^6 CFU/mL	4-mercaptophenylboronic acid	[102, 104]
Escherichia coli 055:B5	Lipopolysaccharides	~ 5 min	330 fmol/mL lipopolysaccharides	5 – 90 pmol/mL	cysteamine	[101]
Human influenza virus X31 (H3N2)	Allantoic fluid	~30 min	~1 µg/mL virus	~1 – 2 µg/mL	trivalent α2,6-thio-linked sialic acid	[106]
Influenza B/Victoria and Influenza B/Yamagata	Culture	~ 10 min	0.156 vol% dilution of Hemagglutination assay titer 512 virus	0.156 – 1.25 vol%	sialic acid (N-acetylneuraminic acid)	[107]

Sensitivity and specificity were not reported for any of the studies

2.7 Comparison of gold nanoparticles to conventional methods

Conventional and gold nanoparticle-based pathogen detection assays can be compared using a variety of metrics reflecting assay performance. The main criteria by which we will be evaluating the

advantages and disadvantages of the previously mentioned assays are time, limit of detection, specificity, technical complexity, and specific limitations. These parameters have been grouped by detection principle, and are summarized in Table 7.

2.7.1 Analysis Time

Analysis times were generally much longer for conventional methods than those using gold nanoparticles. Colony counting was by far the most time-consuming method, due to the need for colonies to be grown on selective media prior to visual identification [108]. Of the organisms presented, the longest culture time was reported for *Campylobacter*, where culture methods require 4 – 9 days for negative results and 14 – 16 days for positive confirmation [35, 109]. In contrast, protein-functionalized gold nanoparticles have been used to detect *Campylobacter* following overnight incubation [96].

The fastest conventional methods are typically PCR-based assays, which can deliver results in 5 – 24 hours, depending on the mode of analysis and pathogen of interest [31]. This processing time is heavily dependent on the time required for sample enrichment and nucleic acid amplification, and is related to the detection limit [110, 111]. Amplification-based techniques with gold nanoparticles can improve upon conventional PCR-based methods by generating rapid color changes in response to pathogens, thereby simplifying the detection of target amplicon, and reducing the time required to obtain a result. Furthermore, emerging biosensors which do not involve the time-consuming step of nucleic acid amplification reported the shortest processing times with several groups reporting results within an hour (Table 3, 5, and 6).

2.7.2 Limit of detection

Despite advances in analysis time, reducing detection limits remains a key challenge for gold nanoparticle-based assays. Conventional methods of colony counting and PCR are typically capable of detecting pathogens at concentrations in the range of 1 CFU/mL or 10 copies/µL DNA (Velusamy et al. 2010; Lazcka et al. 2007). Nanoparticle-based methods reported a wide variety of detection limits, ranging from $7 – 10^8$ CFU/ml or $10^1 – 3 \times 10^{11}$ copies/µL DNA depending on the target [67, 70, 73]. While some groups reported detection limits much higher than those for conventional

methods, particularly those assays without target amplification, other nanoparticle-based assays were comparable in terms of detection limit.

2.7.3 Specificity

Specificity of colony counting methods is dependent on the ability to selectively isolate and culture particular pathogen strains. Due to the use of morphological and physiological characteristics for pathogen identification, specificity may be lower for closely related strains which are less distinguishable based on phenotypic traits. Similarly, immunological assays may suffer from low specificity if antibodies are selected for target analytes that are present on more than one pathogen variety. However, with proper antibody selection and species enrichment, immunological assays have good specificity. PCR-based methods achieve specificity by targeting nucleic acid sequences with selected primers and/or probes. Excellent assay specificity can be achieved when the sequences targeted by PCR are unique to the strain of interest since single base pair mismatches can often be discriminated.

Specificity of gold nanoparticle-based assays is determined by either nucleic acids or antibodies in most cases. Thus, the specificity of these assays is comparable to the methods based on PCR and immunological assays. In the case of small molecule modified nanoparticles and non-functionalized nanoparticles, the assays detect general targets and hence, the specificity suffers. One method for overcoming this specificity challenge is to adopt a “chemical nose” type system, where each analyte presents a unique set of responses and hence can be distinguished [84, 103]. The limitation of a “chemical nose” approach is that the system needs to be trained for each analyte of interest before attempting the detection.

2.7.4 Technical requirements

Procedures for bacterial plating, colony counting, and species identification vary according to the target organism. Generally, the first step involves serial dilution of a sample or automatic plating [108] onto agar plates with selective media. Plates must then be incubated to allow for colony growth to a visually detectable level. This incubation period is dependent on the bacterial species and growth conditions. The number of resulting colonies is counted to infer pathogen concentration in the original sample. This is a time consuming step which can be done by hand or using automated systems [108].

Pathogen identity is determined using various morphological and biochemical tests. The colony counting method is good for workers in microbiology laboratories due to its reliability and use of common laboratory equipment and reagents, however the laborious process is not adequate for rapid diagnostics and requires specialized training.

Immunological assays rely primarily on specificity of antibodies to antigens from the target pathogen. A wide variety of characterized antibodies and kits are available for most pathogens and complexity is dependent on the particular detection strategy [108]. While common immunological methods (e.g. ELISA) do not require specialized lab equipment, they typically require some form of sample enrichment due to decreased sensitivity [109].

PCR-based methods are typically less laborious and time-consuming than previously mentioned conventional methods [31]. Specific DNA or RNA sequences amplified using PCR can be subsequently visualized using a number of ways, depending on the type of PCR. The most common methods are sample separation using gel-electrophoresis and fluorescence observation during real-time PCR with probes. Primer and probe selection is dependent on the target pathogen being investigated. While traditional PCR-based methods require access to a thermal cycler, advances in lab-on-a-chip and isothermal amplification techniques are reducing this barrier to out-of-laboratory field applications.

Some of the main aims of nanoparticle assays are to simplify assay procedure, reduce the need for complex lab equipment, and minimize labor. Nucleic acid amplification-based techniques require either thermal cycling or isothermal amplification equipment which is a significant issue for point-of-care or field applications. However, emerging amplification-free techniques require only basic laboratory equipment. In these cases, the primary technical requirement remains the ability to extract and purify the target analyte (i.e. nucleic acids, proteins, or whole cells) from the sample.

Table 7: Comparing conventional and nanoparticle-based assays

Category	Detection principle	Analysis time	Detection limit	Specificity	Technical requirements	Limitations	References
Conventional	Colony counting	1 - 16 days	10^0-10^1 CFU/mL	Good	Basic microbiology lab equipment and training	Only culturable strains are detected	[108, 109]
	Immunological assay	1 - 5 days	10^3-10^6 CFU/mL	Good	Specific antibodies for pathogen	Sample enrichment is often necessary for high sensitivity	[31, 108]
	PCR	5 - 48 hours	< 10 copies/µL	Excellent	Thermal cycling or isothermal amplification, gel electrophoresis equipment	Distinguishing live and dead cells, presence of inhibitors in complex media	[31, 110, 112]
Nucleic acid amplification-based gold nanoparticle assays	Non-functionalized	3 - 8 hours	2×10^1 – 3×10^9 copies/µL DNA	Excellent	Thermal cycling or isothermal amplification equipment	Need to design specific probes for every pathogen of interest	[38, 54, 56]
	Functionalized (nucleic acid)	1.5 - 8 hours	10^1 – 3×10^{11} copies/µL DNA	Excellent	Thermal cycling or isothermal amplification equipment	Functionalization requires purification, can affect stability and yield of nanoparticles	[67, 70, 73]
Gold nanoparticle assays without nucleic acid amplification	Non-functionalized	5 minutes - 21 hours	$2.5 – 6 \times 10^7$ copies/µL RNA/DNA 10^5 – 10^8 CFU/mL	Good	Minimal equipment	Nanoparticle stability in detection media can be limited	[78, 79, 81, 83]
	Functionalized (nucleic acid)	5 minutes – 2 hours	2.2×10^4 - 1×10^9 copies/µL DNA	Excellent	Basic lab equpiment for nucleic acid extraction	Nucleic acid extraction can consume considerable time compared to assay time	[88, 89, 91]
	Functionalized (protein)	3 minutes - overnight	10^2 – 1.5×10^7 CFU/mL	Good	Often need filtration or centrifugation equipment	Throughput limited by filtration/centrifugation	[95-98]
	Functionali	5	$7 – 10^2$	Poor	Minimal	Cross-reactivity is	[103,

	zed (small molecule)	minutes – 2 hours	CFU/mL	equipment	often present	104]

2.8 Conclusions

Gold nanoparticles with a variety of surface features have been used for the colorimetric detection of pathogens either by detecting nucleic acids, surface proteins, or whole cells. While the majority of the literature has focused on the use of gold nanoparticles as a replacement for gel electrophoresis after nucleic acid amplification, there is a growing body of work in detecting unamplified targets. There is a growing drive towards developing methods or devices that could be used at the point-of-care or in the field by providing a simple visual output. Overall, although gold nanoparticles have facilitated the development of simple and sensitive assays that are replacing conventional methods of pathogen detection, current technologies are not yet ready to be translated directly to the point-of-care or field use because the current methods require extensive sample processing before analysis. Additionally, current biosensors with gold nanoparticles suffer from lower sensitivity when complex media are involved because of non-specific adsorption, which can be mitigated in the future by modifying the surface of gold nanoparticles with non-fouling coatings.

This chapter highlights that non-functionalized gold nanoparticles hold great potential because of their ability to provide a rapid response and detect a variety of targets. Yet, very few studies have explored non-functionalized nanoparticles for pathogen detection. In the following chapters, we will exploit the dependence of colorimetric properties of gold nanoparticles on their size, shape, and aggregation state for the detection and identification of pathogenic bacteria.

Chapter 3

CTAB-coated gold nanostars for the colorimetric detection of *Staphylococcus aureus*

3.1 Summary

Rapid detection of pathogenic bacteria is challenging because conventional methods require long incubation times. Nanoparticles have the potential to detect pathogens before they can cause an infection. Gold nanostars have recently been used for colorimetric biosensors but they typically require surface modification with antibodies or aptamers for cellular detection. Here, CTAB-coated gold nanostars have been used to rapidly (<5 min) detect infective doses of a model Gram-positive pathogen *Staphylococcus aureus* by an instrument-free colorimetric method. Varying the amounts of gold nanoseed precursor and surfactant can tune the size and degree of branching of gold nanostars as studied here by transmission electron microscopy. The size and morphology of gold nanostars determine the degree and rate of color change in the presence of *S. aureus*. The optimal formulation achieved maximum color contrast in the presence of *S. aureus* and produced a selective response in comparison to polystyrene microparticles and liposomes. These gold nanostars were characterized using UV-Visible spectroscopy to monitor changes in their surface plasmon resonance peaks. The visual color change was also quantified over time by measuring the RGB components of the pixels in the digital images of gold nanostar solutions. CTAB-coated gold nanostars serve as a promising material for simple and rapid detection of pathogens.

3.2 Introduction

Gold nanostars are an interesting class of materials because of their excellent performance in colorimetric biosensors [93, 113-115], surface enhanced Raman spectroscopy [116-122], imaging and therapy [123, 124], as well as recently in solar cell power conversion [125]. The optical and electrical characteristics of gold nanostars are governed by their size and degree of branching [122, 126]. Hence, control over these parameters is essential and has previously been demonstrated using methods such as seed-free growth [127], the use of poly(vinylpyrrolidine) [122, 128, 129], and even surfactant-free synthesis [123], but a systematic study of seed-mediated synthesis assisted by the

surfactant, cetyltrimethylammonium bromide (CTAB) is lacking. The use of nanoseed precursor and surfactant offers the opportunity to control the size and degree of branching of the nanostars using these two simple parameters. The morphology of nanostars determines the peak wavelength of light absorption and hence the color of gold nanostars. The peak of absorption in gold nanoparticles changes with their aggregation state. The shift in this peak causes a drastic color change that is detectable by the naked eye and is ideal for application in a biosensor. Furthermore, nanoparticles have increased kinetics in solution when compared with their microparticle counterparts, suggesting that rapid detection may be feasible using a biosensor platform at the nano-scale [130, 131].

Food poisoning continues to cause severe illness around the world and leads to hospitalization of unsuspecting patients. The concentration of pathogens necessary for successfully infecting the host is known as the infective dose. Simple and rapid detection of foodborne pathogens at their infective dose is a key step in preventing the spread of contamination [132]. As mentioned in Chapter 2, conventional methods for the detection of food-borne pathogens include culture counting, immunology, and polymerase chain reaction, but these methods suffer from the drawbacks of long incubation time, interference from contaminants and the requirement of specialized equipment, respectively [35].

These shortcomings have inspired the advancement of biosensors that utilize optical, electrochemical and mass-based transduction. Typically, these biosensors involve the use of specialized equipment such as a spectrophotometer, electrochemical cell, or quartz crystal microbalance and hence cannot be easily implemented outside the laboratory [35, 131, 133]. Thus, there exists a need for a simple and rapid method of pathogen detection that does not require specialized training or expensive equipment [134]. We chose *S. aureus*, a Gram-positive bacterium, as a model pathogen for testing the detection capabilities of our gold nanostars. *S. aureus* often causes food poisoning by producing enterotoxins which induce symptoms of sudden vomiting, diarrhea, nausea, malaise, abdominal cramps, and pain. Since the main mechanism of infection for *S. aureus* involves secreted toxins that need to diffuse out of the bacterium, it is considered a distant action pathogen. Such pathogens require a high concentration (10^5 to 10^6 CFU/mL for *S. aureus*) in the inoculum to successfully infect the host [135].

We expect that aggregation of gold nanostars can be induced by the presence of *S. aureus* via electrostatic interactions between the positively charged CTAB-coated gold nanostars and negatively charged cell walls of *S. aureus*. Such aggregation will lead to a rapid and drastic color change. This principle has been demonstrated in the literature when gold nanoparticles were modified by either antibodies [93] or aptamers [136] specific to the pathogen of interest. While a recent detection method of *S. aureus* claims to be rapid, it still requires 1.5 hours, complex modification of gold nanoparticles, and specialized equipment [136]. The control of the assembly/disassembly of non-functionalized gold nanoparticles has led to detection of small molecules, metal ions, DNA, and proteins but not whole cells. Studies suggest that cationic gold nanoparticles might aggregate around bacteria [137, 138] but the effect of size and morphology of gold nanostars on the aggregation kinetics has not been explored before. Here, we demonstrate that CTAB-coated gold nanostars can be used for rapid (<5 min) instrument-free colorimetric detection of pathogens in solution. We hypothesize that the degree and rate of color change of gold nanostars in the presence of *S. aureus* will be defined by the degree of branching and the particle size.

3.3 Experimental

3.3.1 Materials

Gold (III) chloride hydrate ($HAuCl_4 \bullet xH_2O$), Hexadecyltrimethylammonium bromide (CTAB), sodium borohydride, silver nitrate, and L-ascorbic acid were purchased from Sigma-Aldrich (Oakville, ON, Canada). Trisodium citrate dihydrate was purchased from Thermo Fisher Scientific (Burlington, ON, Canada). All materials were used without further purification. Transparent 96-well microplates, BD trypticase soy agar (TSA) culture plates, BD nutrient broth, sodium chloride (ACS grade), Nalgene sterilization filter units and calcium alginate swabs were purchased from VWR (Mississauga, ON, Canada). Polybead® Carboxylate Microspheres 3.00 µm, 1.00 µm and 0.10 µm were purchased from Polysciences, Inc. (Warrington, PA, USA) and used as model negatively charged polystyrene microparticles. 1,2-dimyristoyl-*sn*-glycero-3-phosphocholine (DMPC), 1,2-dimyristoyl-*sn*-glycero-3-phospho-(1'-*rac*-glycerol) (DMPG) and 1,2-dimyristoyl-*sn*-glycero-3-phosphoethanolamine (DMPE) phospholipids were purchased from Avanti Polar Lipids, Inc. (Alabaster, AL, USA). 400 mesh formvar/carbon coated copper grids were obtained from Canemco

Inc (Gore, QC, Canada). *S. aureus* (ATCC 6538) was purchased from Cedarlane (Burlington, ON, Canada). The vials used for gold nanostar synthesis were rinsed with Millipore water before use.

3.3.2 Synthesis of gold nanoseed precursor

The gold nanoseed precursor was synthesized using a modified version of a previously described simple two-step one pot process [124]. First, a gold (III) chloride hydrate and trisodium citrate dihydrate solution was prepared with final concentrations of 2.5×10^{-4} M and 10^{-4} M, respectively, in 20 mL of Millipore water. Then, under moderate stirring, freshly prepared ice-cold solution of sodium borohydride (0.1 M, 60 µL) was quickly added. Immediately, the solution turned brown-pink and slowly developed into its final red color. The sample was stored overnight in the dark under ambient conditions. The solution was then filtered (0.2 µm) and stored at 4 °C until use. Gold nanoseed solutions were found to be stable for weeks at this temperature. Uniform spherical gold nanoparticles approximately 4-5 nm in diameter were produced.

3.3.3 Synthesis of CTAB-coated gold nanostars

Gold nanostar samples were synthesized using CTAB as a negative template using a modified procedure [124]. The amount of CTAB and gold (III) chloride hydrate were varied to yield the entire nanostar set (n = 30) with varying sizes and morphologies. CTAB (7.33 mM; 125 mg CTAB in 46.88 mL Millipore water) was dissolved by probe sonication (2 seconds on, 1 second off; 25% amplitude) for 20 minutes. This concentration was designated as 125 mg CTAB, based on the initial dissolved amount, for ease of naming convention. After this, the 125 mg CTAB solution was diluted with Millipore water 1:5 (1.466 mM, designated 25 mg CTAB), 2:5 (2.932 mM, designated 50 mg CTAB), 3:5 (4.398 mM, designated 75 mg CTAB), and 4:5 (5.864 mM, designated 100 mg CTAB) for 30 total samples (15 mL, 6 per CTAB concentration). In these dilution ratios and other instances when dilution is mentioned in the thesis, the first number refers to the volume of aliquot added and the second number refers to the total volume of diluted solution. Gold (III) chloride hydrate (0.64 mL, 11 mM) and silver nitrate (0.096 mL, 0.01 M) were added to the CTAB solution under vigorous stirring for 1 minute. Then, L-ascorbic acid (0.103 mL, 0.1 M) was added dropwise. Upon addition of the last drop of L-ascorbic acid, the solution turned clear, and the appropriate volume of gold nanoseed was immediately added. For each CTAB concentration 400, 320, 240, 160, 80, or 32 µL of

gold nanoseed was added for 15 mL of initial CTAB solution, resulting in a final 5 x 6 set. After seed addition, each sample was allowed to stir for another 1.5 minutes. The samples were left in the dark in ambient conditions until use. Gold nanostars were found to be stable in the dark at room temperature for months.

3.3.4 Characterization of gold nanostars

The gold nanostars were characterized using transmission electron microscopy (TEM) for sizing and Ultraviolet-Visible (UV-Vis) spectrophotometry for absorbance spectra. TEM and UV-Vis spectrophotometry were performed using a Philips CM10 and BioTek Epoch Microplate Spectrophotometer, respectively. TEM samples were prepared by drying 5 µL of the samples described above overnight on formvar/carbon coated copper grids. UV-Vis absorbance spectroscopy was performed in duplicates for 300 µL samples in a 96-well plate. Zeta potential was measured using Malvern Zetasizer and gold nanostars as well as bacteria were suspended in 0.85% saline (with ~0.006% broth) to mimic the testing conditions.

TEM images (92,000x) of the all gold nanostars were sized manually with National Institutes of Health ImageJ software (n = 10 each). Calibrated by the scale bars, nanostars were profiled, and five particularities were measured for each nanostar: branch length (Figure 6 a), branch width (Figure 6 b), minor diameter (Figure 6 c), and total diameter (Figure 6 d) as highlighted in Figure 4 b. Total diameter was defined as the longest total length of a nanostar given that the length passes through its geometric center. Conversely, minor diameter was defined as the shortest length through the geometric center. A branch was defined as an extrusion from the expected curvature of a nanostar given that the branch width is less than or equal to half the minor diameter. Branch length and width were defined as the measurement from the expected curvature of the nanostar to the branch tip and the perpendicular width at half the branch length, respectively (Figure 4 b). The number of branches were also counted and are presented along with their distribution in Figure 7.

3.3.5 *Staphylococcus aureus* culture

S. aureus was cultured on TSA plates by using alginate swabs and incubating the plates at room temperature for two nights. A 2.55% saline solution was prepared and sterilized by using Nalgene filters and ~0.006% of nutrient broth was added to the saline to preserve *S. aureus* during tests [139].

Since 0.85% saline is considered isotonic [140] and the bacterial solution is diluted 3x when the gold nanoparticles are added, a 2.55% saline solution was chosen for suspending bacteria to maintain isotonic nature in the final mixture of bacteria and gold nanoparticles. *S. aureus* was transferred to saline solution by adding 5 mL of saline (with ~0.006% broth) to the TSA plate and using alginate swabs to dislodge the bacteria from the plates. *S. aureus* was washed with saline (with ~0.006% broth) solution seven times by centrifugation at 4,000 rpm for 10 minutes. The stock solution of *S. aureus* was diluted 100 times in saline (with ~0.006% broth) and used for testing with gold nanostars. The concentration of *S. aureus* was determined by direct plate counts method.

3.3.6 Colorimetric detection of *Staphylococcus aureus* using various gold nanostars

All 30 of the gold nanostars synthesized were tested to characterize their potential as an instrument-free colorimetric detection platform. 200 µL of each nanostar solution was added into a 96-well microplate placed on top of an X-ray film viewer for homogenous white light illumination. The nanostars were arranged such that columns corresponded increasing (25 to 125 mg from left to right) CTAB amount, while rows corresponded to decreasing (400 to 32 µL from top to bottom) seed volume. The nanostars were then imaged using a Canon EOS Rebel T3 with constant settings. Subsequently, 100 µL of $5x10^5$ CFU/well *S. aureus* was added to each well at time = 0. The color change was then imaged for 2 hours using intervals of about 25 seconds. The image for each subsequent time point was normalized by subtracting the initial image without *S. aureus* using MathWorks MATLAB®. The red, green, blue (RGB) values of the subtracted images were extracted from 200 pixels per well. These values were averaged for each time point and plotted against time for obtaining Figure 10 c. After determining the optimal formulation of gold nanostars, the effect of purification and excess CTAB concentration on bacteria detection was evaluated. The gold nanostars were centrifuged at 10000 rpm for 15 minutes. The supernatant was discarded and the precipitate was resuspended in either Millipore water (0 mg CTAB) or solutions with CTAB concentrations matching those used during synthesis (25, 50, 75, 100, 125 mg). Next, 100 µL of saline (with ~0.006% broth) or *S. aureus* with a normalized absorbance of 0.1 at 660 nm was added to 200 µL of each of the gold nanostar solutions and incubated overnight. Photographs were then obtained using the digital camera.

3.3.7 Comparison of *Staphylococcus aureus* to charged particles

In order to demonstrate selectivity, a solution of *S. aureus* was prepared in saline (with ~0.006% broth) to obtain normalized absorbance of 0.1 at 660 nm and this results in a concentration of approximately 8 x 10^6 CFU/well as determined by plate counts method. Since bacteria and particles cannot be exactly at the same concentration, they were compared by preparing the solutions at the same normalized absorbance of 0.1 at 660 nm. Polystyrene particles were diluted in saline (with ~0.006% broth). Liposomes were prepared according to manufacturer's recommendation. DMPC was dissolved in chloroform at a concentration of 10 mg/mL, while DMPG and DMPE were dissolved in a mixture of chloroform:methanol:water (65:35:8 v/v/v) at a concentration of 10 mg/mL. The phospholipid solutions were first dried under nitrogen and then *in vacuo* overnight. Saline (with ~0.006% broth) was added to the vials containing DMPC and DMPG at 30 °C, and DMPE at 60 °C. The phospholipids were allowed to rehydrate for several hours at the respective elevated temperatures. Size reduction was performed by sonicating each of the samples using a Branson probe sonicator for 10 minutes at 25% amplitude and 1 second on, 0.5 second off pulses. Each of the solutions were diluted in saline (with ~0.006% broth) to obtain the appropriate absorption. 100 µL of the particle solutions were then added to the 200 µL of optimal gold nanostar solution in a 96-well microplate. The solutions were incubated overnight and UV-Vis absorption spectra were obtained.

3.4 Results and Discussion

3.4.1 Synthesis of gold nanostars and morphology characterization

Gold nanostars were synthesized at room temperature via a seed-mediated growth mechanism using CTAB surfactant as a template [124]. The mechanism of anisotropic growth in gold nanoparticles is currently being investigated and often the growth of gold nanostars is compared to that of gold nanorods, because both morphologies use CTAB surfactant as a negative template and silver ions for creating active sites [141-145]. Twin defects have been observed in gold nanoparticles, where two crystals share some of the same crystal lattice points [143]. In the case of nanostars, twin defects on the surface of the seed are postulated to weaken the binding of the positively charged CTAB surfactant, which allows the growth of branches at these sites [143]. Also, silver can be deposited on the surface of the seed by underpotential [142] and produce additional defects, which in turn act as

active sites for growth of branches [143, 144, 146]. We hypothesize that the surface morphology and particle size of gold nanostars can be controlled by changing the amount of gold seed precursor (32, 80, 160, 240, 320 or 400 µL) and CTAB (25, 50, 75, 100, 125 mg) added to the formulation. To test this hypothesis, we synthesized 30 types of gold nanostars by using all possible combinations of these two parameters, while keeping the amount of silver nitrate, L-ascorbic acid, and gold salt in solution constant. These nanostars were characterized using transmission electron microscopy (TEM) to determine their size and surface morphology and using UV-Vis spectroscopy to determine their absorption spectra. We then demonstrated that the gold nanostars change color drastically in the presence of *S. aureus* as compared to a saline (with ~0.006% broth) control.

The TEM images of the 30 samples of gold nanostars show that the total size of nanostars is mostly controlled by the amount of gold nanoseed added, while the degree of branching and branch length are controlled by the CTAB amounts (Figure 4 a). Increasing the amount of seed decreases the total size because more growth sites are present and the total amount of gold available for growth in solution is kept constant. Increasing the amount of CTAB increases the branch length and the average number of branches because the number of CTAB micelles per seed increases, ranging from approximately 10^4 to 10^6 assuming an aggregation number of 60 for CTAB micelles [147]. CTAB is expected to form a bilayer around the gold nanoparticles in a manner similar to that observed for gold nanorods [148] and this is shown in Figure 4 b. We quantified the size and degree of branching for each of the 30 samples by measuring the minor diameter, total diameter, branch length, and branch width, as defined in Figure 4 b. We also quantified the number of branches and some sample images are presented in Figure 5 for the nanoparticle using 125 mg CTAB and 240 µL seed. Since TEM can only provide 2D images of 3D nanoparticles, the number of branches is an underestimate of the actual number of branches but the trends between different nanoparticles can be extrapolated from 2D to 3D. The minor diameter (Figure 6 c) and total diameter (Figure 6 d) showed similar dependence on seed and CTAB concentration, as diametric and branch growth occurs simultaneously when gold is available in solution. This also leads to the relatively uniform growth of branch width under the same conditions as growth of the stars (Figure 6 b). The total diameter ranged from 31 nm to 113 nm for 400 µL and 32 µL seed sets respectively, while the length of branches ranged from 3 nm to 17 nm for 25 mg CTAB and 125 mg CTAB sets respectively (Figure 6 a, d). The changes in surfactant and seed not only affect the dimensions of the branches but also the average number of branches, which ranges

from one to six (Figure 7 a). We believe this is because the higher concentration of CTAB per seed allows better adsorption of CTAB, which in turn promotes anisotropic growth at multiple sites. The concentration of CTAB used in all conditions is above the critical micelle concentration of 1 mM and thus, CTAB would be present in the micellar form. At room temperature, the concentration of CTAB used is well below 25 % (w/v) and thus, CTAB is expected to be in micellar phase and not undergo any other phase transitions [149]. Additionally, the distribution of stars with increasing number of branches also varies with the amount of seed and CTAB. Low seed volumes and high concentration of CTAB are necessary for a higher fraction of highly branched nanostars (Figure 7 b-d). Although there are some rare outliers in the TEM images of single nanostars due to the nature of selecting individual nanoparticles, the trends of size and branching are clearly visible in the images (Figure 4) as well as the plots that follow (Figure 6).

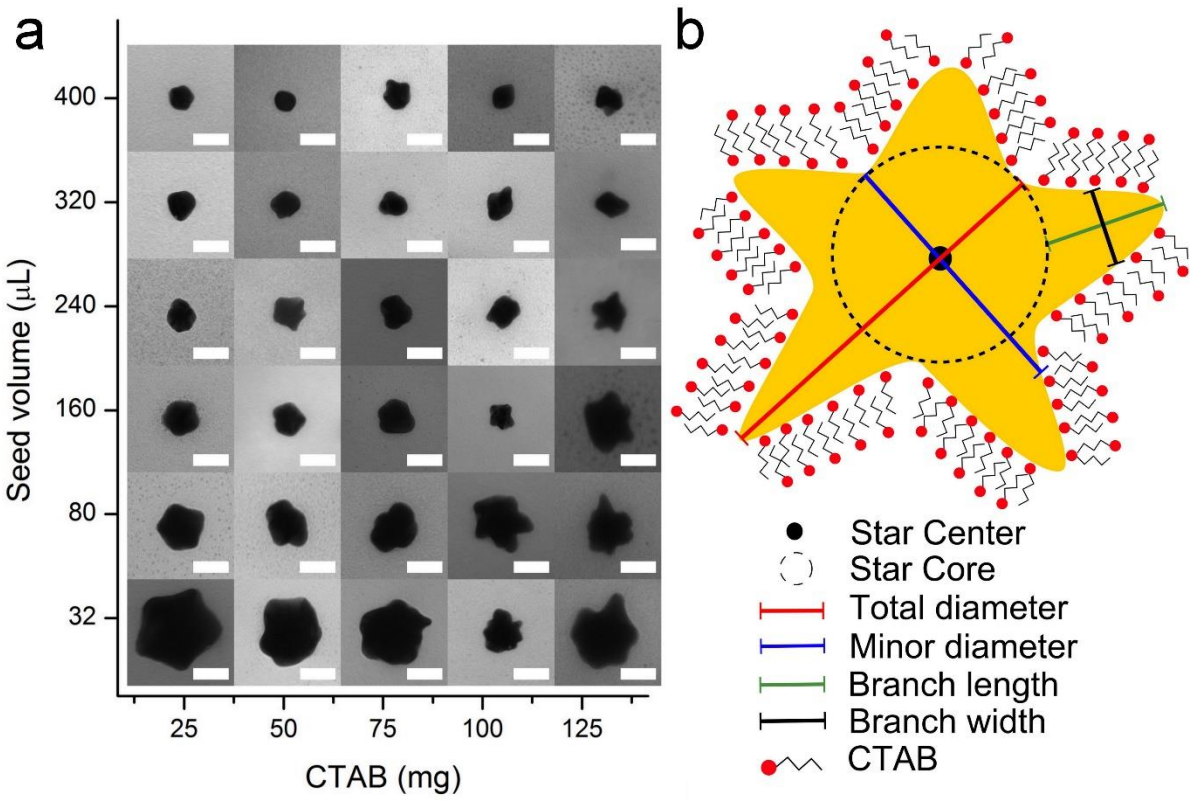

Figure 4: a) Transmission electron microscopy (TEM) images of thirty nanostar samples (scale bar: 50 nm). The mass of CTAB represents the mass added to 46.88 mL of Millipore water such

that 125 mg CTAB is 7.33 mM. b) Schematic showing a CTAB-coated gold nanostar and the definition of various parameters for characterizing a gold nanostar.

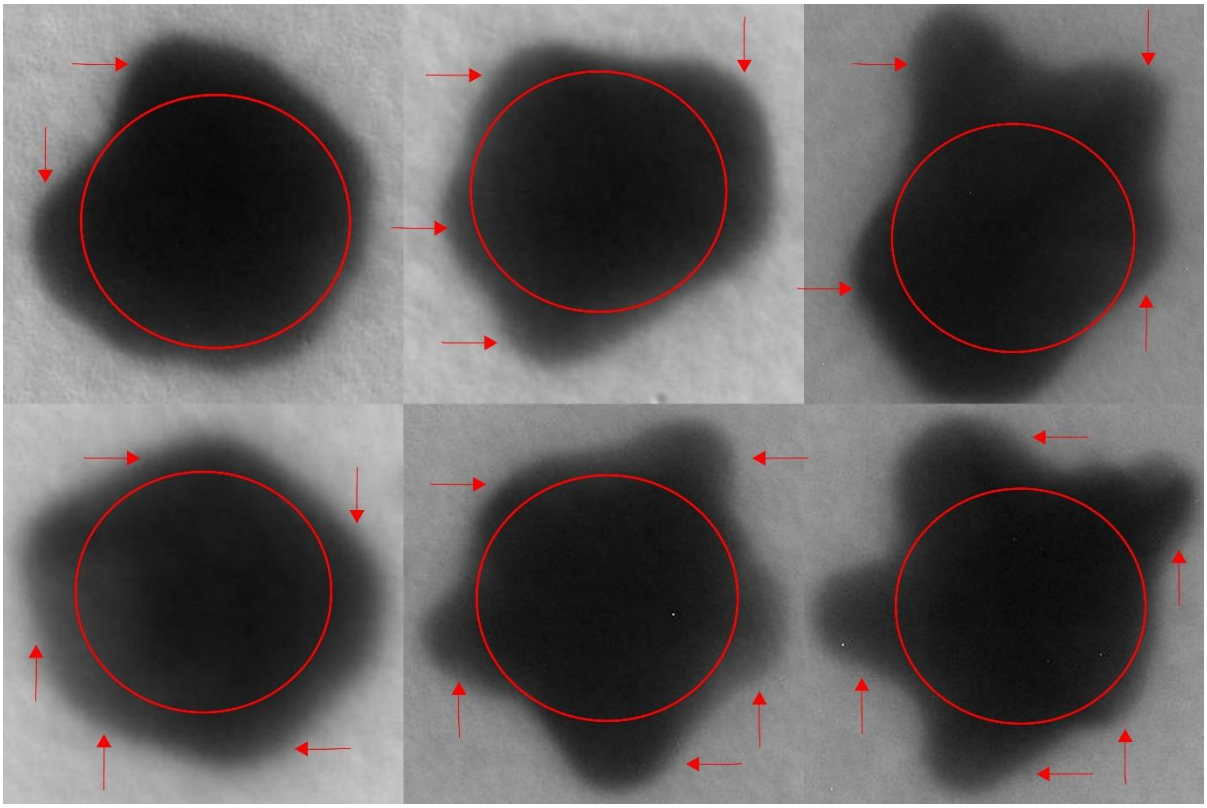

Figure 5: Sample TEM images of gold nanostars synthesized with 125 mg CTAB and 240 µL seed, showing different number of branches ranging from 2 to 5.

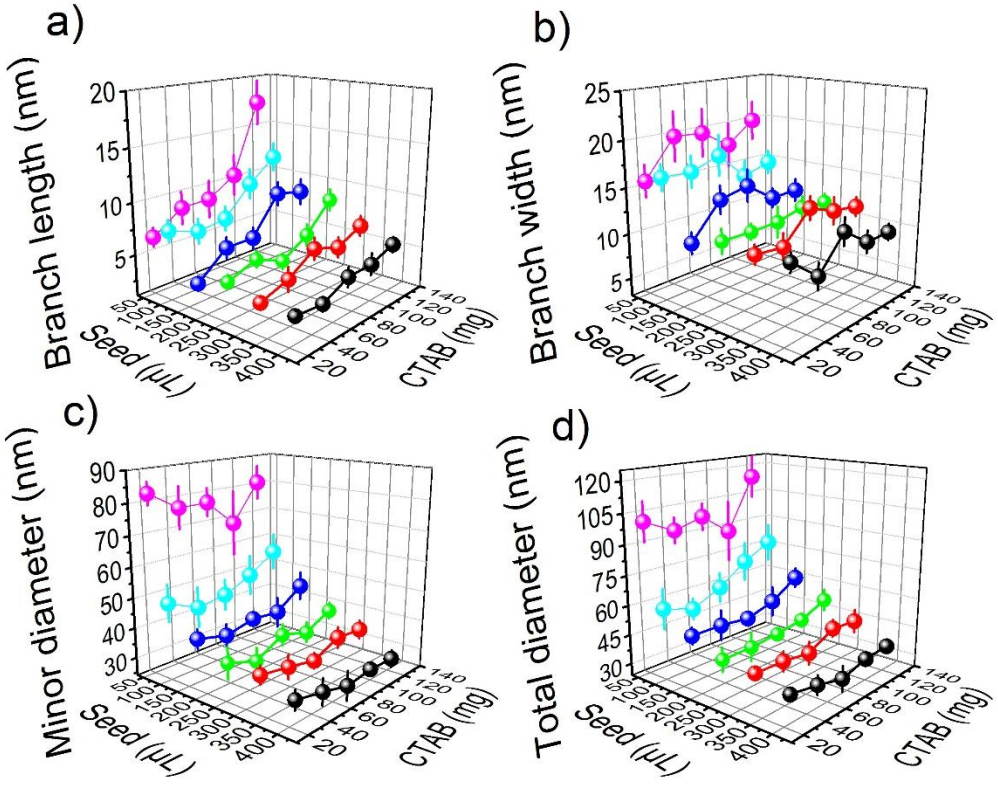

Figure 6: Various parameters defined in Figure 4 b, measured from the TEM images for nanostars: a) Branch length (n = 10; mean ± S.E) b) Branch width (n = 10; mean ± S.E), c) Minor diameter (n = 10; mean ± S.D.), d) Total diameter (n = 10; mean ± S.D.)

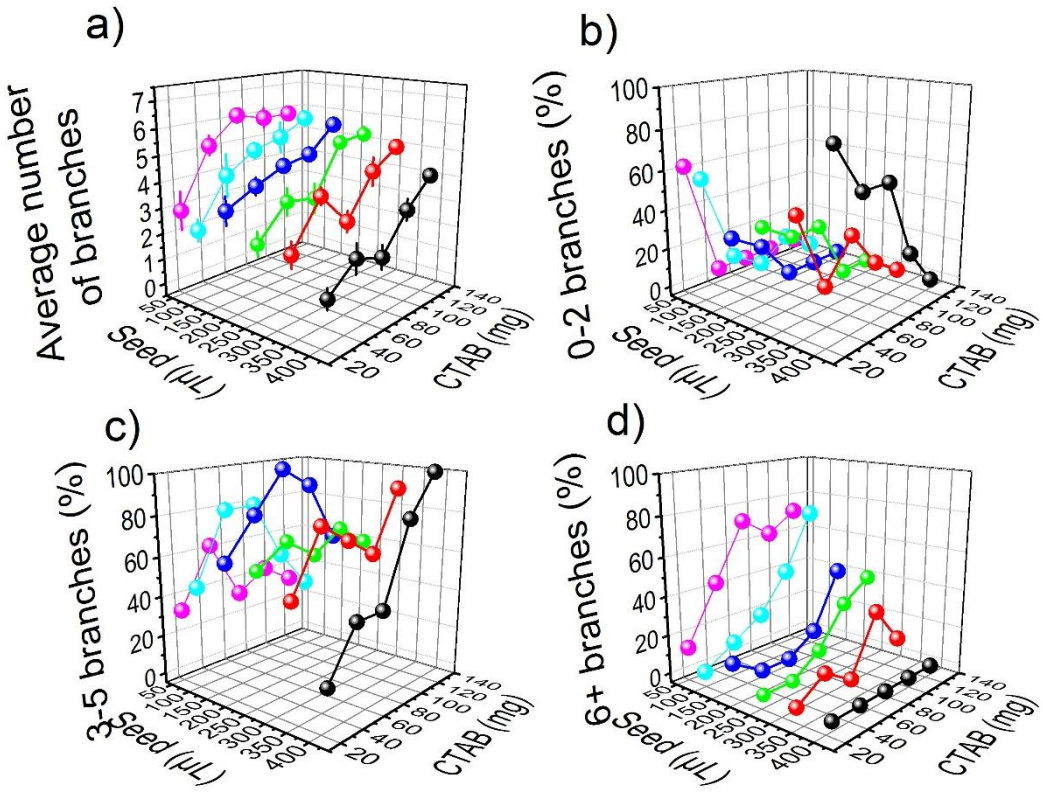

Figure 7: The distribution of branches for the entire 30 nanostar set was characterized using TEM images, and is recorded above, corresponding to a) average number of branches, and bins of b) 0-2 branches, c) 3-5 branches, and d) 6+ branches.

3.4.2 Colorimetric characterization of gold nanostars

The color of gold nanoparticles is determined by the size of the particles because of their surface plasmon resonance. A change in the surface plasmon resonance of the particles can be characterized by the absorption peak of UV-Vis spectroscopy [143, 145, 150]. As seen in Figure 8 a), varying size and the degree of branching yields nanostars with different solution colors. The lowest CTAB, highest seed sample yields a red color. This sample lacks significant branching and thus is found to have a more spherical morphology, as we previously described. Spherical gold nanoparticles have been extensively studied in the past, and as we observed, give the solution a distinct red color [151].

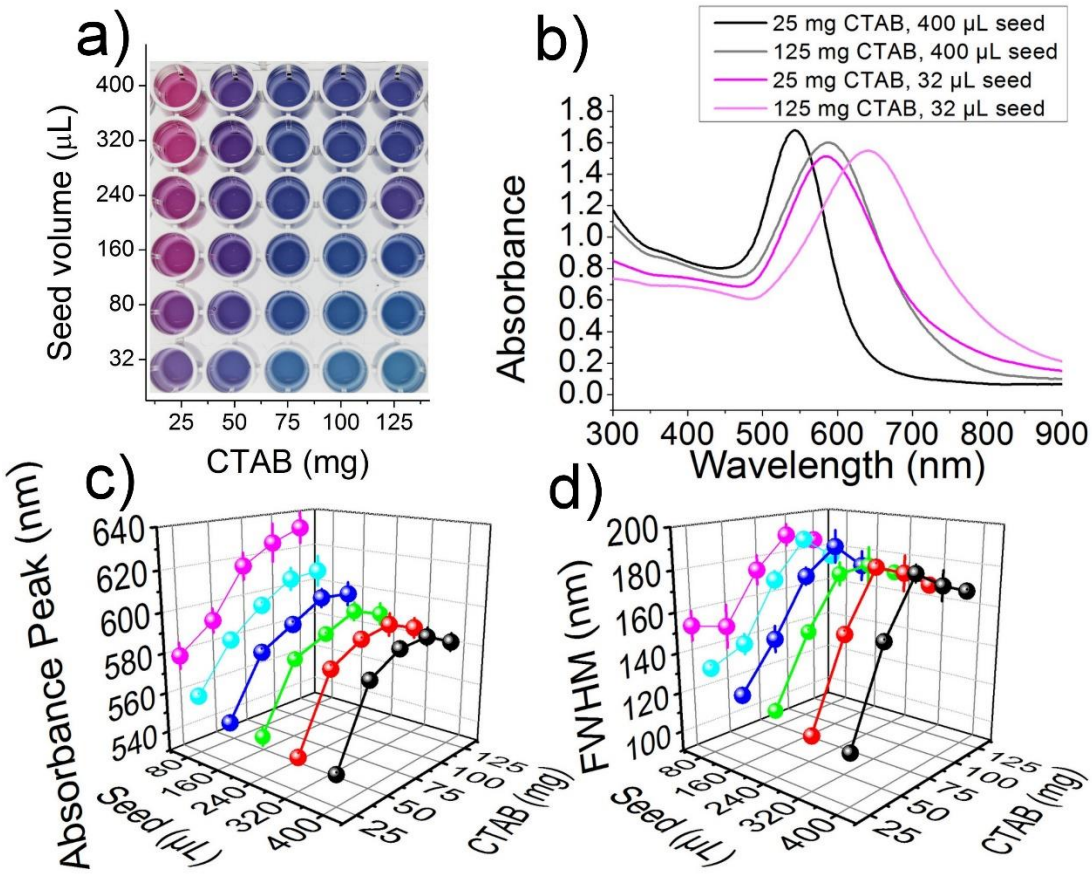

Figure 8: Optical properties of gold nanostars: a) Photograph showing the color of gold nanostars b) UV-Visible absorption spectra for four of the gold nanostars with varying seed and CTAB concentrations. Effect of CTAB and seed concentrations on c) UV-Visible absorbance peaks (n = 6, mean ± S.D.), and on d) Full Width Half Maximum (FWHM) (n = 6, mean ± S.D.)

Decreasing seed and increasing CTAB causes the gold nanostar solutions to be violet and then blue, resulting from a shift in plasmon resonances caused by increased degree of branching and general star-like morphology [124, 152]. A similar color shift from red to blue can happen when spherical nanoparticles aggregate, but our case the color shift is because of growth as we have confirmed from TEM images and dynamic light scattering measurements (DLS). In TEM images, we did not observe aggregates of small gold nanoseeds, instead we observed gold nanostars (Figure 4 a). DLS measurements are not reliable for anisotropic nanoparticles such as gold nanostars because the technique assumes a spherical particle and because light absorption from solution is assumed to be

minimal. Both of these assumptions fail in the case of gold nanostars and hence, an accurate estimate of sizes cannot be obtained but DLS can show if nanoparticles are aggregating and we observed that the particle sizes were in the range of 35-80 nm (Figure 9), similar to those from TEM measurements. The dependence of absorption peak and width on the degree of branching has rarely been explored [123]. We repeated the synthesis of the 30 stars three times and measured the absorption spectra from 300 nm to 900 nm with a step size of 1 nm. As an example, we plotted the complete spectra of the four extreme synthesis data points (Figure 8 b). We also extracted the peaks and full width half maximum values (FWHM) from the spectra of all the nanostars (Figure 8 c,d). The relatively small standard deviations and consistent trends in absorption spectra suggest that the synthesis of nanoparticles is reproducible. Increasing size of the nanostars by decreasing seed leads to a red shift in the absorption peak and also broadens the width. Additionally, there is a significant jump in the peak and FWHM when increasing the CTAB from 25 to 50 mg even though the size of the particles only varies slightly. This jump suggests that a minimum concentration of CTAB is necessary for changing the morphology of nanoparticles from spheres to stars and causing a shift in absorbance peak of about 60 nm as observed in literature [124]. Interestingly, a characteristic drop in the peak position and FWHM occurs at the highest CTAB concentration for all seed volumes when the number and length of branches is the highest. This drop is in agreement with previously modeled data, where a slight blue shift in absorbance peak is observed when the number of branches was increased from four to ten [123]. The drop in the FWHM at highest CTAB concentration also suggests that the size distribution of nanostars is narrower [123]. This is most likely because a higher concentration of CTAB allows for more homogenous adsorption of CTAB on the seeds, thereby synthesizing more monodisperse gold nanostars. Here, DLS could not be used for characterizing the distribution of particles because of the limitations of DLS in measuring solutions that absorb light and have irregularly shaped particles. Other components that could exist in solution are CTAB micelles, gold nanoseeds and unreacted salts. CTAB and other salts do not significantly absorb visible light and hence would not contribute to the UV-Visible absorbance spectra. Gold nanoseeds produce a strong absorption peak at 520 nm and the presence of excess unreacted gold nanoseeds could also cause the drop in absorption peak at the highest CTAB concentration but this would not explain the drop in FWHM because the distribution of nanoparticles and hence FWHM should have been broader.

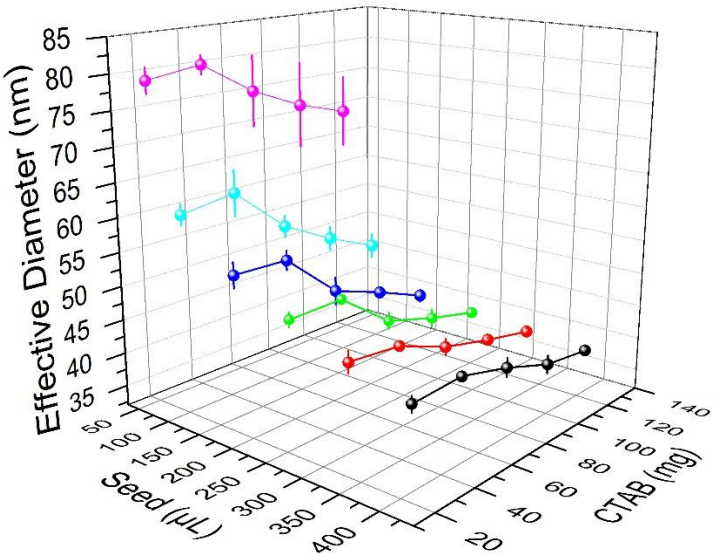

Figure 9: Dynamic light scattering (DLS) measurements of gold nanoparticles for various CTAB and seed concentrations (n = 3, mean ± S.D.)

3.4.3 Colorimetric detection of *Staphylococcus aureus*

Next, we tested the ability of each of the gold nanostars to detect Gram-positive bacteria *S. aureus* by adding them to gold nanostars in 96-well microplates. *S. aureus* was suspended in 2.55% saline solution (with ~0.006% broth) and thus this saline was used as a negative control. Figure 10 a) shows that the stars synthesized with the lowest seed amounts turn clear in saline (with ~0.006% broth) solution. This color change can be explained by the colloidal instability of larger gold nanostars. In contrast, nanostars synthesized with higher seed values are more stable and only change color in the presence of *S. aureus*. While qualitative color change is intense and can be easily observed using the naked eye, quantification of the color was achieved by measuring the RGB components of each sample. We collected several images over two hours at an interval of about 25 seconds while leaving the samples undisturbed and then normalized each image with *S. aureus* by subtracting the initial image of gold nanostars. We measured the RGB values from each well and determined the maximum change in each component. The red component of RGB model showed the maximum change in intensity. Thus, the red component was plotted against the CTAB and gold seed amounts (Figure 10 b). This observation correlates closely with the light absorption peak and FWHM measured

previously (Figure 8 c, d). The green and blue components also change in a similar manner but the magnitude of change is smaller (Figure 11). Figure 10 b) suggests that more branched and larger nanostars show a greater color change in the presence of *S. aureus*. Interestingly, the general trend shown in Figure 10 b) matched the trend throughout our findings in both absorbance peak and FWHM, suggesting a consistent theme that the size and degree of branching of nanostars significantly impact optical properties and govern detection performance in a similar manner. We also studied the evolution of color change over time for each of the nanostars. Initial onset of color change was immediate and visually discernible in less than 5 minutes for most samples. This is seen in Figure 10 c) as the contour plot shows a change of up to 60 units of intensity within 300 seconds in the red component for the most sensitive gold nanostars. We observed that the color changes saturated after about 40 minutes. The plot confirms that the highest seed volume nanostars with smallest sizes and least branching show negligible color change due to high colloidal stability, while the most rapid color change occurs in nanostars synthesized using lowest seed volumes with biggest sizes and highest branching. This is in part because branching increases effective surface area and spatial extent, allowing gold nanostars to aggregate around the bacteria and therefore produce a more substantial change in color. While Figure 10 b) shows the change of gold nanoparticles from their initial state upon addition of *S. aureus*, the ideal formulation of nanostars would not only need to change color drastically in the presence of *S. aureus* but also be stable in saline. We quantified this criterion by subtracting the two images in Figure 10 a) and determining the RGB values of the subtracted image. Since the red component demonstrates maximum change, the well with the highest difference in red provides the best formulation for application in pathogen detection. The resulting RGB values from subtracting images in Figure 10 a) were different from the results presented in Figure 10 b). We observed that the nanostar solution synthesized using 125 mg CTAB and 240 µL gold nanoseed precursor provided the most difference between saline and bacteria solutions. These nanostars have a small enough size to be stable in high salt concentrations and yet are branched enough to aggregate around *S. aureus* and cause a drastic color change. This optimal formulation of gold nanostars was used to test the effect of excess CTAB concentration on the detection of *S. aureus*. The results, seen in Figure 12, demonstrate that there was negligible change between different concentrations of excess CTAB used. If the solution was devoid of CTAB (as in the Millipore water resuspension) after synthesis, gold nanostars would aggregate and change color in saline control as

well. Thus, a small amount of CTAB is indeed necessary in solution after synthesis to prevent aggregation of the gold nanostars in saline (with ~0.006% broth).

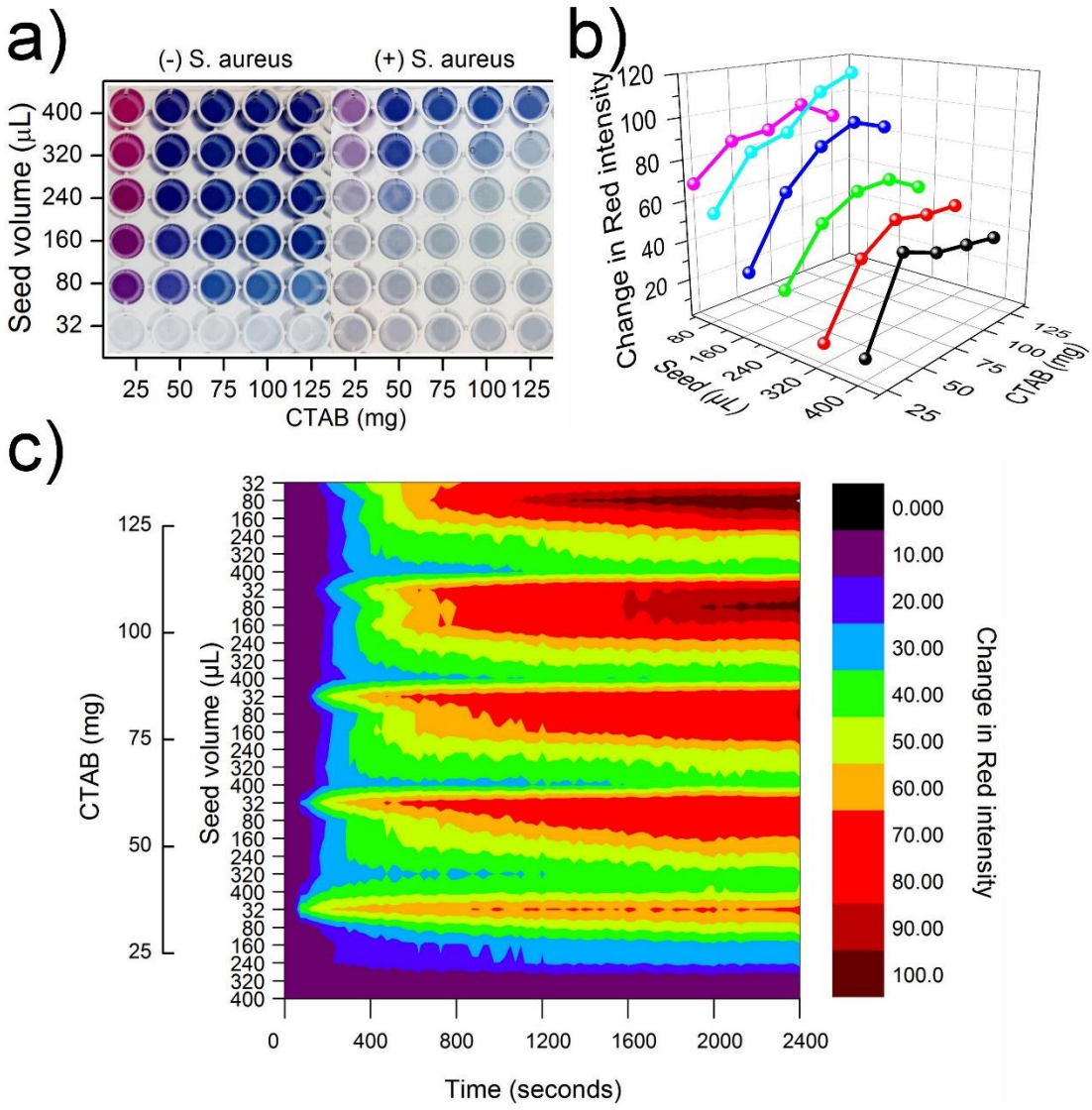

Figure 10: Color change of gold nanostars in the presence of *Staphylococcus aureus*: a) Significant visible color change in the presence of 5x10^5 CFU/well *S. aureus* in a 96-well microplate; b) the final, maximum color change in the red component of RGB color model plotted against the gold seed and CTAB amounts; c) Evolution of the change in intensity of red component of color over time for each sample.

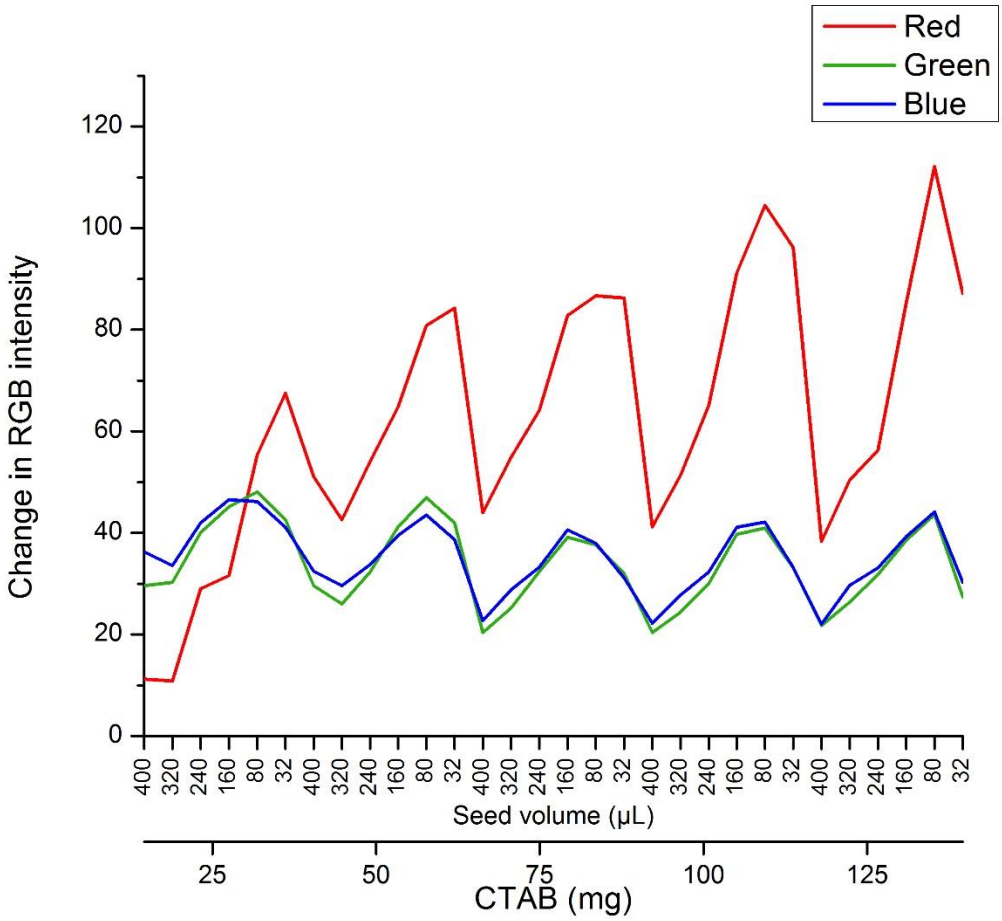

Figure 11: Maximum change in RGB values for color change in the presence of S. aureus is plotted against gold nanostar sample. The red component (solid red line) was found to have the greatest representation of color change for the nanostars. The blue (solid blue line) and green (solid green line) components were found to correspond to the red components, as expected due to overall color change in the wells.

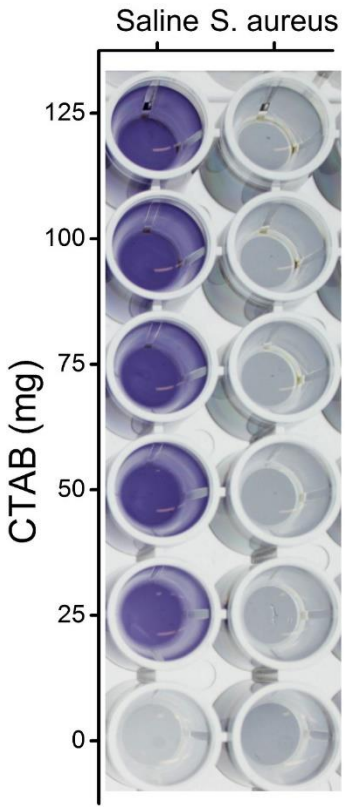

Figure 12: The effect of CTAB concentration on the ability to detect bacteria. Saline (with ~0.006% broth) was used as control and *S. aureus* was prepared at a normalized absorption of 0.1 at 660 nm.

3.4.4 Selectivity of gold nanostars: UV-Visible absorption spectra

In order to better understand the cause of aggregation of CTAB-coated gold nanostars around *S. aureus*, we tested the interaction of gold nanostars with a variety of charged particles. Polystyrene microparticles functionalized with carboxylic acid were used to provide a negative surface charge, which have the potential to aggregate the positively charged CTAB-coated gold nanostars. Three different sizes of polystyrene microparticles were used to explore the effect of size on the aggregation of gold nanostars, where the 1 µm microparticles are most similar in size to *S. aureus*. We also used three different kinds of liposomes to explore the interaction between gold nanostars and charged phospholipids which could be responsible for the attraction between bacteria and gold nanostars. DMPC and DMPE terminate in a choline and ethanolamine group respectively and thus are

zwitterionic. DMPG terminates in a glycerol group and hence the phosphate causes the liposomes to be overall negatively charged. Figure 13 a) shows the UV-Vis spectra of the optimal formulation of gold nanostars (125 mg CTAB, 240 µL gold seed) in the presence of water, saline, *S. aureus*, polystyrene microparticles, and phospholipid liposomes. The spectra in Figure 13 a) demonstrate minimal change in saline, polystyrene microparticles, and DMPC and DMPE liposomes, while highlighting a drastic broadening and flattening of the peak in *S. aureus* and DMPG liposome solutions which confirms the shift in plasmon resonance of the gold nanostars. These spectra are consistent with the observed color change in the microplates from solid blue to a translucent grey in the presence of *S. aureus*. We confirmed that the color change of gold nanostars was due to near complete aggregation around the *S. aureus* (Figure 13 b) by imaging the samples using TEM. This aggregation is caused by electrostatic interactions between the CTAB-coated gold nanoparticle surface that is positively charged (zeta potential of +38.0 mV) and the cell wall of *S. aureus* that is negatively charged (zeta potential of -24.2 mV). Our results are in agreement with the work of Berry *et al*. where they explained that the mechanism of aggregation of CTAB-coated gold nanorods around Gram-positive *Bacillus cereus* is the strong electrostatic interactions between positively charged CTAB molecules and negatively charged teichoic acids on the surface of bacteria [137]. Teichoic acid is expressed on the surface of Gram-positive bacteria and it includes several phosphate groups, which provide a polyanionic surface with a high density of negative surface charge. As demonstrated by Figure 13 a), a polyanionic surface is necessary for the aggregation of CTAB-coated gold nanostars since only negatively charged DMPG liposomes led to substantial aggregation. On the other hand, polystyrene particles with monoanionic carboxylic acid and zwitterionic liposomes had insufficient negative charge to cause a significant color change. Since only DMPG liposomes cause a color change comparable to bacteria, the aggregation of gold nanostars requires interaction with several negatively charged groups. Thus, the aggregation and color change of CTAB-coated gold nanostars is selective to bacteria and polyanionic particles in comparison to other particles with only monoanionic or zwitterionic charges. This work avoids the use of antibodies and aptamers and only exploits electrostatic interactions for colorimetric detection. Thus, there are some limits to specificity but since the distribution of charges is expected to be different in different strains of bacteria, these interactions are exploited for differentiating between bacteria in the following chapters.

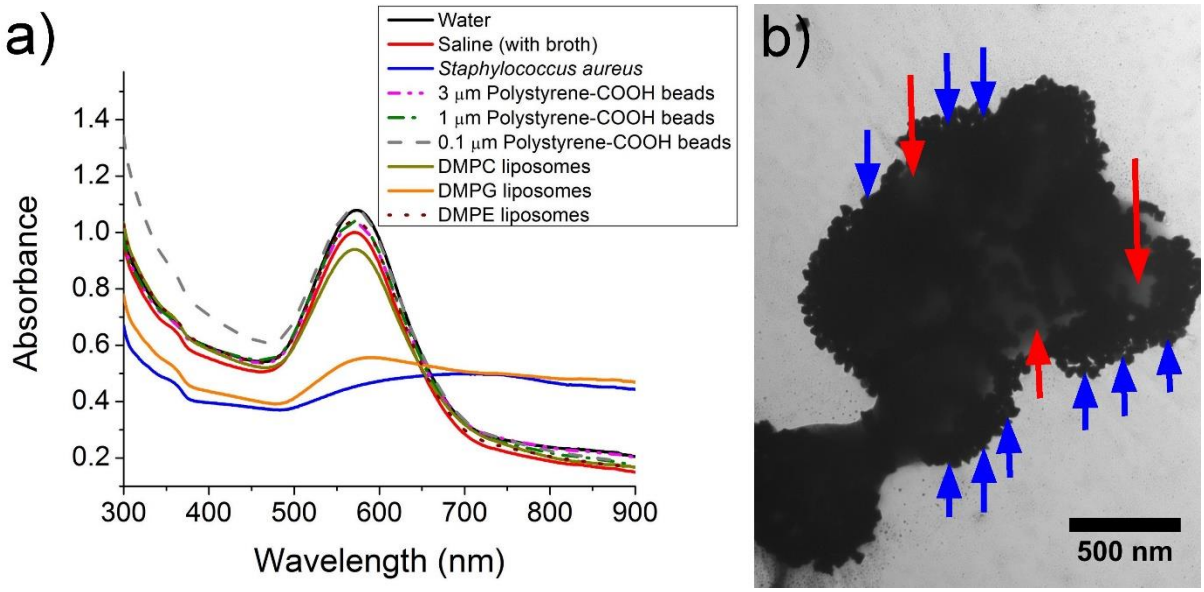

Figure 13: Selectivity of the optimal formulation of gold nanostars: a) UV-Visible absorption spectra of gold nanostars in water, in saline with ~0.006% broth, in the presence of *S. aureus*, in the presence of 3 µm, 1 µm, and 0.1 µm carboxylic acid functionalized polystyrene particles, in the presence of 1,2-dimyristoyl-*sn*-glycero-3-phosphocholine (DMPC) liposomes, 1,2-dimyristoyl-*sn*-glycero-3-phospho-(1'-*rac*-glycerol) (DMPG) liposomes, and 1,2-dimyristoyl-*sn*-glycero-3-phosphoethanolamine (DMPE) liposomes; b) Transmission electron microscopy image of gold nanostars (blue arrows) aggregating around *S. aureus* (red arrows).

3.5 Conclusion

We demonstrated that the size and degree of branching of gold nanostars can be controlled by varying the amount of gold nanoseed precursor and CTAB added to the formulation. We used CTAB-coated gold nanostars for rapid (<5 min) instrument-free colorimetric detection of *S. aureus* at its infective dose without the use of any targeting ligands such as antibodies or aptamers. The size and branching of gold nanostars control the rate and degree of color change in the presence of *S. aureus*. An optimal formulation of gold nanostars (125 mg CTAB and 240 µL gold nanoseed precursor) provides maximum contrast in color between *S. aureus* and saline (with ~0.006% broth) and also a selective response in comparison to polystyrene microparticles and liposomes. TEM confirmed that the mechanism of color change was indeed the aggregation of gold nanostars around the bacteria caused

by electrostatic interactions. Thus, CTAB-coated gold nanostars are a promising platform for rapid colorimetric detection of pathogens at the relevant infective dose.

Chapter 4
"Chemical nose" for the visual identification of emerging ocular pathogens using gold nanostars

4.1 Summary

Ocular pathogens can cause severe damage in the eye leading to severe vision loss and even blindness if left untreated. Identification of pathogens is crucial for administering the appropriate antibiotics in order to gain effective control over ocular infection. Herein, we report a gold nanostar-based "chemical nose" for visually identifying ocular pathogens. Using a spectrophotometer and nanostars of different sizes and degrees of branching, we show that the "chemical nose" is capable of identifying the following clinically relevant ocular pathogens with an accuracy of 99%: *S. aureus, A. xylosoxidans, D. acidovorans* and *S. maltophilia*. The differential colorimetric response is due to electrostatic aggregation of cationic gold nanostars around bacteria without the use of biomolecule ligands such as aptamers or antibodies. Transmission electron microscopy confirms that the number of gold nanostars aggregated around each bacterium correlates closely with the colorimetric response. Thus, gold nanostars serve as a promising platform for rapid visual identification of ocular pathogens with application in point-of-care diagnostics.

4.2 Introduction

Microbial keratitis poses a great risk for vision loss [1]. Contact lenses are the most common risk factor that predispose wearers to keratitis [153-159]. The fundamental challenge in mitigating keratitis is detecting these pathogens early and more importantly, identifying the species for designing a more effective treatment regimen [160-162]. As reviewed in Chapter 2, the current gold standard for identifying the pathogens relies on microbial cultures or genomic analysis, which must be done in a central laboratory [3]. Recent advances in biosensors offer the potential to perform these tests at the point-of-care [5, 6]. Common approaches employ a colorimetric method [98, 163] or microelectronics for sensing [164-167]. A recent study has shown improvement of detection capabilities to allow sub-cellular measurements of individual cells [4]. However, a major challenge remains to be solved: identifying species of bacteria at the point-of-care, which is crucial because of growing antibiotic

resistance [1] and unique drug susceptibility profiles of pathogens [168]. Lately, the prevalence of Gram-negative *Achromobacter* [169-171], *Stenotrophomonas* [172], and *Delftia* [173] has been emphasized because of their innate ability to form biofilms in contact lenses and their accompanying lens cases. Moreover, these pathogens present an increasing problem due to their capability to survive in contact lens care solutions [174] and cause microbial keratitis [158]. Hence, there exists a need for a platform that rapidly identifies multiple pathogens affecting contact lens wearers.

Gold nanoparticles have been used extensively as colorimetric biosensors due to their high extinction coefficients, enhanced scattering, unique localized surface plasmon resonance and high surface area to volume ratio [8, 175, 176]. The optical properties of gold nanoparticles can be further exploited by varying their shape, size and surface characteristics. As demonstrated in Chapter 3, gold nanostars are an interesting class of nanoparticles; their optical properties can be fine-tuned by altering the size and degree of branching [9, 122, 126]. Nanostars coated with specific antibodies have demonstrated the colorimetric detection of a single species of bacteria [93], but a ubiquitous platform for the colorimetric detection and identification of bacteria is rare. A small body of work is present on the use of cationic nanoparticles coupled with fluorescent polymers for identification of bacteria using a "chemical nose" approach, where a unique set of responses is obtained for each species of pathogen [15, 16]. The existing methods require the modification of gold nanoparticles with multiple ligands and the use of a fluorescent spectrometer, which is not easily accessible in a point-of-care setting. In Chapter 3, a library of gold nanostars was developed with tunable color change in the presence of *S. aureus* [9]. Here, we show that gold nanostars can be used as a "chemical nose" not only for detecting bacteria but also identifying their species without the use of antibodies or aptamers. The specificity of the "chemical nose" is a result of the ability of cationic gold nanostars to electrostatically aggregate around bacteria and provide a colorimetric response based on intrinsic physicochemical differences between bacteria, such as surface charge, surface area, and morphology [9].

4.3 Materials and Methods

4.3.1 Materials

All the chemicals and containers used in this study were from the same sources as those mentioned in Chapter 3. Additionally, *Staphylococcus aureus* (ATCC 6538), *Achromobacter xylosoxidans* (ATCC 27061), *Delftia acidovorans* (ATCC 15668), and *Stenotrophomonas maltophilia* (ATCC 13637) were purchased from Cedarlane Labs (Burlington, ON, Canada). All procured chemicals were used without further purification. The vials used for gold nanoseed synthesis were rinsed with Millipore water and air dried before use.

4.3.2 Synthesis of gold nanostars

The gold nanoseed precursor was synthesized using the simple two-step one pot process described in Chapter 3 [9, 124]. Briefly, 60 µL of 0.1 M freshly prepared ice-cold sodium borohydride was added to 20 mL of a gold (III) chloride hydrate (2.4×10^{-4} M) and trisodium citrate dihydrate (10^{-4} M) solution under vigorous stirring. The sample was incubated overnight in the dark in ambient conditions, filtered (0.2 μm), and stored at 4 ^{o}C until use.

To synthesize the gold nanostars, a scaled-up version of procedure from Chapter 3 employing cetyltrimethylammonium bromide (CTAB) as a negative template was used [9]. CTAB (7.33 mM in Millipore water) was dissolved at 60 °C and with magnetic stirring for 10 min. After this, the 7.33 mM CTAB solution was partitioned into two aliquots. The second aliquot was diluted 1:5 (1.47 mM in Millipore water). 210 mL of each CTAB solution was used for synthesis: 7.33 mM CTAB for blue nanostars and 1.47 mM for red nanostars. Gold (III) chloride hydrate (8.97 mL, 11 mM) and silver nitrate (1.34 mL, 10 mM) were added to each CTAB solution under moderate stirring for 1 min. Then, L-ascorbic acid (1.44 mL, 100 mM) was added dropwise. Upon addition of the last drop of L-ascorbic acid, the solutions turned clear, and the appropriate volume of gold nanoseed (2.24 mL for blue nanostars and 5.60 mL for red nanostars) was immediately added. After seed addition, each sample was allowed to stir for another 1.5 min and sit in ambient conditions for an additional 10 min. Centrifugation was then performed at 10,000 rpm for 15 min and the supernatant was removed and replaced with 1 mM CTAB solution (in Millipore water). These two nanostars were mixed (1:1 by volume) to obtain the purple nanostars. When the term ‘mixed’ is used in this thesis, the ratios refer to

the volumes of solutions that were mixed together. For example, when the blue and red nanostars are mixed 1:1 by volume, both the nanoparticles are being diluted by a factor of 2. Thus, it is equivalent to saying that blue nanostars were diluted 1:2 in red nanostars. Gold nanostars were found to be stable in the dark at room temperature for months.

4.3.3 Bacterial culture

S. aureus, A. xylosoxidans, D. acidovorans, and *S. maltophilia* were inoculated on TSA plates and incubated at 37 °C for 24 hours. Bacterial cells were harvested using alginate swabs and suspended in 5 mL of sterile saline (2.55%) with nutrient broth (~0.006%) in a 15 mL centrifuge tube. Each bacterial strain was then washed seven times with 2.55% saline (with ~0.006% nutrient broth) by centrifugation at 4,000 rpm for 10 min. The bacteria were then diluted to obtain an optical density at 660 nm (OD_{660}) of 0.1 (~10^8 CFU/mL [172]). When normalized against blank saline absorbance (0.033), this value becomes 0.067. When added to gold nanostars, the solution is diluted 1:3 to obtain final OD_{660} = 0.02 for bacteria.

4.3.4 Identification of bacterial species

The assay for identification of bacterial strains was performed in 96-well microplates. The plates were prepared by adding 200 µL of blue, red, or purple gold nanostars to the microplate wells. The training set was obtained by adding 100 µL of each bacteria (4 strains) to the gold nanostars at final OD_{660} = 0.02. Saline (with ~0.006% broth) was used as a control group. Each training group had 7-8 replicates. In order to obtain unknown samples, 14-18 samples from each group were selected and added randomly to a sterile storage microplate, resulting in a total of 79 samples. Each of these samples was then added to blue, red, and purple gold nanostar solutions and incubated at room temperature overnight along with the training set. In the case of purple nanostar solution, assuming the concentration of particles is the same as the amount of seed used, the ratio of nanoparticles to bacteria is approximately 10^4.

After incubation, the microplates were illuminated by an X-ray film viewer and imaged using a Canon EOS Rebel T3 digital camera. For spectrophotometric identification, the UV-Visible absorption spectra were obtained for each well in the microplates using a BioTek Epoch microplate spectrophotometer while scanning from 300 nm to 900 nm with a step size of 1 nm.

After obtaining the absorption spectra, the normalized absorbance values were obtained for all samples by using the following equation:

$$\text{Normalized absorbance} = (\text{Average saline control absorbance at } \lambda - \text{Average saline control absorbance at 800 nm}) - (\text{Sample absorbance at } \lambda - \text{Sample absorbance at 800 nm})$$

where λ is the wavelength of particular importance: 583 nm peak for blue nanostars, 541 nm peak for red nanostars, and 544 nm peak and 583 nm for purple nanostars. The absorbance at 800 nm was used as the baseline. The data were then subjected to a classical linear discriminant analysis (LDA) using MySTAT (version 12.02) where each population in the training set was assigned a numerical identifier and this identifier was used as the grouping variable while the normalized absorbance values from the purple nanostars were used as the two predictors. Classification of unknown samples was performed by determining the shortest Mahalanobis distance (a measure of the distance between a point and a distribution) to the groups generated using the training matrix. During the identification of unknown bacteria samples, the experiment preparation and data collection were performed by two different researchers resulting in a blinded process.

4.3.5 Transmission electron microscopy of bacteria and gold nanostars

Blue gold nanostars were chosen as a representative sample for imaging using transmission electron microscopy (TEM). Samples were prepared by adding 5 µL of the overnight incubated bacteria and gold nanostars solution to copper TEM grids and allowed to dry under ambient conditions overnight. Once dry, the samples were washed by placing 5 µL of Millipore water on the TEM grids for 30 seconds and then wicking the liquid using filter paper to remove excess surfactants, salts, and unbound gold nanostars. The samples were then imaged using Phillips CM10 TEM. The total number of gold nanostars aggregated around the surface of each bacterium was manually counted using the National Institutes of Health ImageJ software (n = 8).

4.4 Results and Discussion

4.4.1 Visual color change with gold nanostars

In order to develop a "chemical nose," we need various gold nanoparticles that can interact with bacteria to provide a specific response. We hypothesize that if gold nanostars with different sizes and degrees of branching are incubated with a particular species of bacterium, each nanostar will provide a unique colorimetric response. To test this hypothesis, we chose the commonly occurring Gram-positive *S. aureus* and Gram-negative ocular pathogens *A. xylosoxidans, D. acidovorans,* and *S. maltophilia* as the pathogens of interest [177] and added them to gold nanostars to obtain a drastic colorimetric response. Two types of nanostars were synthesized such that there would be distinct differences in color (blue and red), size, and degree of branching based on Figure 4, 6, and 7 from Chapter 3. Thus, each nanostar solution should interact differently between species of bacteria depending on a species' surface charge, surface area, and morphology to provide a "chemical nose" sensor. The blue nanostars have a greater size and higher degree of branching (Figure 14 a) as compared to the red nanostars, which are smaller and more spherical in shape (Figure 14 b). These two nanostar solutions were also mixed 1:1 by volume to obtain a third solution of purple nanostars in order to investigate the co-operative response from the two nanoparticles. The three nanostar solutions were added to adjacent microplate wells and mixed with saline with nutrient broth (as control) and different species of bacteria at the same optical density. A sample image is presented in Figure 14 c), where the bacterial species are visually discernible. Amongst these species, *S. aureus* and *S. maltophilia* present the most striking differences as compared to saline. In the case of *S. aureus*, the gold nanostar solutions have a tinge of their respective original color whereas for *S. maltophilia*, the samples lose their original color to nearly clear. This suggests a more complete aggregation of gold nanostars in the presence of *S. maltophilia* as compared to other species of bacteria. *D. acidovorans* and *A. xylosoxidans* produce a lower degree of color change. In the case of *D. acidovorans*, a color change of the red nanostars is seen to a slight purple, which is unique in comparison to other species. Thus, the red nanostars show a more drastic color change as compared to blue nanostars which allows for visual distinction between *A. xylosoxidans* and *D. acidovorans*. The purple nanostar solution behaves similar to blue stars in the case of *S. aureus* but it appears to be a superposition of blue and red nanostar responses in the presence of all other species of bacteria.

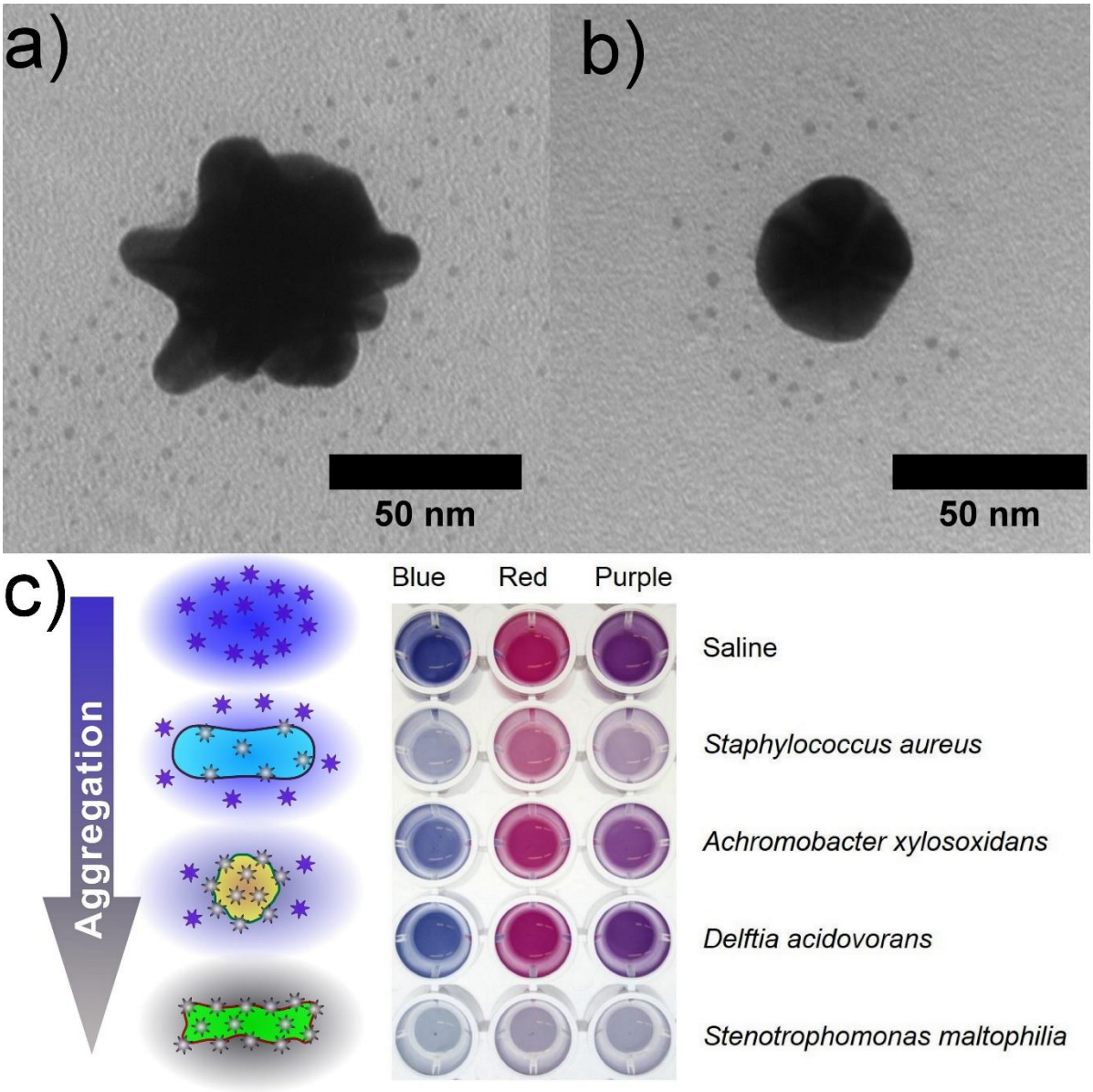

Figure 14: Transmission electron microscopy images of a) branched blue gold nanostar and b) spherical red gold nanostar. c) Change in color of gold nanostars caused by varying degrees of aggregation due to the differences in surface charge, surface area and morphology of bacteria. The photograph shows the color when species of bacteria prepared at OD_{660} = 0.02 are added to different gold nanostars.

4.4.2 Colorimetric identification of bacteria

The absorption spectra of each gold nanostar solution in the presence of bacteria are presented in Figure 15 a-c. The observations from the spectra are consistent with the visual observations where *S. maltophilia* shows the most drastic change in spectra. In the case of blue nanostars, the peak with *S. maltophilia* is almost flattened whereas for red nanostars, there is partial flattening. The purple nanostar responses appear to be a linear combination of blue and red nanostars. In the case of *D. acidovorans*, while the absorbance peak does not drop significantly for red and purple nanostars, a red shift and drop is observed for blue nanostars (Figure 15 a). In all other bacterial species, the location of absorbance peak remains consistent but the absorbance values are reduced. Each gold nanostar solution has a unique absorption peak, which resembles the localized surface plasmon resonance wavelength. As shown in Figure 15 a-b, blue and red nanostars have peaks at 583 nm and 541 nm respectively. Purple nanostars have a peak at 544 nm (close to that of red nanostars); however, the absorbance at 583 nm is also of interest to determine the response characteristics from the blue nanostars constituents. The absorbance at 541 nm of red nanostars constituents was not found to be important since it was close to the natural peak of 544 nm of purple nanostars. The absorbance values from these peaks were obtained and normalized against saline with broth as well as baseline absorbance at 800 nm. These normalized values are presented in Figure 15 d) and demonstrate that each species of bacteria interacts in a unique manner with blue, red, and purple nanostar solutions. We further analyzed these normalized values to create a training set for the identification of species of bacteria.

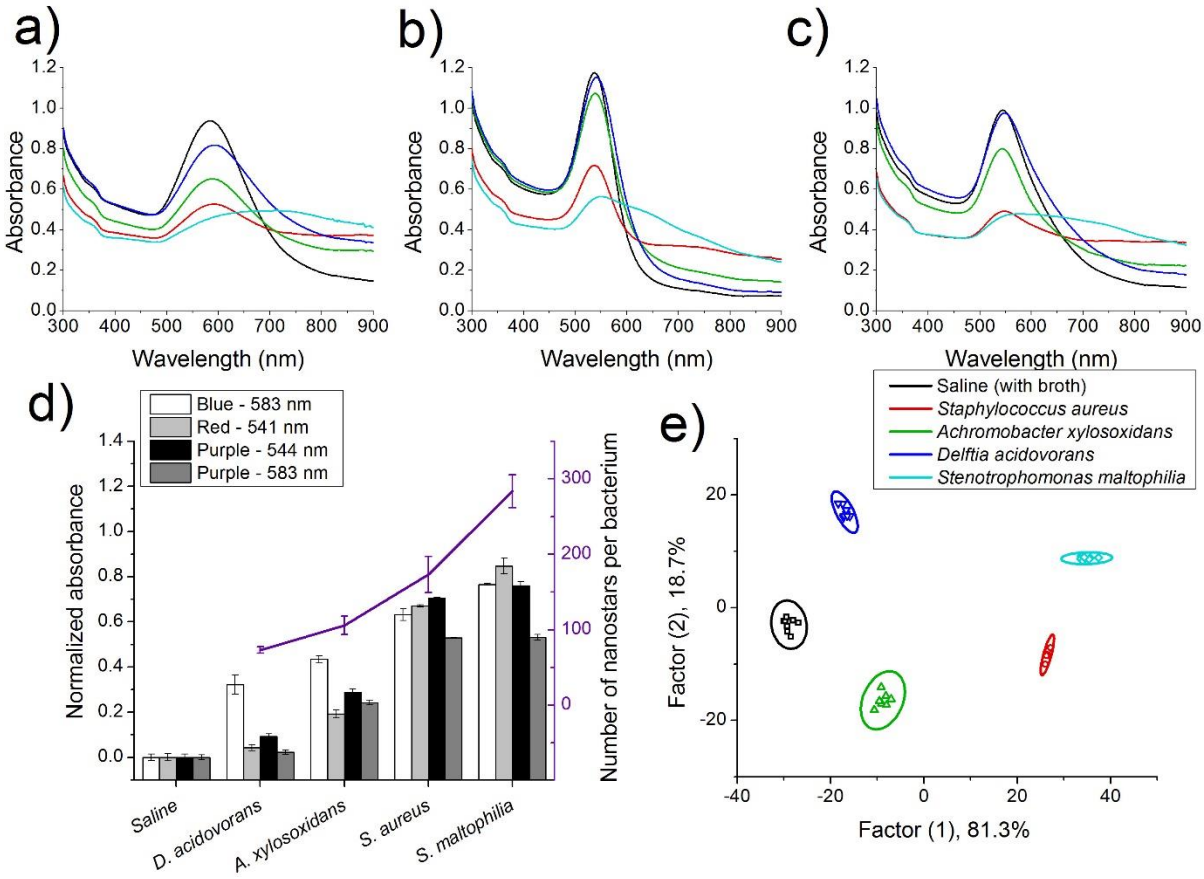

Figure 15: Response of gold nanostars to saline (with broth) control and different species of bacteria at OD_{660} = 0.02. Absorption spectra of: a) blue nanostars; b) red nanostars; c) purple nanostars. d) Normalized absorbance response (n = 7–8; mean ± S.D.) and average number of aggregated gold nanostars per bacterium by transmission electron microscopy (n = 8; mean ± S.E.). e) Canonical scores plot of the response from linear discriminant analysis of purple nanostars (544 nm and 583 nm) for different species of bacteria. 95% confidence ellipses are presented for each population.

Using LDA, we observed that identification of each population of bacteria was possible by using the two normalized absorbance values from purple nanostars (544 nm and 583 nm). This is demonstrated in Figure 15 e), where each species of bacteria as well as saline control is statistically discernable using 95% confidence intervals. LDA is a useful technique in this scenario because it maximizes inter-group variance while minimizing intra-group variance. Here, factors are a linear

combination of the absorbance values from purple nanostars as determined by their respective canonical discriminant functions using MySTAT:

$$\text{Factor (1)} = -28.9 + 154.9 * \text{Purple}_{544\text{ nm}} - 101.8 * \text{Purple}_{583\text{ nm}}$$

$$\text{Factor (2)} = -3.0 + 325.0 * \text{Purple}_{544\text{ nm}} - 443.3 * \text{Purple}_{583\text{ nm}}$$

Thus, factor (1) gives a greater weight to the absorbance at 544 nm while factor (2) gives more weight to absorbance at 583 nm but the values from both of these wavelengths are required for discriminating the populations of bacteria since neither coefficients are negligible as compared to the other. This training set was then used to identify unknown samples using MySTAT ($p > 0.95$), and it was demonstrated that 99% (78/79 samples) of the samples could be identified accurately with their respective group. Only one of the samples was incorrectly classified as *S. aureus* when it was supposed to be *A. xylosoxidans*. We are currently investigating this outlier and also methods to eliminate misclassification. Overall, these are noteworthy results since only two inputs are being used to identify five different populations of samples. It has been demonstrated that the unique surface charge on different species of bacteria can be utilized for identification when electrostatic interactions are used [15]. Previous work required the modification of gold nanoparticles with a variety of molecules to provide unique surface charges and hydrophobicity for enhancing the interaction with bacteria. Additionally, these gold nanoparticles are generally coupled with fluorescent polymers to provide the response and hence require fluorescence spectrometry. In the present study, identifying bacterial species was possible visually as well as spectrophotometrically. We exploit the inherent properties of gold nanostars rather than modifying them with specific surface ligands. The CTAB surfactant of gold nanostars is present on as-synthesized nanoparticles and serves as the source of positive surface charge. We have shown in Figure 13 of Chapter 3 that the CTAB-coated nanostars (zeta potential of +38.0 mV) require a polyanionic surface for aggregation and color change [9]. Such a polyanionic surface is provided in Gram-positive bacteria by teichoic acids [137, 178] and in Gram-negative bacteria by lipopolysaccharides and phospholipids [101, 179]. The intrinsically different distribution of charges on the surface of bacteria caused by the composition of proteins, polysaccharides, and lipids [180-182] is responsible for causing the unique electrostatic interactions with gold nanostars. This unique surface composition can be considered to be a fingerprint of the bacteria and probed using the gold nanostars to obtain a colorimetric response. It is expected that gold

nanostars with significant protruding branches will interact more strongly with the surface of bacteria due to higher effective surface area and spatial extent as compared to more spherical nanostars [9]. These inherent differences in branching and size provide different colorimetric outputs since their localized surface plasmon resonance is sensitive to the degree of aggregation [150].

4.4.3 Transmission electron microscopy imaging of bacteria

We used TEM to confirm that the gold nanostars were aggregating around the bacteria of interest (Figure 16). It was observed that gold nanostars aggregate around bacteria with different shapes (spherical or rod-like) as well as types (Gram-positive or Gram-negative). The TEM samples were rinsed with Millipore water once before drying to remove excess gold nanostars and assist in visualization. Since gold nanostars remained on the bacteria even after rinsing, the images suggest a strong electrostatic interaction, which governs the degree of aggregation and hence the colorimetric response provided by the gold nanostars. This is shown in Figure 15 d) since a close correlation is observed between the number of blue gold nanostars aggregated per bacterium and the normalized absorbance observed for the blue nanostars.

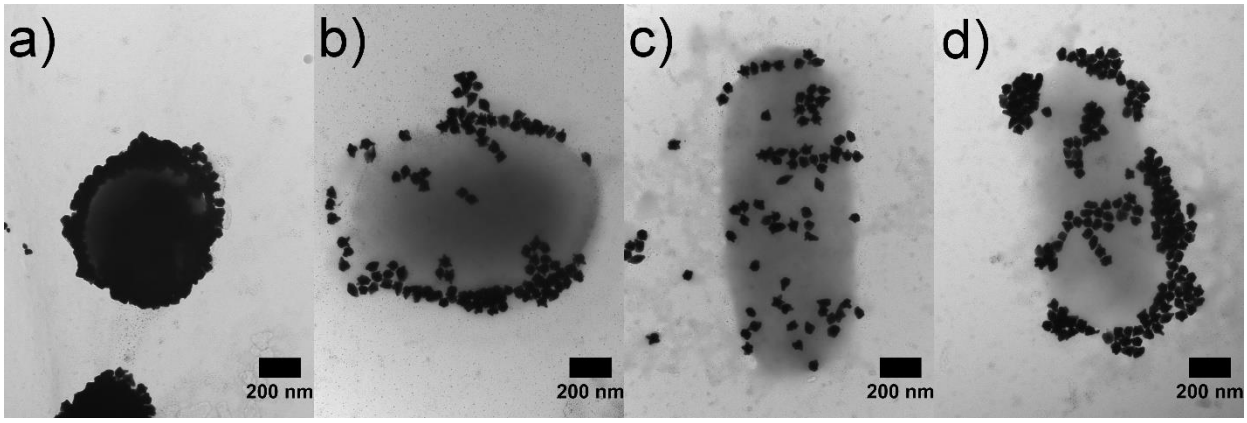

Figure 16: Transmission electron microscopy images of blue gold nanostars aggregating around bacteria: a) *Staphylococcus aureus*, b) *Achromobacter xylosoxidans*, c) *Delftia acidovorans*, d) *Stenotrophomonas maltophilia*. Scale bars are 200 nm each.

In contrast to the results reported in Figure 15 d), at the relevant pH (~7) and electrolytic condition (0.85% NaCl, 1:1) one might expect that *S. aureus* would have a greater number of gold nanostars

aggregated – thus greater normalized absorbance – when compared to *S. maltophilia* due to surface charge since the former is Gram-positive and the latter is Gram-negative [183]. Moreover, there appears to be a higher density of gold nanostars aggregated around *S. aureus* than *S. maltophilia* in Figure 16 a) and d), respectively. However, total gold nanostar aggregation response depends on surface area in addition to surface charge as previously mentioned. Thus, as seen in the TEM images the greater size and rod shape of *S. maltophilia* leads to a much greater surface area. Despite *S. aureus* being Gram-positive, the combination of greater surface area and relatively high number of polyanionic surface charges of *S. maltophilia* yield to a greater number of total gold nanostar aggregated per bacterium and thus a greater normalized response, as was reported in Figure 15 d).

In addition to the number of gold nanostars per bacterium, the pattern of aggregation also seems to be unique. For example, in Figure 16 c), the gold nanostars around *D. acidovorans* are distributed throughout the cell and form a sparse coating. On the other hand, in Figure 16 d), there appear to be patches of aggregated gold nanostars in localized areas on the surface of *S. maltophilia*, while some areas are completely devoid of gold nanostars. In a previous study, the aggregation of 6 nm cationic gold nanoparticles has shown a unique aggregation pattern around the Gram-positive bacteria *Bacillus subtilis* as compared to the Gram-negative *Escherichia coli* [138]. It was demonstrated that the patterns disappeared once the bacteria were exposed to proteolytic cleavage suggesting the importance of surface proteins in the aggregation of gold nanoparticles [184]. We demonstrate that aggregation patterns are not limited to Gram-positive bacteria as they also appeared on Gram-negative *S. maltophilia* (Figure 16 d). Gold nanostars can thus be used as probes for exploring the surface morphology, protein and lipid distribution, and local charge densities of bacteria in future studies.

Additionally, aggregation of gold nanoparticles around bacteria has been observed when modified with specific antibodies against the bacteria [93, 185] but these studies typically detect a single bacterial species. In past work, biomodification becomes necessary when the detection of multiple species of bacteria is involved [186]; however, in the current work we have demonstrated the ability to distinguish between species without adding specific ligands to the surface of gold nanostars, while relying on the intrinsic response of gold nanostars to bacteria instead. The simplicity and rapid

response of the assay gives the potential of implementation in a consumer product or at the point-of-care.

4.5 Conclusions

We demonstrated that gold nanostars are a versatile platform for identifying species of bacteria such as *S. aureus, A. xylosoxidans, D. acidovorans*, and *S. maltophilia*, where all the species were visually discernible and 99% of the samples were identified correctly using a spectrophotometer and LDA. The use of two different CTAB-coated gold nanostars provided unique colorimetric outputs corresponding to the dependence of electrostatic interactions on size and shape of nanostars and surface characteristics of bacteria. TEM was used to show a correlation in the degree and pattern of aggregation and the colorimetric response of gold nanostars in the presence of both Gram-positive and Gram-negative bacteria. Thus, CTAB-coated gold nanostars are a promising "chemical nose" platform for simple visual identification of bacterial contaminants for point-of-care diagnostics.

Chapter 5
Quantification of bacteria and detection of polymicrobial mixtures using “chemical nose”

5.1 Summary

Rapid and portable diagnosis of pathogenic bacteria can save lives lost from infectious diseases. Current biosensor technologies normally require sophisticated instruments and highly skilled personnel to detect bacteria with high accuracy. Here, we show that a “chemical nose” based on spherical and branched gold nanoparticles can accurately detect pathogenic bacteria in monomicrobial and polymicrobial samples. A unique colorimetric response is obtained from the “chemical nose” for each pathogen, depending on the size and morphology of gold nanoparticles, the lipid distribution of the bacterial membrane, and the surface configuration of the cell wall. The “chemical nose” serves as a universal platform for simple colorimetric detection and identification of eight species of bacteria across two orders of magnitude of concentration (89% accuracy), as well as binary and tertiary mixtures of the three most common hospital-isolated pathogens: *Staphylococcus aureus*, *Escherichia coli*, and *Pseudomonas aeruginosa* (100% accuracy). Using transmission electron microscopy and blot assays, we demonstrate that extracellular polymeric substances play an important role in controlling the degree of interaction between gold nanoparticles and bacterial cell surface. Simulations of nanoparticle aggregates using Maxwell-Garnett theory show that distinguishable color changes between bacteria are due to different types and extent of aggregation of nanoparticles. We present a versatile biosensor that does not require complex modification of gold nanoparticles with biomolecules nor expensive equipment and hence can be implemented at the point-of-care.

5.2 Introduction

Detecting and identifying multiple bacteria in a complex microbial community is challenging due to the large number of possibly interacting components. Conventional biosensors focus on a ‘lock and key’ recognition strategy [12], which utilizes biomolecules such as aptamers and antibodies to offer high sensitivity and specificity [31, 187-190]. However, detecting multiple pathogens requires the use of unique biomolecules for each target of interest, which makes the development of broad-spectrum

biosensors cumbersome. An alternative method for developing versatile biosensors involves the use of a “chemical nose” where a set of interactions between the pathogen and sensors produce unique patterns of response, in a manner similar to the functioning of our sense of smell [12-14]. Designing a “chemical nose” biosensor requires minimal prior knowledge of the analyte because the system can be ‘trained’ to recognize various analytes [12]. Such “chemical nose” sensors have been used for detecting various targets such as amino acids [191], proteins [192], carbohydrates [193], volatile organic compounds [194], bacteria [15, 16, 84, 195], and cancer cells [130, 196-198].

Typically, nanoparticle-based “chemical nose” biosensors require the modification of nanoparticle surface with multiple ligands where each ligand is responsible for a unique interaction with the target [13, 16]. These modifications can add complexity to the synthesis of the biosensor. Additionally, existing “chemical nose” biosensors are unable to detect and identify mixtures of bacteria, which is crucial for diagnosing polymicrobial infections. Here, we show that a “chemical nose” biosensor based on gold nanoparticles can be used to detect and identify bacteria at various concentrations and combinations. We have utilized a single molecule, cetyltrimethylammonium bromide (CTAB)—a typical surfactant used for synthesis of gold nanoparticles—for providing electrostatic interactions between nanoparticles with various morphologies and surface features of bacteria. The inherent differences in nanoparticle size, shape, and aggregation behaviour produce unique changes in the absorption spectra and hence produce a versatile “chemical nose” biosensor.

In Chapter 3, using a few Gram-positive and Gram-negative organisms, we demonstrated that the size and shape of gold nanoparticles can govern the colorimetric response [9, 199]. In Chapter 4, using a limited set of four ocular pathogens at a single concentration, we have also shown that discriminating between bacterial species requires the use of a mixture of nanoparticles such that each type of nanoparticle contributes uniquely to the observed color change [84]. In this chapter, we provide a “chemical nose” that is able to not only detect and identify a much larger set of eight different species of bacteria at three different concentrations, but also discriminate between polymicrobial mixtures by using the entire absorption spectrum instead of just the peaks. We also demonstrate the crucial role of extracellular polymeric substances in controlling the response of the “chemical nose” to the different bacterial species. Simulations of gold nanoparticle aggregation

highlight that different types of aggregates are responsible for producing unique colorimetric responses to bacteria.

5.3 Materials and Methods

5.3.1 Materials

All the chemicals and containers used in this study were from the same sources as those mentioned in Chapter 3. Additionally, Amersham™ Protran® Supported nitrocellulose (NC, 0.2 μm pore size) membrane, lipopolysaccharides (LPS-S) from *P. aeruginosa* 10, rough strain (Rd) lipopolysaccharides (LPS-R) from *E. coli* F583, peptidoglycan (PepG) from *S. aureus*, and lipoteichoic acid (LTA) from *S. aureus* were purchased from Sigma-Aldrich (Oakville, ON, Canada). BD TSA with 5% sheep blood (TSA II) culture plates and Amersham™ Hybond™ polyvinylidene difluoride (PVDF, 0.45 μm pore size) membrane were purchased from VWR (Mississauga, ON, Canada). Cardiolipin (CL), L-α-phosphatidylglycerol (PG), and L-α-phosphatidylethanolamine (PE) from *E. coli* were purchased from Avanti Polar Lipids (Alabaster, AL, USA). Also, *Pseudomonas aeruginosa* (ATCC 9027), *Staphylococcus aureus* (ATCC 6538), *Escherichia coli* (ATCC 10798), *Achromobacter xylosoxidans* (ATCC 27061), *Delftia acidovorans* (ATCC 15668), *Stenotrophomonas maltophilia* (ATCC 13637), *Enterococcus faecalis* (ATCC 29212), and *Streptococcus pneumoniae* (ATCC 6305) were purchased from Cedarlane Labs (Burlington, ON, Canada). All procured chemicals were used without further purification. The 20 mL vials used for gold nanoseed synthesis were cleaned using 12M sodium hydroxide and larger glassware was cleaned using aqua regia as described in published protocol [200].

5.3.2 Synthesis of gold nanoparticles

The gold nanoseed precursor was synthesized using the simple two-step one pot process described in Chapter 3 and 4 [9, 84, 124]. To synthesize gold nanostars and nanospheres, the procedure from Chapter 3 and 4 was used with changes in the amount of silver nitrate to get a greater distinction between the morphologies of nanoparticles [9, 84]. Briefly, 210 mL of 7.33 mM CTAB and 1.46 mM CTAB were used for nanostars and nanospheres respectively. Gold (III) chloride hydrate (8.97 mL, 11 mM) was added to each CTAB solution, followed by silver nitrate (1.34 mL for nanostars and 0.67 mL for nanospheres, 10 mM) under moderate stirring. Then, L-ascorbic acid (1.44 mL, 100 mM) was

added dropwise and the solution turned clear. The appropriate volume of gold nanoseed (2.24 mL for nanostars and 5.60 mL for nanospheres) was immediately added. The nanoparticles were purified by centrifugation at 10,000 rpm for 15 min resuspended in 1 mM CTAB solution. These two gold nanoparticle solutions were mixed (1:1 by volume) to obtain the purple "chemical nose" solution.

5.3.3 Bacterial culture

P. aeruginosa, S. aureus, E. coli, A. xylosoxidans, D. acidovorans and *S. maltophilia* were inoculated on Trypticase Soy Agar (TSA) plates and incubated at 37 °C for 24 hours. *E. faecalis* and *S. pneumoniae* were inoculated on TSA II plates and incubated at 37 °C for 24 hours, where *S. pneumoniae* was placed in a 5% CO_2 environment. Bacterial cells were harvested using alginate swabs and suspended in 5 mL of sterile saline (2.55%) with nutrient broth (~0.006%) in a 15 mL centrifuge tube. In the case of *S. pneumoniae,* cultures from two TSA II plates were combined due to low OD_{660} values of the culture, which is used for normalization. Each bacterial strain was then washed seven times with 2.55% saline (with ~0.006% nutrient broth) by centrifugation at 4,000 rpm for 10 min. The bacteria were then diluted to obtain an optical density at 660 nm (OD_{660}) of 0.10 ± 0.005 (~10^8 CFU/mL) [172]. The wavelength of 660 nm was chosen because it has previously been used for similar bacteria [172]. When the bacteria are added to gold nanoparticles, the solution is diluted 1:3 to obtain final OD_{660} = 0.03 for bacteria. The actual concentrations of bacteria were determined by plate counts method and is summarized in Table 8. Other concentrations of bacteria were obtained by diluting the bacteria solutions 1:5 or 1:25 in 2.55% saline (with ~0.006% nutrient broth).

Table 8: Concentration of bacteria determined by plate counts method when they are normalized to OD_{660} = 0.03. Here, 'well' refers to the microplate well which has a volume of 300 µL

Bacteria	Concentration (CFU/well)
Pseudomonas aeruginosa (ATCC 9027)	1.2×10^7
Staphylococcus aureus (ATCC 6538)	7.3×10^6
Escherichia coli (ATCC 10798)	5.4×10^6
Achromobacter xylosoxidans (ATCC 27061)	2.2×10^7
Delftia acidovorans (ATCC 15668)	8.1×10^6

Stenotrophomonas maltophilia (ATCC 13637)	1.1×10^7
Enterococcus faecalis (ATCC 29212)	1.1×10^7
Streptococcus pneumoniae (ATCC 6305)	4.8×10^4

5.3.4 Identification and quantification of bacteria

The assay for identification and quantification of bacterial species was performed in 96-well microplates. The plates were prepared by adding 100 µL of the bacteria or saline control in replicates of eight. This was followed by the addition of 200 µL of the purple "chemical nose" solution. The microplates were then placed on a Stovall Life Science Inc. (Peosta, IA, USA) Belly Dancer orbital shaker for 2 mins and then incubated overnight at room temperature in the dark. Although the color change is visible within five minutes for some samples [9], the color continues to evolve over time. The acquisition of absorption spectra for a microplate full of samples requires a few hours. Thus, the overnight incubation ensures that changes in spectra during acquisition are insignificant compared to the changes during incubation time. After incubation, the UV-Visible absorption spectra were obtained for each well in the microplates using a BioTek (Winooski, VT, USA) Epoch microplate spectrophotometer while scanning from 300 nm to 999 nm with a step size of 1 nm.

The training set was obtained by selecting three replicates out of eight and the other five replicates were randomized by an independent researcher. The researcher performing data analysis remained blind to the identity of the randomized samples. Using MathWorks® MATLAB®, the spectral data from the training set was used for performing hierarchical clustering analysis (HCA) on bacteria with $OD_{660} = 0.03$, using Euclidean distance and Ward's method and the corresponding dendrogram is presented in Figure 21 a. For classification, the training set was used to perform principal component analysis (PCA) and obtain the corresponding scores as well as coefficients. These principal component scores were used in the training of the linear discriminant analysis (LDA). Since obtaining the principal scores requires normalization by the mean of each response (wavelength), the randomized samples were normalized by these mean values and then translated to principal scores using the coefficients obtained from PCA. The gold nanoparticles show a unique spectral shift for each bacterial species and thus, the shape of the absorption spectra is unique for each species. Thus, all 700 wavelengths (300-999 nm) were used for PCA instead of selecting specific wavelengths to

avoid biasing the data towards one specific pattern. Also, the use of all wavelengths allows this analysis to be adaptable if a more complex mixture of nanoparticles is used with multiple absorption peaks. PCA will assign a low weight to the wavelengths that do not significantly contribute to the variance of responses. The PCA scores were used for determining the group in which the unknown samples belonged, by LDA, where each group corresponds to either control or a bacterium at a particular concentration.

Furthermore, a concentration dependent response for each bacterial species was obtained by normalizing each species to OD_{660} = 1.0 ± 0.05, then diluting them in 2.55% saline 16x, 32x, 64x, 128x, 256x, and 512x. Then, 100 µL of each of these dilutions were added to 200 µL of the purple gold nanoparticle solutions and absorption spectra were obtained after overnight incubation. After obtaining the absorption spectra, the normalized absorbance values were obtained for all samples by using the following equation:

$$\begin{aligned} &Normalized\ absorbance \\ &\quad = (Average\ saline\ control\ absorbance\ at\ 540\ nm \\ &\quad - Average\ saline\ control\ absorbance\ at\ 800\ nm) \\ &\quad - (Sample\ absorbance\ at\ 540\ nm - Sample\ absorbance\ at\ 800\ nm) \end{aligned}$$

where absorption at 540 nm is the absorbance at the peak of nanoparticles in saline and absorbance at 800 nm serves as a baseline. The normalized absorbance is plotted for each bacteria assuming that OD_{660} = 1.0 has an approximate concentration of 10^9 CFU/mL [172].

5.3.5 Identifying mixtures of bacteria

Mixtures of *P. aeruginosa*, *S. aureus*, and *E. coli* were prepared by using the OD_{660} = 0.10 ± 0.005 solutions and mixing them 1:1 and 1:1:1 by volume for binary and tertiary solutions respectively. Saline control and each of the bacteria samples were added to the 96-well microplate as before, and then the purple "chemical nose" solution was added and mixed. Three out of eight replicates were used as a training set, while the other five were randomized and used for identification. PCA and LDA was performed using MATLAB® as before.

5.3.6 Removal of extracellular polymeric substances (EPS)

An EPS extraction protocol was used on *S. aureus*, *E. coli*, and *A. xylosoxidans* with a slight modification of published method [201]. The bacteria were first incubated on TSA plates at 37 °C for 24 hours. Bacterial cells were harvested using alginate swabs and suspended in 10 mL of sterile saline (2.55%) with nutrient broth (~0.006%) in 15 mL centrifuge tubes. 60 µL of formaldehyde was added to a 5 mL aliquot of the bacterial suspension and the rest of suspension was used as a control. The tubes were incubated at 4 °C for 1 hour. Then, 4 mL of 1M sodium hydroxide was added to the treatment tube and saline was added to control tubes and incubated at 4 °C for an additional 3 hours. In order to remove EPS from the cells, the bacteria were washed by centrifugation at 4000 rpm for 10 minutes seven times. The bacteria concentration was then normalized to obtain $OD_{660} = 0.10 \pm 0.005$ (~10^8 CFU/mL) [172] as before and 100 µL of bacteria were added to 200 µL of purple "chemical nose" solution.

When extracting EPS for lipid blots, only *E. coli* was cultured on TSA plates and extracted using alginate swabs. First 60 µL of formaldehyde was added to 10 mL suspension of *E. coli* in saline and then treatment with sodium hydroxide was implemented as outlined above. The tubes were then centrifuged at 10,000 rpm for 30 minutes. Supernatant containing EPS was collected, filtered (0.2 µm), and dialysed (3,500 Da) for 24 hours at 4 °C before vacuum drying for 48 hours.

5.3.7 Cell surface component blotting on membranes

Phospholipids (PG, PE, CL) were dissolved in chloroform to a final concentration of 2 mM. Other cell surface components (LPS-S, LPS-R, LTA , PepG) were dissolved or suspended in Millipore water to a final concentration of 2.86 mg/mL. Chloroform-based solutions were blotted onto PVDF in 2 µL volumes and water-based solutions were blotted onto NC in 2 µL volumes. Chloroform and water blanks (2 µL) were included on PVDF and NC blots, respectively. Membranes were then dried in the dark for 1 hour under ambient conditions.

In order to test the effect of EPS, it was dissolved in Millipore water to a final concentration of 2.86 mg/mL (15x) and 0.191 mg/mL (1x). After drying, PG, PE, and CL blots on PVDF were overlaid with 30 µL of 1x EPS solution and vacuum dried for 2 hours. Also, after drying of other component blots, 2 µL of 15x EPS solution was blotted overtop the LPS-S, LPS-R, LTA, and PepG blots and

dried for an additional 1 hour in the dark under ambient conditions. Control blots of chloroform- and water-based solutions were overlaid with 30 μL and 2 μL of Millipore water, respectively.

Once dried, membranes were transferred into a 10 mL bath of purple "chemical nose" solution and incubated on the Belly Dancer orbital shaker for 10 minutes. Following nanoparticle incubation, membranes were transferred to 100 mL of Millipore water and washed for 1 minute with gentle shaking. Washed PVDF and NC membranes were photographed using a Canon EOS REBEL T3 digital camera. Image processing and data collection was done using ImageJ (National Institutes of Health). Images were first separated into RGB color channels. Background illumination was normalized by plotting Mean Green Values for 22-26 empty membrane regions (circular selection, 150 px diameter) against centroid coordinates. Linear regression was then performed using Microsoft Excel to generate x- and y-coordinate correction factors. Mean Green Values were then collected for each blot center (circular selection, 150 px diameter). These values were normalized for background illumination by applying the following transformation:

$$Value_{corrected} = Value_{raw} - x_{centroid} * m_x - y_{centroid} * m_y$$

where x and y are the x and y co-ordinates, m_x is the slope of the x co-ordinate vs. background green values, and m_y is the slope of the y co-ordinate vs. background green values.

Group means and standard deviations for each experimental condition were then determined using the corrected values and normalized against the control blots (chloroform + water and water + water, for PVDF and NC respectively). Statistical significance was determined in Microsoft Excel using one-tailed heteroscedastic t-tests.

5.3.8 Transmission electron microscopy

Red gold nanosphere and blue gold nanostar solutions were prepared for transmission electron microscopy (TEM) by adding 5 μL to a copper grid and drying under ambient conditions overnight. Similarly, mixtures of bacteria and gold nanoparticles (5 μL) were added to formvar coated copper TEM grids and allowed to dry under ambient conditions overnight. Once dry, the bacteria samples were washed by placing 5 μL of Millipore water on the TEM grids for 30 seconds and then wicking the liquid using filter paper to remove excess surfactants, salts, and unbound gold nanoparticles. The samples were then imaged using a Phillips (Eindhoven, The Netherlands) CM10 TEM.

5.3.9 Modeling of gold nanoparticle aggregation

The optical characteristic of gold nanoparticle aggregates was estimated using Maxwell-Garnett effective medium theory [202]. Here, spherical gold nanoparticles with a radius of 15 nm and six different types of aggregates (Figure 17 a) were simulated. Every aggregate was assumed to be a compact cluster which was smaller than optical wavelength and well-separated to other aggregates in solution. The effective permittivity (ε_{eff}) of these six different aggregation types was calculated with the Maxwell-Garnett equation:

$$\frac{\varepsilon_{eff} - \varepsilon_s}{\varepsilon_{eff} + 2\varepsilon_s} = V_a \times \frac{\varepsilon_a - \varepsilon_s}{\varepsilon_a + 2\varepsilon_s}$$

where V_a is the volume fraction of gold nanoparticles in solution as shown by boxes in Figure 17 a, ε_a is the complex permittivity of gold [203], and ε_s is the permittivity of water [204]. The absorption coefficient (α_{abs}) of the six aggregate types was then calculated [205]:

$$\alpha_{abs} = \frac{4\pi}{\lambda}\kappa = \frac{4\pi}{\lambda}\sqrt{\frac{\sqrt{\varepsilon_1^2 + \varepsilon_2^2} - \varepsilon_1}{2}}$$

where κ is the extinction coefficient, λ is the wavelength of light, ε_1 and ε_2 denotes the real and imaginary parts of effective permittivity of aggregates respectively.

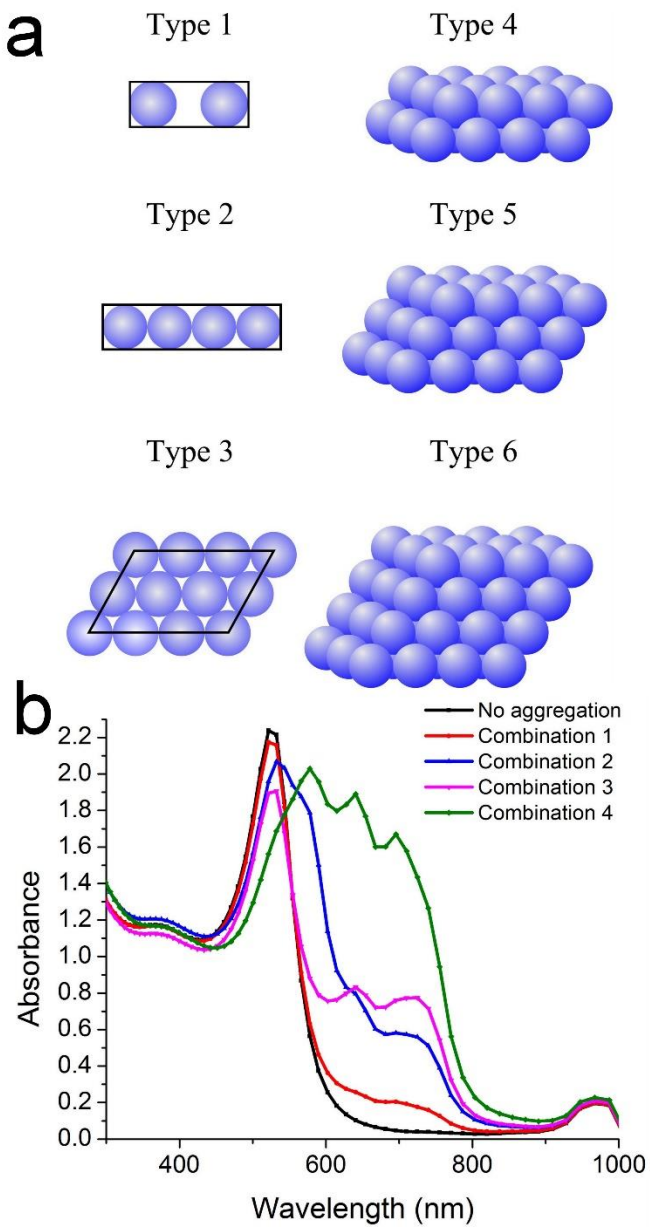

Figure 17: Different types of nanoparticle aggregates and their modeled absorbance spectra: a) schematic of aggregate types, the quadrilaterals in Types 1-3 indicates the volume used to calculate volume fraction occupied by the aggregate (Va), a hexagonal close packed structure is used for Types 4-6; b) absorbance spectra obtained for various combinations of aggregate types detailed in Table 9.

The absorption spectrum of partially aggregated colloidal gold solutions was then predicted using a gold concentration of 0.10 mg/mL, which resembles the concentration of gold in the "chemical nose" after they are mixed with bacterial samples. First, the testing solution with one centimeter optical length was divided into many thin layers with a thickness of 120 nm each. The occupied volume and the composition of different aggregates were then assigned to each layer based on the information presented in Table 9. Then, the volume fraction and absorption coefficient of the free particles in the remaining volume were calculated. Finally, the absorption spectrum of the partially aggregated colloidal solution was determined using Beer-Lambert Law [206, 207]:

$$A = -\log\left(\frac{I}{I_0}\right) = -\log(e^{-\alpha z}) = -\log(e^{-\alpha 1 z 1 - \alpha_2 z_2 - \alpha_3 z_3 \cdots})$$

where A is the absorbance, I_0 is the incident light intensity, I is the transmitted light intensity, α is the absorption coefficient, and z is the optical length. The optical length z for different types of aggregate was weighted by the percent volume occupied by aggregates (Table 9). It should be noted that Maxwell-Garnett effective medium theory is suitable for isolated particles where interaction between particles is ignored [208]. The model assumes one material as the host and considers the volume fraction of the other material.

Table 9: Volume fractions occupied by the aggregate types shown in Figure 17a and the percentage of total solution volume covered by the given aggregate type for various combinations

Aggregate type	Volume fraction (V_a)	Combination 1	Combination 2	Combination 3	Combination 4
Type 1	0.4189	0.0000000%	0.0003000%	0.0000000%	0.0002000%
Type 2	0.5236	0.0000000%	0.0000020%	0.0000000%	0.0000200%
Type 3	0.6046	0.0000080%	0.0000400%	0.0000400%	0.0001000%
Type 4	0.6910	0.0000070%	0.0000140%	0.0000175%	0.0000700%
Type 5	0.7255	0.0000050%	0.0000200%	0.0000300%	0.0000500%
Type 6	0.7441	0.0000065%	0.0000260%	0.0000390%	0.0000650%

5.4 Results and Discussion

5.4.1 Detecting bacteria at various concentrations

We use a 1:1 volume mixture of CTAB-coated gold nanospheres and nanostars to obtain a purple colored solution as a "chemical nose." The difference in size and morphology of gold nanoparticles is chosen such that each set of particles can respond to the various species of bacteria in a unique manner and thus provide additional features to the colorimetric response [9, 84]. When the solution of gold nanoparticles is added to bacteria, the nanoparticles aggregate around the bacteria due to electrostatic interactions between the cationic CTAB and anionic segments of cell walls, which leads to a color change due to a shift in the localized surface plasmon resonance. The color change is characterized by obtaining absorption spectra in the presence of various bacteria (Figure 18 a, c). The spectra demonstrate that the presence of bacteria causes broadening of the absorption peak due to higher absorption at longer wavelengths, which is typical when gold nanoparticles aggregate. The aggregation of gold nanoparticles on bacteria is mostly caused by teichoic acids in Gram-positive bacteria and lipopolysaccharides and phospholipids in Gram-negative bacteria [15, 84, 101, 137, 138, 178, 179]. The replicates for these responses are plotted in Figure 18 c and they show minimal variation within species and a drastic difference between species. This suggests that absorption spectra can be used for identification of the organism. Additionally, the colorimetric response highlighted by the absorption curves is also concentration dependent, as shown in Figure 18 b, where *P. aeruginosa* was normalized to a final OD_{660} = 0.03 and then diluted 5x and 25x in saline. Similarly, all other bacteria were also diluted and their spectra are presented as contour plots in Figure 19 and Figure 20. It can be observed that as the concentration of bacteria decreases, the differences between bacteria start to diminish yet subtle unique features are present. These data can now be used as a reference for testing the platform's ability to identify and quantify bacteria.

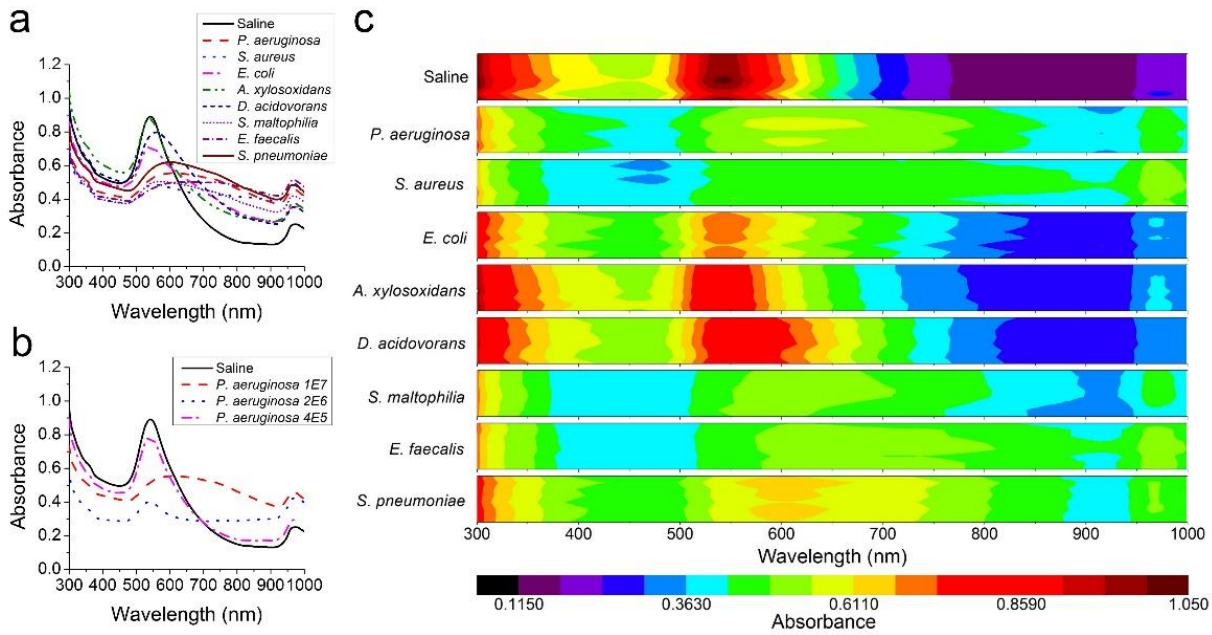

Figure 18: Absorption spectra of gold nanoparticles in the presence of bacteria: a) response for saline control and eight different species of bacteria normalized to OD_{660} = 0.03, b) response in the presence of various concentrations (approximately $1x10^7$, $2x10^6$, and $4x10^5$ CFU/well) of *Pseudomonas aeruginosa,* and c) contour plot of replicates (n = 8) for each bacteria normalized to OD_{660} = 0.03 and saline control, where each band consists of 8 slices (one per replicate).

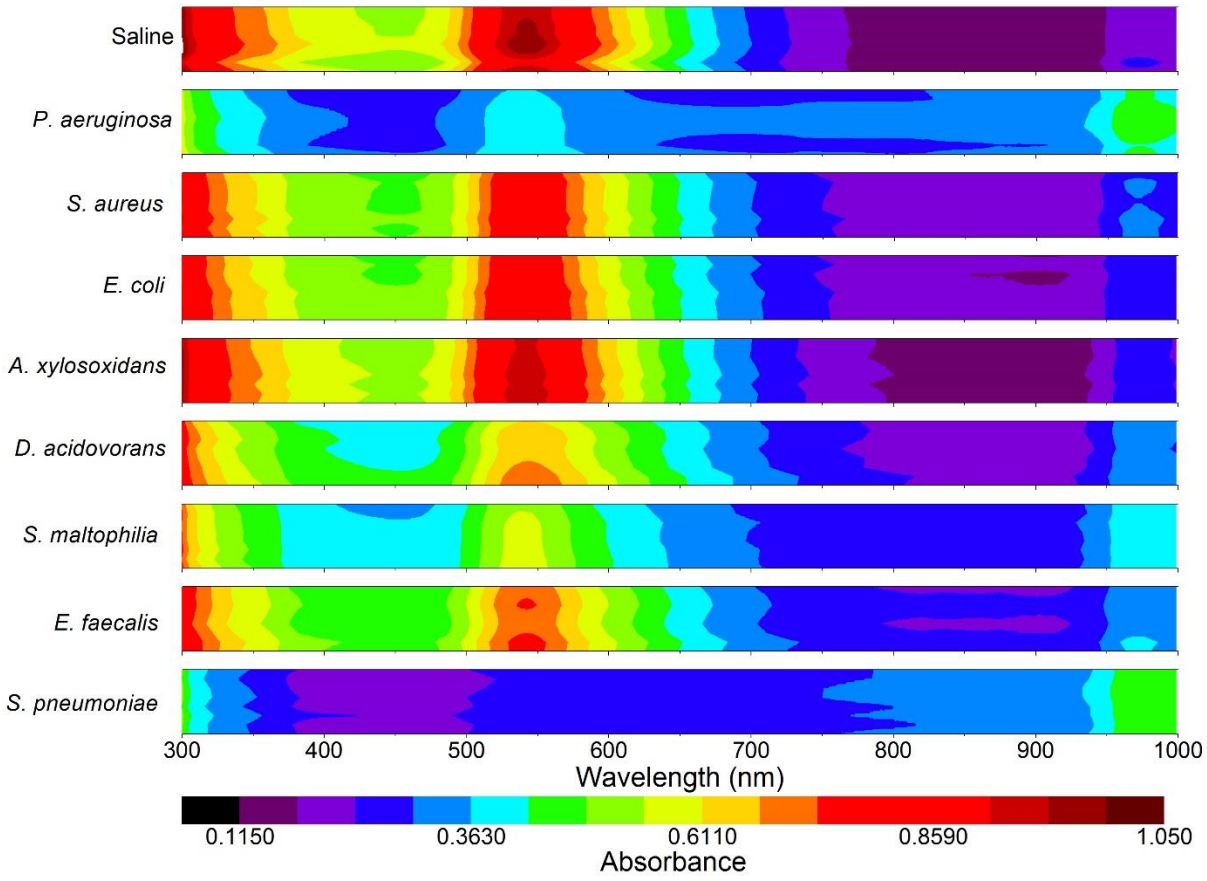

Figure 19: Contour plots of absorption spectra when bacteria (n=8) at OD_{660}= 0.006 are added to gold nanoparticles, each band consists of eight slices (one per replicate).

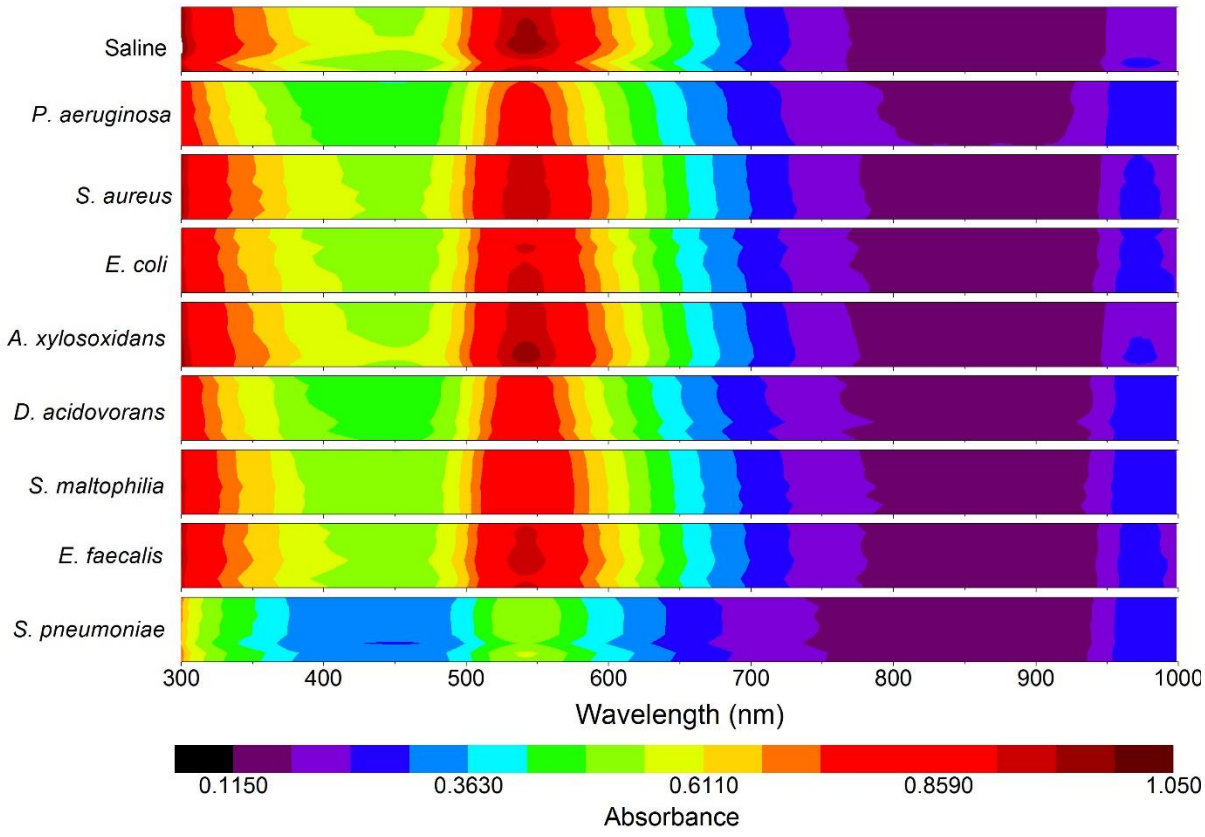

Figure 20: Contour plots of absorption spectra when bacteria (n=8) at OD_{660}= 0.0012 are added to gold nanoparticles, each band consists of eight slices (one per replicate).

HCA is a useful technique for visualizing data with multiple dimensions [209]. We performed HCA on three out of the eight replicates, using each wavelength for the absorption spectra as a variable. The dendrogram resulting from HCA is presented in Figure 21 a for bacteria that were normalized to OD_{660} = 0.03. The dendrogram shows that there is no misclassification, since all the replicates have minimal Euclidean distance. In general, the dendrogram seems to separate Gram-positive and Gram-negative bacteria, where Gram-negative bacteria provide a lower response and are clustered closer to saline. Yet, *P. aeruginosa* and *S. maltophilia* provide a drastic enough response to be clustered together with the Gram-positive bacteria and TEM analysis will shed some light on these peculiarities. In order to use these data for identification of unknown samples, PCA is suitable for

reduction of the dimensions. PCA on each of the eight bacteria at three different concentrations demonstrated that the first three principal components could explain 100% of the variability amongst bacterial samples. PCA scores for bacteria normalized to OD_{660} = 0.03 are presented in Figure 21 b and they confirm the observations from HCA by highlighting clustering of the same bacteria species. The PCA scores for all other concentrations and the HCA dendrogram derived from these scores are presented in Figure 22 and Figure 23 respectively. The principal components were used to classify the other five replicates for each of the 25 groups (saline and three concentrations for each of the eight bacteria) using the coefficients from PCA model followed by LDA. An accuracy of 89% (111/125) was achieved, which is impressive because this suggests that an unknown sample can be characterized using the gold nanoparticle based "chemical nose" platform to detect whether there is bacteria, identify the species of bacteria, and also approximate the concentration present simply based on the colorimetric response. Most of the error in identification results from misclassification of bacteria at the lowest concentration samples as indicated by the clusters in Figure 23. The working concentration of the biosensor can be expanded since each species of bacteria under consideration exhibits unique concentration dependent responses, as highlighted in Figure 24. We hypothesize that a more complex mixture of nanoparticles with various sizes, shapes, or functionalities might assist in discriminating bacteria at lower concentrations and some of these parameters are explored in a later chapter.

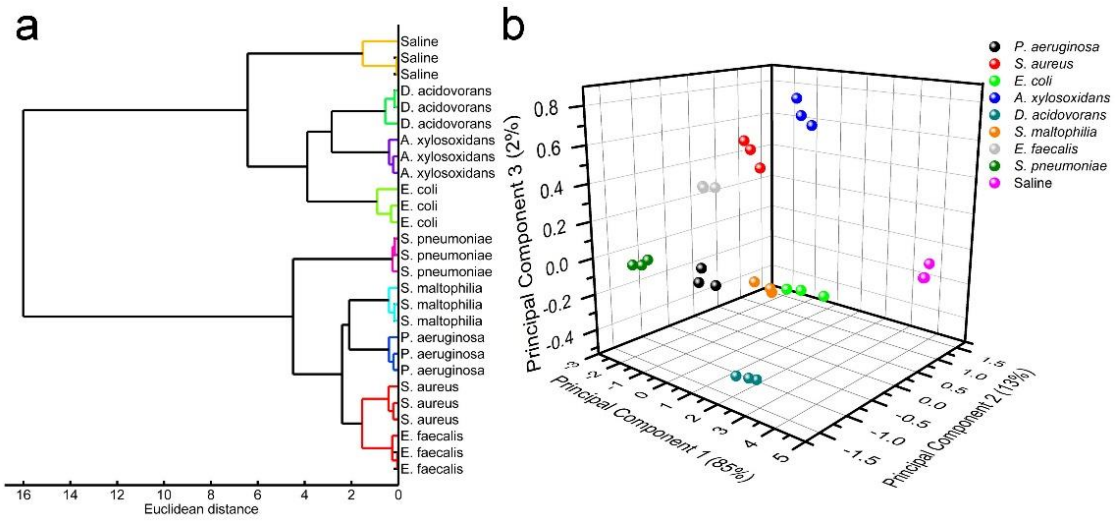

Figure 21: a) Dendrogram obtained using hierarchical clustering analysis (HCA) on the spectra (Ward's linkage method) of gold nanoparticles in the presence of bacteria normalized to OD_{660} = 0.03 and the color threshold was set to 10% of the maximum Euclidean distance using MathWorks® MATLAB® b) Principal component analysis (PCA) scores plot of the response of gold nanoparticles in the presence of bacteria. The percent variability explained is indicated on the axes. PCA model was built by using the spectral data in the range of 300-999 nm using MathWorks® MATLAB®

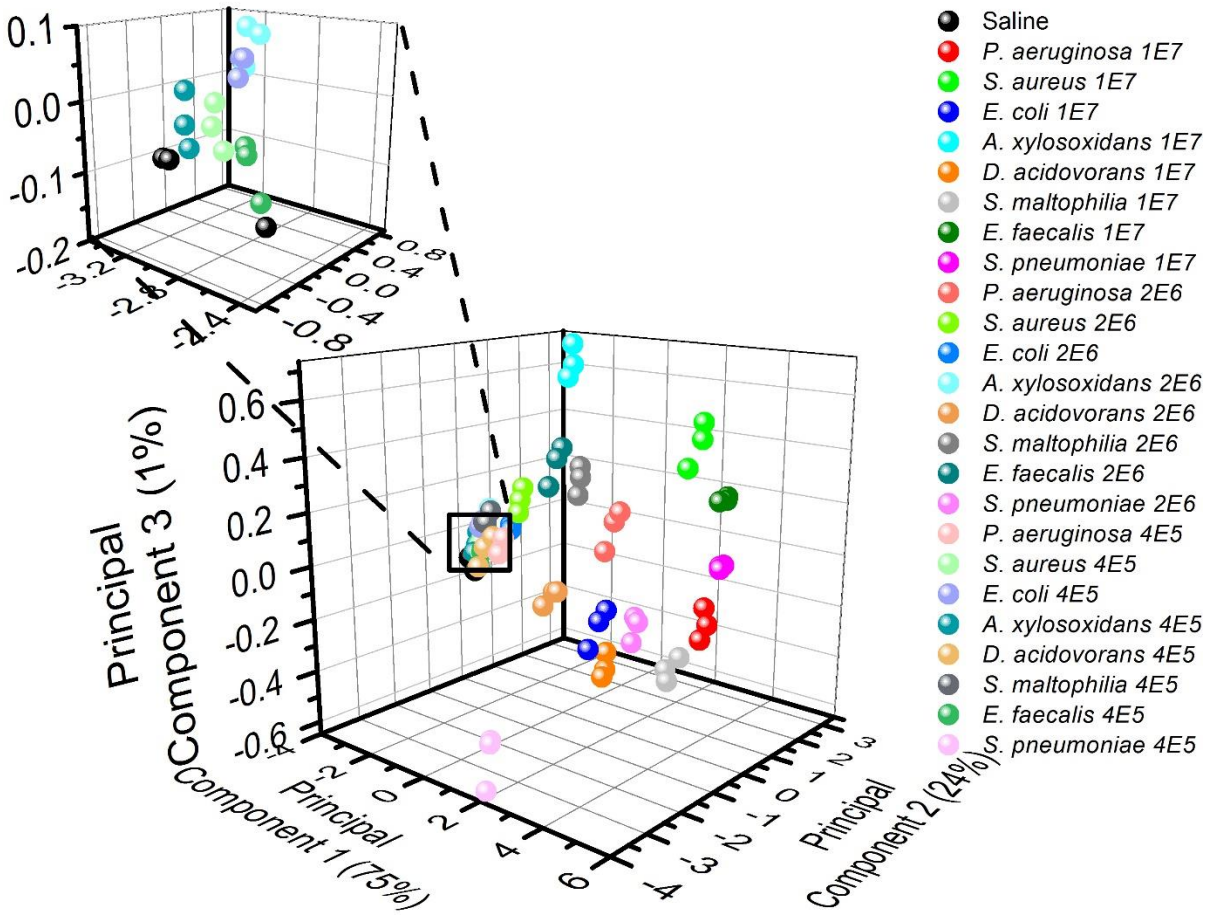

Figure 22: Principal component scores of the colorimetric responses of saline control and bacteria at different approximate concentrations, indicated by the number next to the names, in the units of CFU/well where well corresponds to a microplate well with a volume of 300 µL.

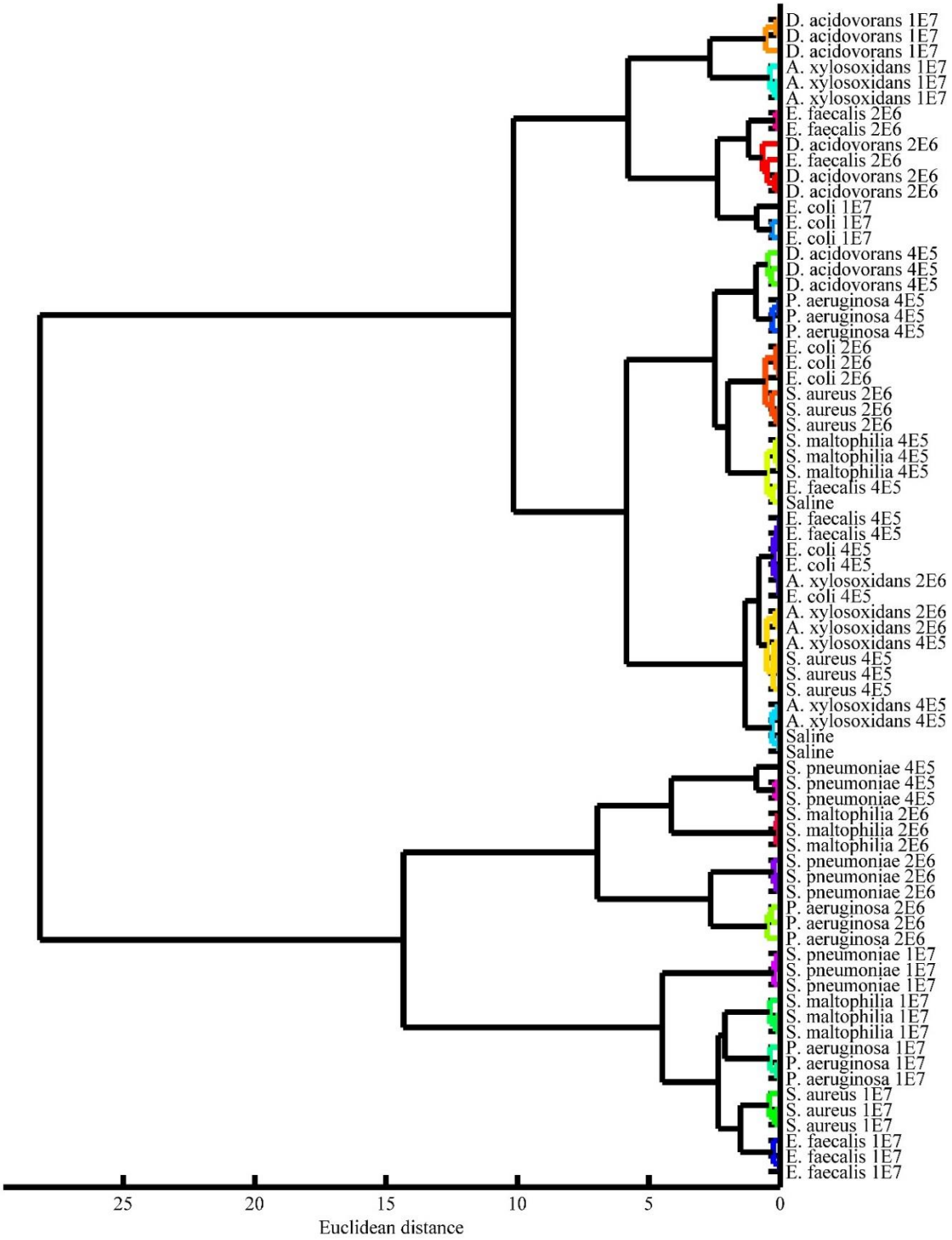
D. acidovorans 1E7
D. acidovorans 1E7
D. acidovorans 1E7
A. xylosoxidans 1E7
A. xylosoxidans 1E7
A. xylosoxidans 1E7
E. faecalis 2E6
E. faecalis 2E6
D. acidovorans 2E6
E. faecalis 2E6
D. acidovorans 2E6
D. acidovorans 2E6
E. coli 1E7
E. coli 1E7
E. coli 1E7
D. acidovorans 4E5
D. acidovorans 4E5
D. acidovorans 4E5
P. aeruginosa 4E5
P. aeruginosa 4E5
P. aeruginosa 4E5
E. coli 2E6
E. coli 2E6
E. coli 2E6
S. aureus 2E6
S. aureus 2E6
S. aureus 2E6
S. maltophilia 4E5
S. maltophilia 4E5
S. maltophilia 4E5
E. faecalis 4E5
Saline
E. faecalis 4E5
E. faecalis 4E5
E. coli 4E5
E. coli 4E5
A. xylosoxidans 2E6
E. coli 4E5
A. xylosoxidans 2E6
A. xylosoxidans 2E6
A. xylosoxidans 4E5
S. aureus 4E5
S. aureus 4E5
S. aureus 4E5
A. xylosoxidans 4E5
A. xylosoxidans 4E5
Saline
Saline
S. pneumoniae 4E5
S. pneumoniae 4E5
S. pneumoniae 4E5
S. maltophilia 2E6
S. maltophilia 2E6
S. maltophilia 2E6
S. pneumoniae 2E6
S. pneumoniae 2E6
S. pneumoniae 2E6
P. aeruginosa 2E6
P. aeruginosa 2E6
P. aeruginosa 2E6
S. pneumoniae 1E7
S. pneumoniae 1E7
S. pneumoniae 1E7
S. maltophilia 1E7
S. maltophilia 1E7
S. maltophilia 1E7
P. aeruginosa 1E7
P. aeruginosa 1E7
P. aeruginosa 1E7
S. aureus 1E7
S. aureus 1E7
S. aureus 1E7
E. faecalis 1E7
E. faecalis 1E7
E. faecalis 1E7
25
20
15
10
5
0
Euclidean distance

Figure 23: Hierarchical clustering analysis dendrogram after analyzing the principal component scores used for training sets in linear discriminant analysis. The number in the names corresponds to the concentration of bacteria in CFU/well where well corresponds to a microplate well with a volume of 300 µL.

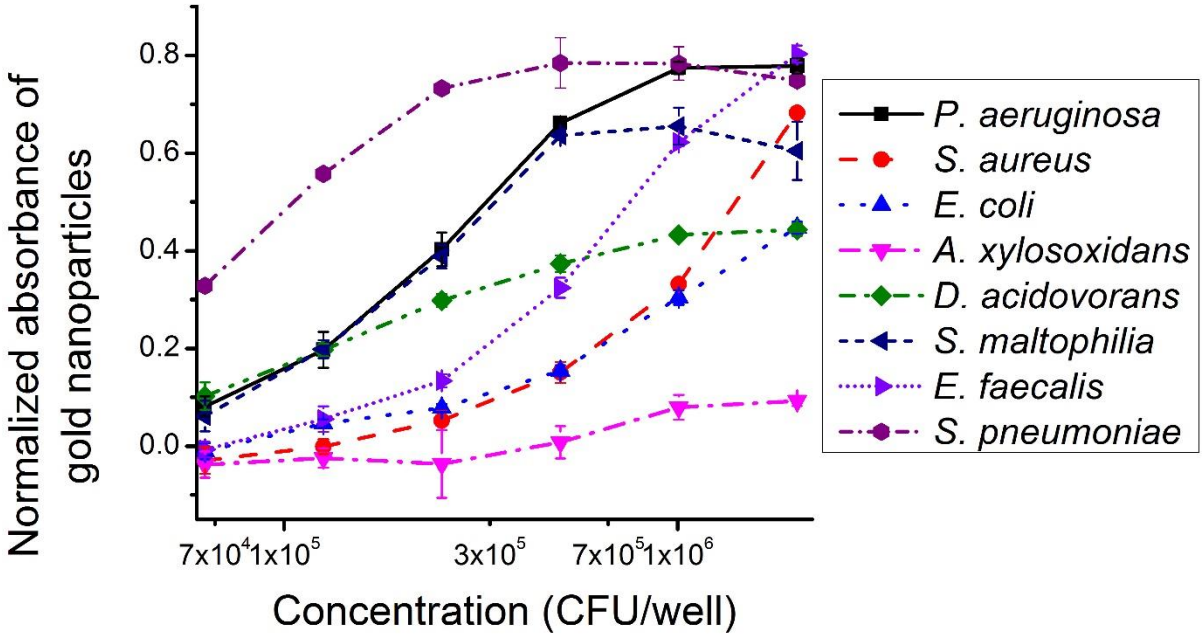

Figure 24: Concentration dependent response given by normalized absorbance at 540 nm for approximate concentrations of each bacteria which were normalized to OD_{660} = 1.0 ± 0.05 (assuming a concentration of 10^9 CFU/mL) and then diluted 16-512x in saline. Here well corresponds to a microplate well with a volume of 300 µL.

5.4.2 Detection of polymicrobial mixtures

Hospitals have become a major source of antibiotic-resistant infections and are a threat for vulnerable patients. Three of the most common hospital-isolated pathogens are: *S. aureus, E. coli* and *P. aeruginosa* [210, 211]. These pathogens often exhibit unique antibiotic susceptibility profiles, which evolve over time and require timely monitoring using antibiograms [212]. In order to administer the appropriate antibiotic therapy, there is an urgent need for a biosensor to distinguish between bacterial species. Additionally, the detection of multiple bacterial species is especially

important in the diagnosis of polymicrobial infections because certain species such as *P. aeruginosa* can express increased virulence in the presence of other bacteria [213]. The "chemical nose" based on gold nanoparticles can detect mixtures of bacterial species once the system is trained. Binary and tertiary mixtures of *P. aeruginosa, S. aureus* and *E. coli* were prepared (final OD_{660} = 0.03, 1:1 v/v or 1:1:1 v/v/v) and then mixed with gold nanoparticles. The responses obtained from these mixtures are presented in Figure 25 a and the mixtures appear to be dominated by the bacteria that cause higher aggregation. For example, in the case of a binary mixture of *P. aeruginosa* and *E. coli*, even though a pure *E. coli* sample does not cause a drastic color change, the mixture does cause a significant drop in the absorption peak and yet, the response is distinct from pure *E. coli* and *P. aeruginosa* cultures. Thus, in the case of infections, the "chemical nose" has the potential to distinguish between monomicrobial and polymicrobial instances, which will facilitate a more effective and rapid antimicrobial treatment without the need for extensive and lengthy testing of the sample. We analyzed these data using PCA and the scores are presented in Figure 25 b, where the variance was explained completely by using the first three components. Although the third principal component only accounts for 0.4% of the variance, this value is still significant compared to the variance between replicates, which is in the range of 0.01-0.04% for the saline and bacterial samples. Once again, three replicates were used for training the system and the other five were randomized for blind identification and an accuracy of 100% (40/40) was obtained for each of the pure cultures and mixtures using LDA. Thus, the "chemical nose" can not only detect and discriminate between pure cultures but also identify species in mixed cultures, after it is trained appropriately. Given enough training sets, the "chemical nose" platform presented here can identify species within mixtures and approximate their concentrations. Adding more nanoparticles with unique shapes such as gold nanorods, nanocubes, and nanoprisms can then expand the specificity and range of application for the "chemical nose" platform [199].

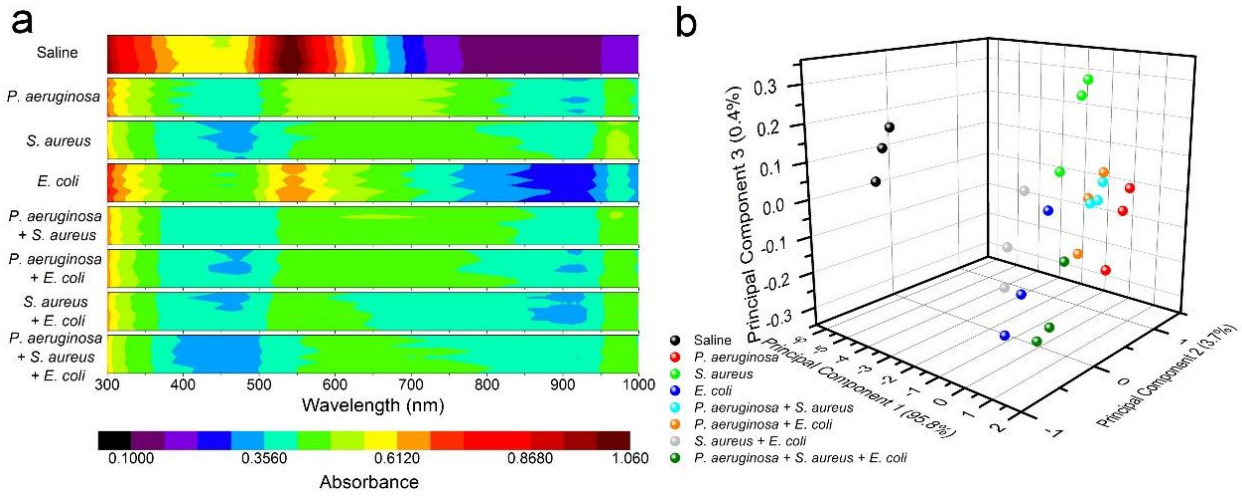

Figure 25: Response of gold nanoparticles in the presence of mixtures of bacteria: a) Contour plots of absorption spectra showing replicates for each sample (n = 8), each band consists of eight slices (one per replicate) b) principal component analysis scores for three of the replicates that were used as training sets in linear discriminant analysis. The variance explained by each component is included in parenthesis with axes labels.

The colorimetric response provided by this "chemical nose" is dependent on the degree of aggregation of gold nanoparticles, which varies based on the surface features of the bacteria as well as the morphology of the particles as seen in Chapter 4 [84]. In addition to the polyanionic charge presented on the cell walls, the amount of extracellular polymeric substances produced by bacteria can determine the extent of aggregation of gold nanoparticles. The TEM images of gold nanoparticles around bacteria tested here are shown in Figure 26 and it is clear that in the cases of *A. xylosoxidans* and *D. acidovorans*, there is a layer of polymeric substance around the bacteria which prevents extensive aggregation of gold nanoparticles on the surface and hence causes a lower response for these bacteria. In other cases, the gold nanoparticles are heavily aggregated around the pathogen and adhere to the pathogen despite being rinsed once with water, which suggests strong electrostatic binding. Additionally, in cases of *P. aeruginosa* and *S. maltophilia*, the nanoparticles seem to aggregate around specific sections of the cell instead of evenly distributing throughout the surface, which might have led to a greater response compared to other Gram-negative species. This also suggests the role of lipid domains that are present around specific proteins [214] or can form in the

presence of cationic molecules such as CTAB [215]. Specifically, phosphatidylglycerol and diphosphatidylglycerol (cardiolipin) possess an overall negative charge which is expected to be probed by the cationic nanoparticles while phosphatidylethanolamine (PE) being zwitterionic would show lower affinity as seen with the liposomes in Chapter 3 [9]. Thus, the nanoparticle aggregation and hence the colorimetric response is governed by the complex composition and configuration of the bacterial cell surface.

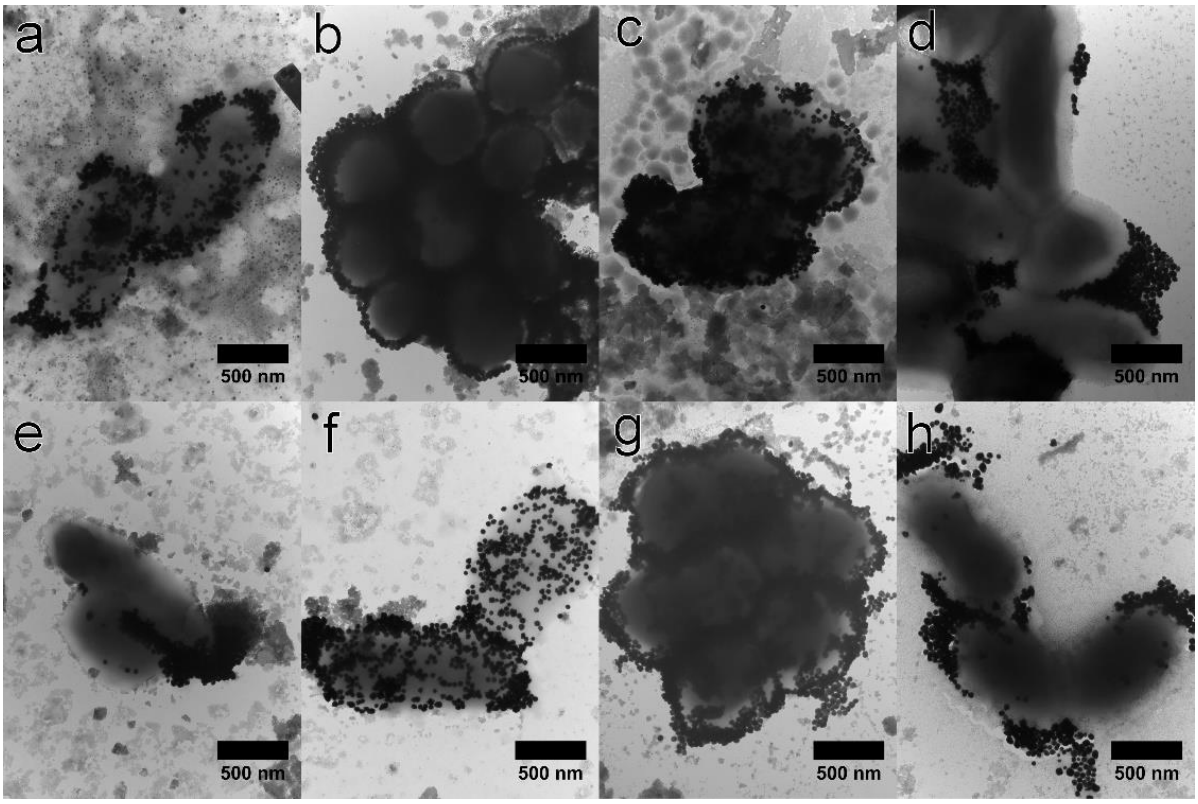

Figure 26: Transmission electron microscopy images of gold nanoparticles aggregating around bacteria: a) *Pseudomonas aeruginosa*, b) *Staphylococcus aureus*, c) *Escherichia coli*, d) *Achromobacter xylosoxidans*, e) *Delftia acidovorans*, f) *Stenotrophomonas maltophilia*, g) *Enterococcus faecalis*, and h) *Streptococcus pneumonia*

5.4.3 Role of EPS

One of the main parameters that determine colorimetric response seems to be the presence of EPS on bacteria. In order to confirm the effect of EPS, we executed an EPS extraction protocol for *S. aureus*

(control), *E. coli*, and *A. xylosoxidans* as per published methods [201]. *S. aureus* serves as a control because it seems to lack EPS that would prevent binding of nanoparticles. After extraction, the cells were mixed with the "chemical nose" solution and their colorimetric response are presented in Figure 27. A dramatic increase in response is observed for treated *E. coli* and *A. xylosoxidans* as compared native bacteria while the response of *S. aureus* does not change drastically. TEM images of the treated bacteria and gold nanoparticles (Figure 28) are consistent with the colorimetric response where removal of EPS causes increased nanoparticle aggregation around *E. coli* and *A. xylosoxidans* while a similar coverage of nanoparticles is seen for treated and untreated *S. aureus*.

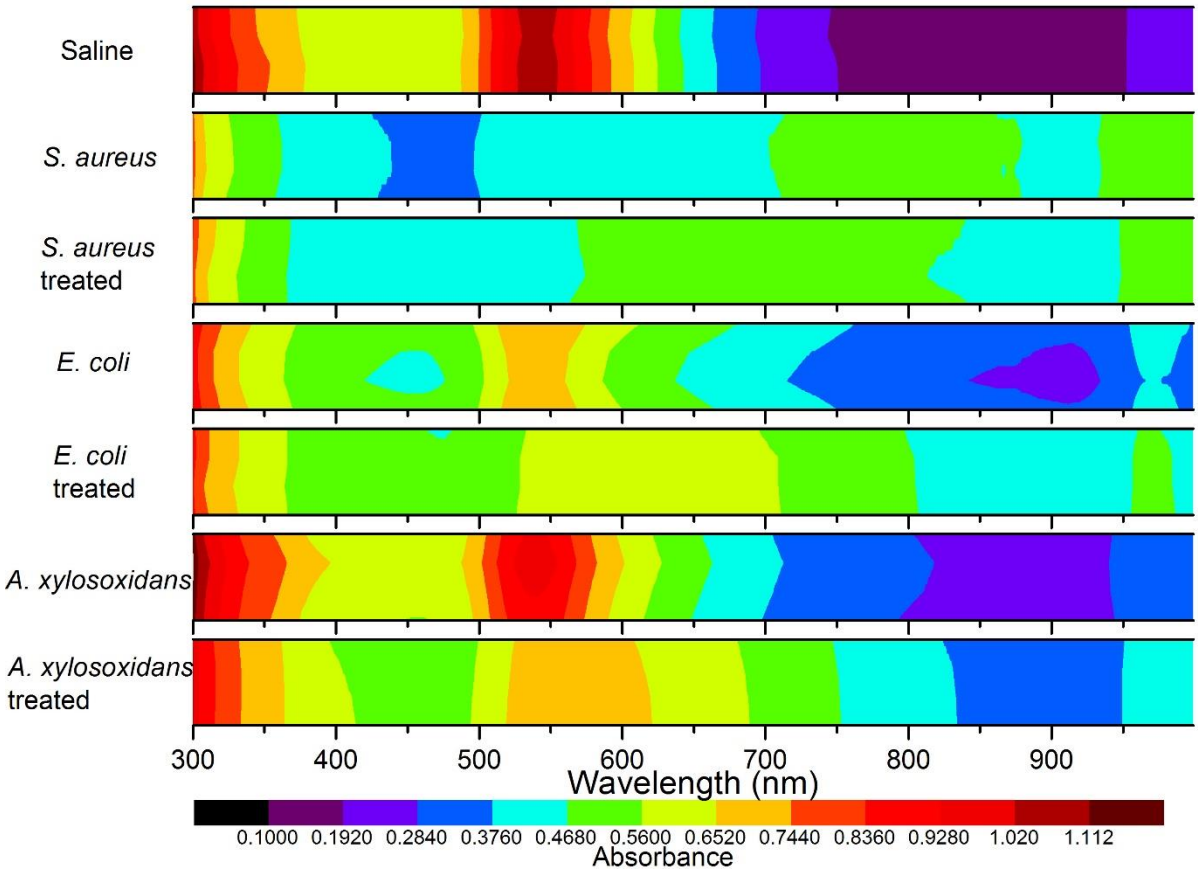

Figure 27: Effect of extracting extracellular polymeric substances (EPS) from bacteria. The treated bacteria were processed by exposing to formaldehyde and then sodium hydroxide and then washed to remove EPS.

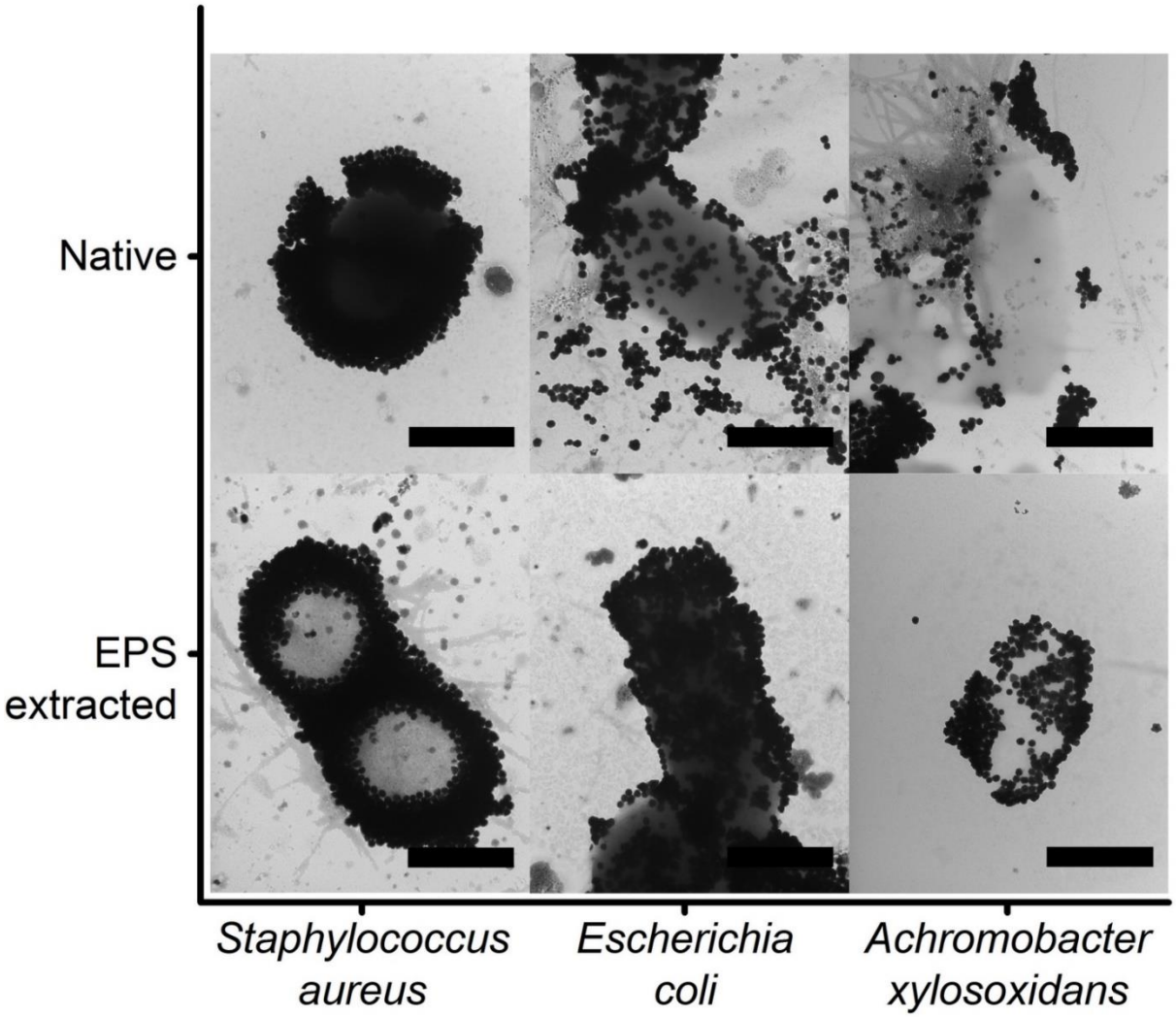

Figure 28: TEM images of gold nanoparticles aggregating around bacteria with or without the extracellular polymeric substances (EPS) extracted. Scale bars are 500 nm each.

EPS can have an impact on various components of the cell surface such as phospholipids, lipopolysaccharides, teichoic acids, and peptidoglycan. EPS typically contain high fractions of carbohydrates and proteins [201], which could provide steric hindrance to the nanoparticles and thus cause a decrease in binding. In order to study the effects of EPS on these individual components, we used blot assays on PVDF and NC membranes to quantify nanoparticle binding. This strategy is adapted from protein lipid overlay assays for investigating the binding of proteins to lipids [216]. A

similar approach has been used for the detection of glycoproteins by immobilizing antibodies on the membrane and using peptide coated gold nanoparticles [217]. PVDF was used for components that required chloroform for dissolution while NC was used for water-soluble components due to the hydrophobic and hydrophilic nature of PVDF and NC respectively. The visual binding of various cell surface components with and without EPS is presented in Figure 29. Digital blot images can be characterized by analyzing color using RGB model [218]. Since the "chemical nose" absorbs mostly green light, we expect that an increased binding of nanoparticles to the membrane will show a decrease in the green component of RGB. The response is normalized by subtracting it from the background white color of the membrane. Figure 30 highlights the binding of nanoparticles to various components of the cell walls. In the case of phospholipids, it is observed that at the same molar concentration, PG and CL demonstrate a higher binding compared to PE (Figure 30 a), which is expected because of the anionic nature of PG and CL and zwitterionic nature of PE. On the other hand, the water-soluble components have unknown molecular weights and hence cannot be directly compared to each other. All cell surface components demonstrate a significant reduction in binding of nanoparticles in the presence of EPS, except for rough strain (Rd) lipopolysaccharide (LPS-R) from *E. coli* F583 (Figure 30 a, b). Additionally, to confirm that the reduction in binding is due to the presence of EPS, various masses of EPS were added to PG blots by changing the concentration of EPS in solution. Figure 30 c highlights that increasing the mass of EPS leads to significant decrease in nanoparticle binding. Therefore, the presence of EPS is an important characteristic that determines the colorimetric response from the "chemical nose" biosensor.

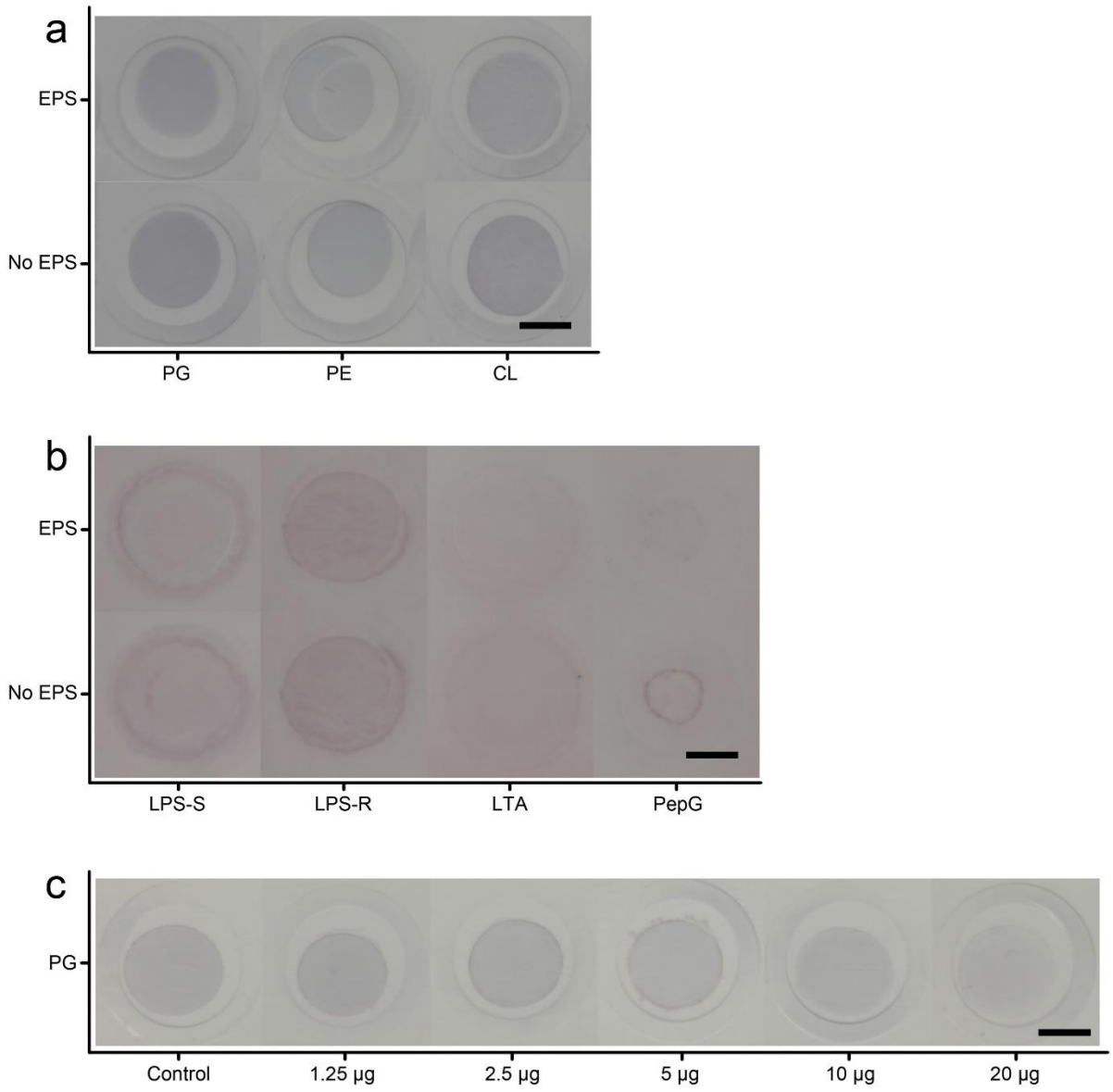

Figure 29: Photos of blots on a) PVDF membrane with phosphatidylglycerol (PG), phosphatidylethanolamine (PE), and cardiolipin (CL); b) nitrocellulose membrane (NC) with smooth lipopolysaccharides (LPS-S), rough lipopolysaccharides (LPS-R), lipoteichoic acids (LTA), and peptidoglyclan (PepG), and c) PVDF membrane with PG and varying mass of extracellular polymeric substances (EPS). Scale bars are 2 mm each.

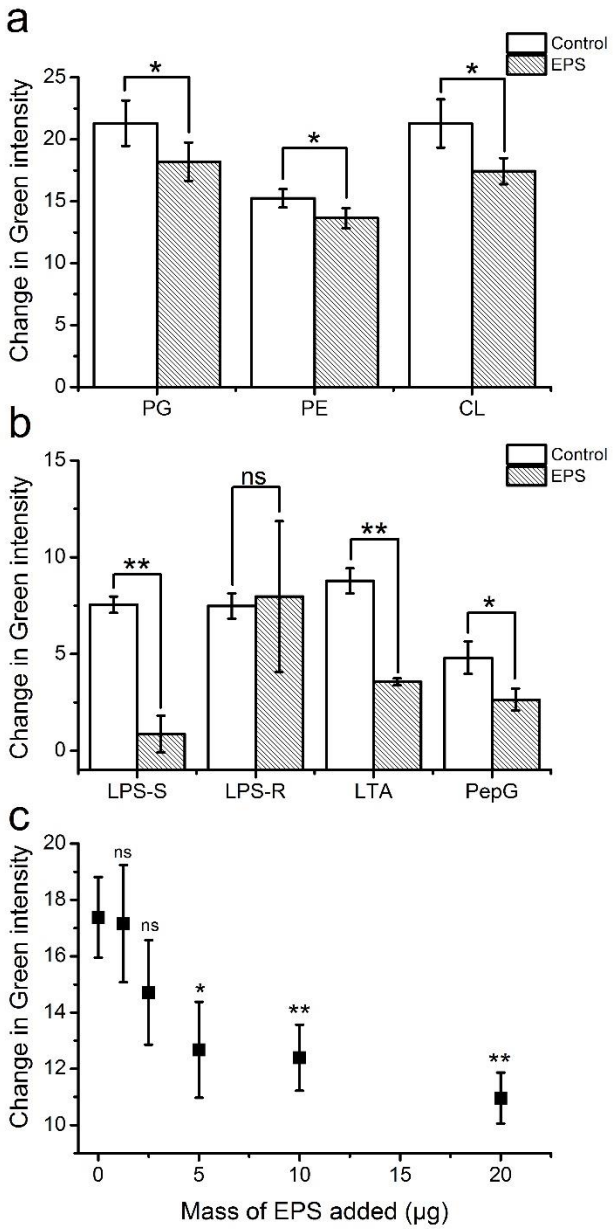

Figure 30. Normalized Green intensity values from the RGB color model for images shown in Figure 29: a) Polyvinylidene difluoride (PVDF) membrane with L-α-phosphatidylglycerol (PG), L-α-phosphatidylethanolamine (PE), and cardiolipin (CL); b) nitrocellulose membrane (NC) with smooth lipopolysaccharides (LPS-S), rough strain (Rd) lipopolysaccharides (LPS-R),

lipoteichoic acids (LTA), and peptidoglyclan (PepG), and c) PVDF membrane with PG and varying mass of extracellular polymeric substances (EPS). All values are reported as means ± S.D. (n = 3), ns = not significant ($p \geq 0.05$), * $p \leq 0.05$, and ** $p \leq 0.01$.

5.4.4 Modeling gold nanoparticle aggregation states

Different types of gold nanoparticle aggregates are observed in TEM images. Some bacteria lead to formation of multiple layers around the cell walls (Figure 26 b), while some have aggregates only in specific regions (Figure 26 a, f) and yet, some others have nanoparticles dispersed throughout the cell surface (Figure 26 c). In order to determine the relationship between gold nanoparticle aggregation type and their colorimetric response, we simulated aggregation of nanoparticles using Maxwell-Garnett effective medium theory [202], which has previously been implemented for metallic thin films [219-221] and particle clusters [222]. Six different types of gold nanoparticle aggregates were modeled, as shown in Figure 17 a and their ratios in solution were varied as described in Table 9. The expected absorption spectra in Figure 17 b show representative responses for different combinations of aggregate types. Each of these combinations shows a characteristic change as seen in Figure 18 a for the response of gold nanoparticles to bacteria. The modeled spectra only consider spherical nanoparticles with fixed size and one type of aggregate packing (hexagonal close packed) while the "chemical nose" consists of a distribution of size and degree of branching of nanoparticles. Thus, the model provides coarse predictions compared to the experimental observations but the trends provide insight into the relationship between colorimetric response and aggregation on bacteria. Combination 1 uses a low total percent of aggregation using Type 3-6 aggregates. The obtained absorption spectrum correlates to the observed spectrum for *A. xylosoxidans* (Figure 18 a), which suggests that the overall degree of aggregation is low, as confirmed in TEM images (Figure 26 d). As we increase the overall percent of volume fraction occupied by aggregates in Combination 2 and introduce Type 1 aggregates, where nanoparticles are not in contact but rather separated by their radius, a slight peak shift is observed in addition to the increase in absorption in the 620 nm and 720 nm regions. The obtained absorption spectrum correlates to that of *D. acidovorans* (Figure 18 a), suggesting that some nanoparticles might be close to each other on the bacterial surface but not coming in contact. A further increase in planar and multi-layer stacking fraction in Combination 3 shows a significant drop of the 530 nm peak and an increase in the absorption at 620 nm and 720 nm, presenting a spectrum

similar to the response from *E. coli* (Figure 18 a). Finally, Combination 4 has a significant fraction of nanoparticles aggregated including all types of aggregates and the absorption spectrum broadens significantly as is the case with *P. aeruginosa*, *S. aureus*, *E. faecalis*, *S. maltophilia*, and *S. pneumoniae*. These bacteria have a high fraction of aggregation either due to multiple layers around the cell wall (eg. *S. aureus* Figure 26 b) or due to patterns of aggregation (eg. *P. aeruginosa* Figure 26 a). In Combination 4, the absorbance at 530 nm also drops significantly due to the loss of free particles. Thus, Maxwell-Garnett effective medium theory provides some insight into how different types of nanoparticle aggregates around bacteria could be influencing the observed colorimetric changes and thus, how each bacterial species presents a distinguishable color change.

5.5 Conclusions

We demonstrated that gold nanoparticles with varying morphologies are a versatile "chemical nose" platform for detecting, identifying, and quantifying species of pathogenic bacteria. The "chemical nose" can also distinguish between polymicrobial samples of the most prevalent pathogens in hospitals. We also determined that EPS play an important role in influencing the degree of nanoparticle aggregation around bacteria. Additionally, simulations using the Maxwell-Garnett effective medium theory suggest that different aggregation patterns on bacterial cell walls are responsible for providing distinguishable colorimetric responses. Successful identification of bacteria using differential gold nanoparticle aggregation can be complemented with future investigations into nanoparticle-cell surface interactions to improve assay performance and predict response to novel bacterial strains. The simplicity of detection in this system allows for field implementation without extensive technical expertise or training. Additionally, the use of nanoparticles permits employing minimal material for maximum results. Although gold might sound expensive, nanoparticles require few milligrams to produce a strong color, which brings the cost to about $0.25/assay at the lab scale. This is especially important for developing countries, because of their limited resources and education. Thus, gold nanoparticles can be utilized for point-of-care diagnostics in the health industry and in-field testing in food and environmental industries by controlling their morphologies and training the "chemical nose" system.

Chapter 6
Exploiting the kinetics of nanoparticle aggregation for rapid colorimetric detection using “chemical nose”

6.1 Summary

Infectious diseases spread rapidly because current diagnostic methods are slow, expensive, and require technical expertise. Biosensors have recently been used as devices that can be deployed at the point-of-care for rapid and accurate diagnosis. Here, we show that a “chemical nose” biosensor based on gold nanoparticles can be coupled with a portable spectrophotometer to detect monomicrobial and polymicrobial solutions of pathogenic bacteria within two minutes of data collection. The design presented here exploits the rapid kinetics of gold nanoparticle aggregation around bacteria, which leads to a dramatic color change. The “chemical nose” produces unique signals based on the surface characteristics of the bacteria and hence provides a versatile platform for detection. In this chapter, we present a biosensor design that can easily be translated to the point-of-care because of its rapid response and simple output.

6.2 Introduction

Rapid detection of bacteria is crucial in curbing the spread of infectious diseases and preventing epidemics [2, 30]. As highlighted in Chapter 2, current methods for detection of bacteria require considerable sample processing, because they detect either nucleic acids or proteins, which need to be extracted from the bacteria [223, 224]. Culture-based methods are sensitive but slow because the growth of bacteria can require 1-5 days [2]. Additionally, most methods require sophisticated instruments and/or extensive technical training [2, 30]. Rapid diagnosis of infectious diseases needs to be executed at the point-of-care with limited resources. Colorimetric responses are preferred in biosensors because they can be easily deciphered at the point-of-care [2, 7, 10]. Recently, portable scanners and smartphones have been used for measuring, analyzing, and reporting colorimetric responses when sensing analytes such as proteins [225, 226], viruses [227], and bacteria [228].

Gold nanoparticles are playing an increasingly important role in providing a colorimetric response because their color depends on their aggregation state and their local environment [8]. Using gold

nanoparticles for detecting pathogens typically requires biomodification with antibodies or aptamers for targeting specific analytes [2, 7, 37]. As mentioned in Chapter 5, this "lock-and-key" approach is limited [12] because detecting multiple pathogens in a mixture requires a unique targeting biomolecule for each pathogen. A "chemical nose" approach provides a viable alternative to the conventional methods because the "chemical nose" can be trained for various analytes, including mixtures [12, 13, 103]. Chapter 4 and 5 demonstrated that a "chemical nose" based on gold nanoparticles can be used for identification of various unique pathogens and their mixtures once the system has been trained [84]. In order to implement this "chemical nose" at the point-of-care, here we have exploited the kinetics of the color change of gold nanoparticles in the presence of bacteria. The rapid color change provides sufficient data within two minutes to detect bacteria in monomicrobial and polymicrobial solutions. The portable spectrophotometer design used here (Figure 31) has the potential to be translated easily to point-of-care use with the help of smartphone-based spectrophotometers [226, 229].

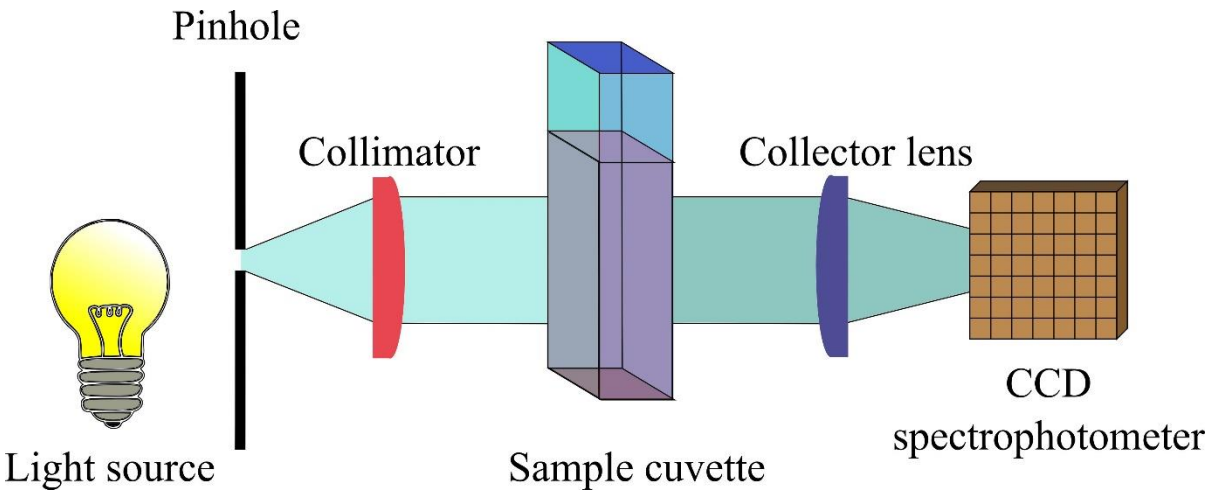

Figure 31: Schematic illustrating the spectrophotometer setup where sample is a mixture of nanoparticles and bacteria.

6.3 Materials and Methods

6.3.1 Materials

The chemicals, containers, and bacteria used in this study were from the same sources as those described in Chapter 5.

6.3.2 Spectrophotometer design

A standard optical extinction arrangement (Figure 31) was used in the spectrophotometer design as previously described [230]. Briefly, a tungsten-filament lamp with fiber coupling (Ocean Optics HL-2000, Dunedin, FL, USA) was used as a light source and the light was collimated before passing through the cuvette containing nanoparticle solutions. The exiting light was collected into another fiber and directed to the portable spectrometer (Ocean Optics USB4000, Dunedin, FL, USA). Micro-volume disposable polystyrene cuvettes were used for the samples. The entire experimental setup was enclosed in a container to minimize external light and dust.

6.3.3 Synthesis of gold nanoparticles "chemical nose"

Gold nanoseeds were first synthesized as described in Chapter 3 [9, 84, 124]. Gold nanostars and nanospheres were synthesized as described in Chapter 5, where CTAB is used as a negative template [9, 84]. The red gold nanosphere and blue gold nanostar solutions were mixed (1:1 by volume) to obtain the purple "chemical nose" solution.

6.3.4 Bacterial culture

Bacteria were cultured and prepared using the methods described in Chapter 5. *Pseudomonas aeruginosa, Staphylococcus aureus,* and *Escherichia coli* were inoculated on Trypticase Soy Agar (TSA) plates and incubated at 37 °C for 24 hours. Bacterial cells were harvested using alginate swabs and suspended in 5 mL of sterile saline (2.55%) with nutrient broth (~0.006%) in a 15 mL centrifuge tube. Each bacterial species was then washed seven times with 2.55% saline (with ~0.006% nutrient broth) by centrifugation at 4,000 rpm for 10 min. The bacteria were then diluted to obtain an optical density at 660 nm (OD_{660}) of 0.10 ± 0.005 (~10^8 CFU/mL [172]). This provides monomicrobial solutions of the bacteria *P. aeruginosa, S. aureus,* and *E. coli.* Each of these solutions was mixed either 1:1 (v/v) to obtain binary mixtures or 1:1:1 (v/v/v) to obtain a tertiary mixture. The 2.55%

saline (with ~0.006%) broth was used as control. This resulted in three monomicrobial and four polymicrobial solutions. When the bacteria are added to gold nanoparticles, the solution was diluted 1:3 to obtain final OD_{660} = 0.03 for bacteria.

6.3.5 Detection of monomicrobial and polymicrobial solutions

Detection of bacteria was performed in polystyrene cuvettes by mixing 1.2 mL of the "chemical nose" solution and 0.6 mL of the bacterial solution using a pipette. The cuvette was then transferred to the spectrophotometer and spectra were acquired 60 s after the mixing of nanoparticle and bacteria solutions. The spectra were acquired using Spectra Suite (Ocean Optics, Dunedin, FL, USA) with an integration time of 200 ms, averaging 5 measurements, and with a boxcar width of 5. Spectra were obtained every 5 s for 10 minutes and only the first two minutes of data were used, because it was the linear region of the response. Principal component analysis (PCA) was performed using MathWorks® MATLAB® on the absorbance data for 400-850 nm. The first principal component was extracted and fitted using a linear fit for the first 120 s of data.

6.3.6 Transmission electron microscopy

Polymicrobial mixtures of bacteria with gold nanoparticles (5 µL) were added to formvar-coated copper TEM grids and allowed to dry under ambient conditions overnight. Once dry, the bacteria samples were washed by placing 5 µL of Millipore water on the transmission electron microscopy (TEM) grids for 30 seconds and then wicking the liquid using filter paper to remove excess surfactants, salts, and unbound gold nanoparticles. The samples were then imaged using Phillips (Eindhoven, The Netherlands) CM10 TEM.

6.4 Results

6.4.1 Rapid colorimetric response from portable spectrophotometer

The "chemical nose" we have developed consists of a 1:1 (v/v) mixture of gold nanospheres and nanostars. These nanoparticles are cationic because of their cetyltrimethylammonium bromide (CTAB) coating. The nanoparticles aggregate around the anionic bacteria and then lead to a rapid and drastic color change. We have demonstrated the potential of this "chemical nose" in differentiating between different species of pathogenic bacteria in Chapter 4 and 5 [84], but rapid detection of

polymicrobial mixtures remained unexplored. With the help of a portable charge-coupled device (CCD) array spectrophotometer, we are translating the "chemical nose" biosensor to point-of-care use. The CCD spectrophotometer provides a rapid response, hence allowing the study of kinetics of color change in gold nanoparticles. The changes in the spectra over two minutes after mixing bacteria and gold nanoparticles are shown in Figure 32. It is observed that saline shows negligible change in the spectra over time, whereas *P. aeruginosa* and *S. aureus* show a drastic change. *E. coli* shows a smaller change compared to the other two bacteria, but a difference can be observed when comparing the response to that of saline. Between *P. aeruginosa* and *S. aureus*, not only is the degree of color change different, but also the rate at which the spectra are changing. These differences are also observed in the responses obtained from binary and tertiary mixtures of these bacteria. It is important to note that the mixtures present a response that can be distinguished from their monomicrobial solutions, which implies that a distinction can be made between monomicrobial and polymicrobial infections in a manner similar to the observations in Chapter 5.

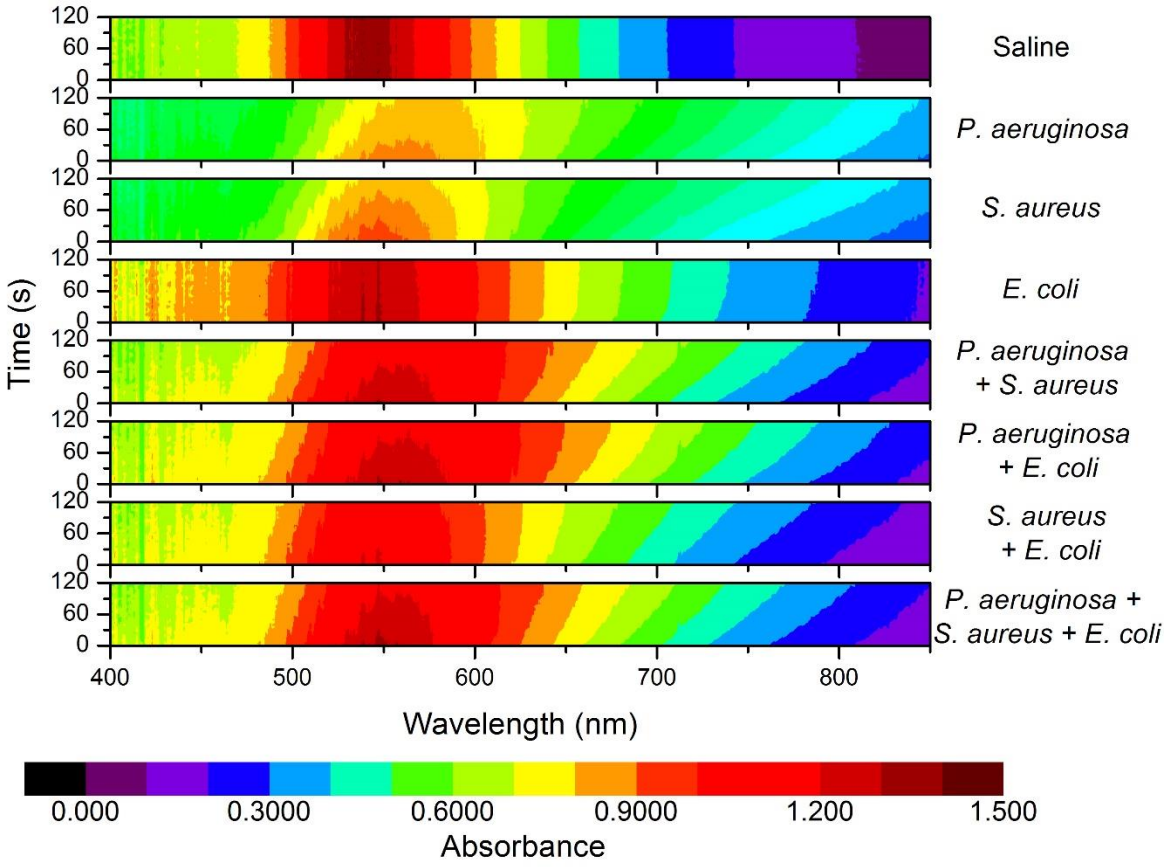

Figure 32: Changes in absorption spectra of gold nanoparticles over time in the presence of bacteria: saline was used as a control, monomicrobial species were prepared such that the final OD_{660} of bacteria = 0.03 (approximately 5 x 10^7 CFU/mL), polymicrobial solutions were prepared by mixing 1:1 (v/v) or 1:1:1 (v/v/v) of the monomicrobial solutions. Initial time of zero indicates one minute after addition of the nanoparticles.

It can be challenging for the untrained eye to distinguish between some of the contour plots. Thus, the data is simplified using principal component analysis (PCA), where the absorbance values of each spectrum are represented by a few principal components. It was determined that the first principal component explained 85.1% of the variance and hence this component was plotted over time for each of the samples, as shown in Figure 33. A linear fit can be obtained for each sample, with the slope and intercept presented in Table 10. The high R^2 values observed for all samples confirm good fit of the

linear model for the first two minutes of data. A low R^2 value is obtained for the saline sample and is expected, because the response does not change over time, resulting in a slope of 0. Table 10 highlights that each sample is defined by a unique line, characterized by its slope and intercept. These values can be used for training the "chemical nose" and then for identifying which bacteria or mixture is present, as demonstrated in Chapter 4 and 5 [84]. Only two minutes of the spectral data was required for generating Figure 33 using the portable spectrophotometer. Thus, if the "chemical nose" is coupled with this spectrophotometer design, polymicrobial infections can be rapidly diagnosed at the point-of-care.

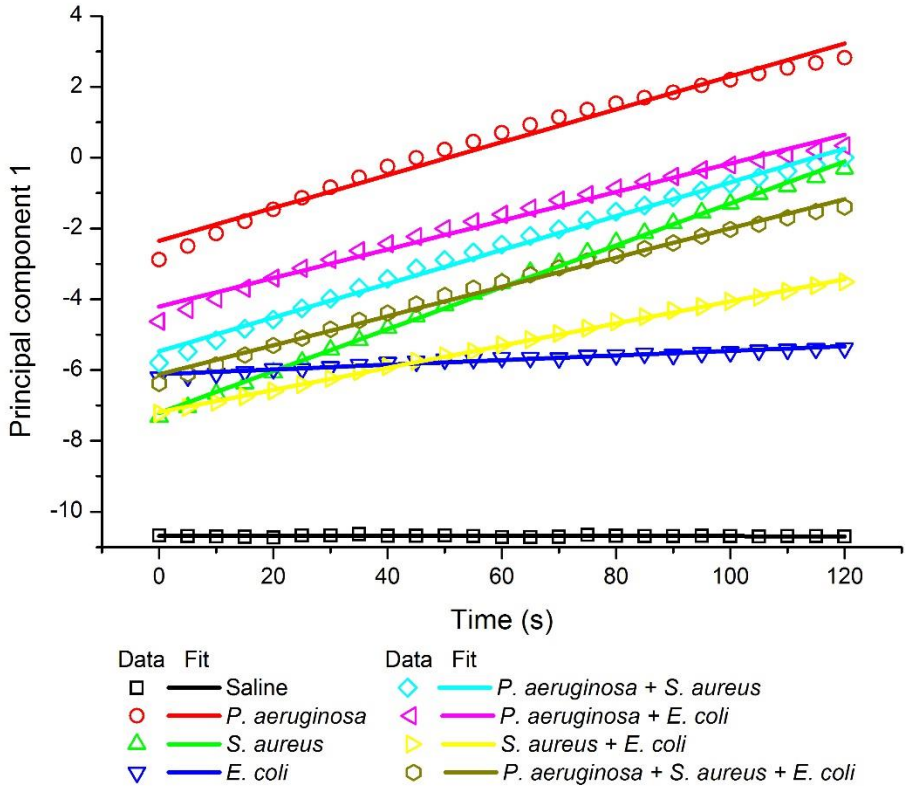

Figure 33: Linear fit of first principal component (85.1% variance explained) showing unique slopes and intercepts for each monomicrobial and polymicrobial samples

Table 10: Slopes and intercepts of linear fits of principal components for each of the bacterial samples

Sample	Slope	Intercept	R^2
Saline	0.000	-10.685	0.006
Pseudomonas aeruginosa	0.046	-2.349	0.980
Staphylococcus aureus	0.059	-7.211	0.998
Escherichia coli	0.007	-6.112	0.959
P. aeruginosa + S. aureus	0.048	-5.468	0.992
P. aeruginosa + E. coli	0.040	-4.206	0.986
S. aureus + E. coli	0.031	-7.186	0.999
P. aeruginosa + S. aureus + E. coli	0.041	-6.124	0.993

6.4.2 TEM images of bacterial mixtures

Chapter 3, 4, and 5 demonstrated that the color change in gold nanoparticles is due to their aggregation around bacteria [9, 84]. In order to study the nanoparticle aggregation in bacterial mixtures, these samples were imaged using TEM and are presented in Figure 34. The TEM images highlight that within the mixtures, each bacterial species maintains their affinity to nanoparticles. This allows us to identify which bacterium is being observed under the microscope. For example, *P. aeruginosa* shows a unique pattern of aggregation, where some areas are left bare and others show high aggregation, which is similar to that seen with *Stenotrophomonas maltophilia* in Chapter 4 [84]. In comparison, *S. aureus* shows almost complete coverage due to the teichoic acids present on the surface. Thus, *P. aeruginosa* and *S. aureus* can be easily distinguished in Figure 34 a, not only by their size and shape but also due to their affinity for nanoparticles. Similarly, *E. coli* generally shows a lower but relatively uniform aggregation of nanoparticles on its cell walls. This is clear in Figure 34 b and Figure 34 c, where *P. aeruginosa* and *S. aureus* show more aggregation than *E. coli* respectively. Finally, Figure 34 d exemplifies all the qualities of the three bacteria observed together, where each bacterial species can still be distinguished. Thus, not only does the "chemical nose" serve as a platform for colorimetric detection, it can also be used as a tool for staining bacteria in a characteristic manner.

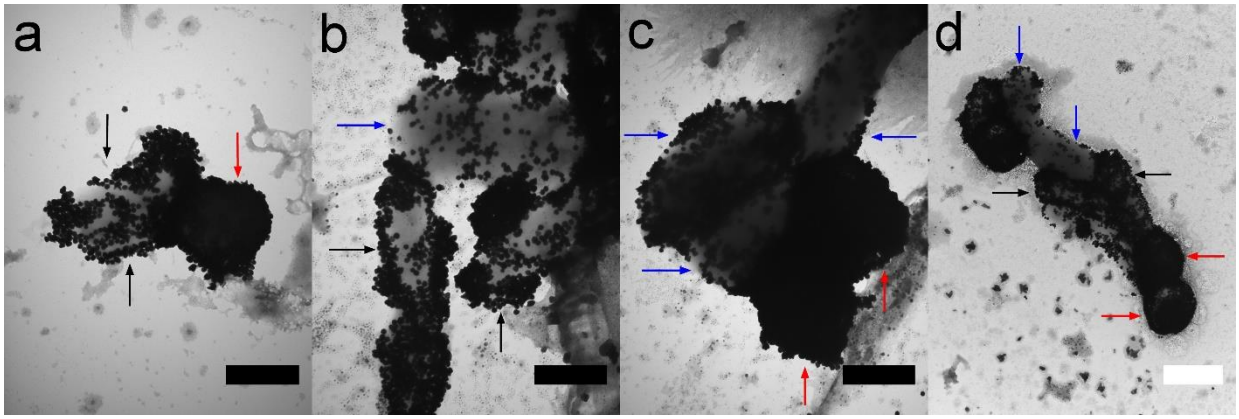

Figure 34. Transmission electron microscopy images of gold nanoparticles aggregating around bacteria mixtures: a) *Pseudomonas aeruginosa* (black arrows) + *Staphylococcus aureus* (red arrows), b) *P. aeruginosa* + *Escherichia coli* (blue arrows), c) *E. coli* + *S. aureus*, d) *P. aeruginosa* + *E. coli* + *S. aureus*, Black scale bars are 500 nm, white scale bar is 1000 nm.

6.5 Discussion

We employed a CCD spectrophotometer to rapidly acquire absorption spectra [230]. Previously, similar designs have been extensively explored for portable detection with the help of smartphones and portable scanners [226, 228, 229]. Thus, the results demonstrated here can be easily translated for use in a smartphone accessary, which would allow for simple deployment at the point-of-care. Additionally, the use of PCA as a mathematical tool overcomes the considerable noise in the spectra, because the noise gets eliminated when principal components are calculated. This analysis can be incorporated into a smartphone application in a manner similar to that used for label-free detection of proteins[226]. An easy-to-use interface will promote the deployment of the detection system in developing countries and in rural areas of developed countries, where resources and levels of education are limited [224, 231].

The "chemical nose" produces a distinct degree and rate of color change for each of the bacterial samples because of the surface features of bacteria [9, 13, 16, 84, 103, 138]. The cell walls of the bacteria contain unique compositions and orientations of lipids, proteins, and polysaccharides, which can interact with cationic gold nanoparticles [180-182]. As mentioned in previous chapters, in the case of Gram-positive bacteria such as *S. aureus*, most of the interactions are due to the polyanionic

teichoic acids [137, 178], while in the case of Gram-negative bacteria such as *E. coli* and *P. aeruginosa*, the interactions are governed by lipopolysaccharides [101, 179]. Additionally, the extracellular polymeric matrix can play a role in preventing aggregation of the gold nanoparticles as may be the case for *E. coli* [232, 233]. It has also been shown that lipids can exhibit specific domains within the cell walls upon addition of a cationic molecule [215] such as CTAB and this would explain the specific patterns of aggregation observed in the case of *P. aeruginosa*. Thus, a unique "smell" in the form of spectral response can be obtained for each sample in question for training the "chemical nose" and then an unknown spectrum can be matched with the training set, using techniques such as linear discriminant analysis to determine its identity.

6.6 Conclusions

A versatile "chemical nose" biosensor has been presented here that can diagnose monomicrobial and polymicrobial infections rapidly at the point-of-care. This was possible without complex modification of gold nanoparticles with biomolecules and by using a simple spectrophotometer design. The design can also be translated to a smartphone for widespread use in health, food, and environmental applications.

Chapter 7
"Chemical nose" biosensors: effects of nanoparticle shape and concentration

7.1 Summary

Gold nanoparticles are a versatile platform for "chemical nose" biosensors. In this chapter, we demonstrate that the shape and concentration of gold nanoparticles can be used to control the specificity and sensitivity in detecting Gram-positive and Gram-negative bacteria. The order of decreasing response from various shapes of gold nanoparticles is: nanostars > nanocubes > nanospheres > nanorods. Decreasing the concentration of nanoparticles increases the sensitivity and shifts the range of detectable concentration of bacteria to lower values.

7.2 Introduction

"Chemical nose" biosensors are gaining considerable attention as a replacement to their conventional counterparts that often require biomolecules such as aptamers and antibodies [13-16, 84, 103, 209, 234]. A "chemical nose" has the ability to produce unique patterns in the presence of the analyte, which facilitate the identification of the analyte [12]. Gold nanoparticles have been implemented as a "chemical nose" biosensor for the detection of proteins [234, 235], cancer cells [12, 196], and bacteria [16, 84].

As shown in previous chapters, a recent strategy for detecting bacteria using gold nanoparticles has been the use of electrostatic interactions between bacterial cell walls and the nanoparticle surfaces coated with cetyltrimethylammonium bromide (CTAB) [9, 84]. This approach provides a versatile platform for applying gold nanoparticles for the detection, identification, and quantification of bacteria. In order to exploit the potential of a gold nanoparticle-based "chemical nose," an understanding of the parameters that control specificity and sensitivity are necessary, but to-date are not well-understood. In this chapter, we show that controlling the shape and concentration of gold nanoparticles determines the specificity and sensitivity of the "chemical nose" biosensor. We used four gold nanoparticle shapes: nanospheres, nanostars, nanocubes, and nanorods to detect two Gram-positive (*Staphylococcus aureus* and *Enterococcus faecalis)* and two Gram-negative (*Escherichia coli*

and *Pseudomonas aeruginosa*) bacteria. These bacteria are notorious for contaminating food, water, and hospital surfaces and leading to antibiotic resistant infections [236]. Detection and identification of these bacteria at the point-of-care using a "chemical nose" biosensor will help to prevent such infections.

7.3 Materials and Methods

7.3.1 Materials

All chemicals, containers, and bacteria used in this study were from the same sources as in Chapter 5. Additionally, gold nanorods (A12-10-780) with 10 nm diameter and 38 nm length were purchased from Nanopartz Inc. (Loveland, CO, United States). All procured chemicals were used without further purification. As in Chapter 5, the 20 mL vials used for gold nanoseed synthesis were cleaned using 12M sodium hydroxide and larger glassware was cleaned using aqua regia as described in a published protocol [200].

7.3.2 Synthesis of gold nanospheres and nanostars

When selecting synthesis procedures, it was important to use CTAB-mediated synthesis such that the nanoparticles were coated with the surfactant, as the cationic head groups are essential to the "chemical nose" for aggregating around bacteria. As described in Chapter 3, the gold nanoseed precursor was synthesized using a previously described simple two-step one pot process [9, 84, 124]. To synthesize gold nanospheres and nanostars, the methods from Chapter 5 were used [9, 84].

7.3.3 Synthesis of gold nanocubes

Gold nanocubes were synthesized using published procedure while aiming for approximately 50 nm particles [237]. The gold seeds were first synthesized by adding an aqueous gold (III) chloride solution (0.25 mL, 10 mM) to a CTAB solution (7.5 mL, 100 mM) at approximately 30 °C. This was followed by reduction of the gold using sodium borohydride (0.8 mL, 10 mM) under vigorous stirring. The seed was then left at 30 °C for at least 3 h and then diluted 1:10 in Millipore water and filtered with a 200 nm filter before further use. The growth solution of nanocubes required addition of CTAB (48 mL, 300 mM) and gold (III) chloride (6 mL, 10 mM) to 240 mL Millipore water. Then, 28.5 mL of 600 mM ascorbic acid were added and the solution was mixed by inversion. Once the

solution turned colorless, 150 µL of the diluted, filtered gold nanoseed were added. The solution was mixed by inversion and left undisturbed for 15 minutes.

Gold nanospheres, nanostars, and nanocubes were purified by centrifugation at 10,000 rpm for 15 min and then resuspended in 1 mM CTAB solution. In the case of gold nanocubes, half the volume of CTAB solution was used for resuspension to increase the concentration of nanoparticles while nanospheres and nanostars were resuspended in the same volume as starting solution.

7.3.4 Bacterial culture

Bacteria were cultured and washed according to methods from previous chapters [84]. *S. aureus, E. coli,* and *P. aeruginosa* were inoculated on TSA plates and *E. faecalis* was inoculated on TSA II plates. All bacteria were incubated at 37 °C for 24 hours. Bacterial cells were harvested using alginate swabs and suspended in 5 mL of sterile saline (2.55%) with nutrient broth (~0.006%) in a 15 mL centrifuge tube. Each bacterial strain was then washed seven times with saline by centrifugation at 4,000 rpm for 10 min. The bacteria were then diluted to obtain an optical density at 660 nm (OD_{660}) of 0.1 (~10^8 CFU/mL) [172]. When the bacteria were added to gold nanoparticles, the solution was diluted 1:3 to obtain final OD_{660} = 0.03 for bacteria. The bacteria were further diluted serially in 2.55% saline (with ~0.006% broth) to obtain dilution factors of 2x, 4x, 8x, 16x, 32x, and 64x.

7.3.5 Response of nanoparticles to bacteria

The assay for measuring response of the nanoparticles to bacterial species was performed in 96-well microplates. The plates were prepared by adding 100 µL of the bacteria or saline control in triplicates. This was followed by the addition of 200 µL of the nanospheres, nanostars, nanocubes, or nanorods. The microplates were then placed on a Stovall Life Science Inc. (Peosta, IA, USA) Belly Dancer orbital shaker for 2 mins and incubated overnight at room temperature in the dark. After incubation, the UV-Visible absorption spectra were obtained for each well in the microplates using a BioTek (Winooski, VT, USA) Epoch microplate spectrophotometer while scanning from 300 nm to 999 nm with a step size of 1 nm. These spectra were plotted using OriginLab® OriginPro®.

The effect of CTAB concentration was studied by centrifuging the gold nanostars at 10,000 rpm for 15 minutes, discarding the supernatant and then resuspending the pellet in the appropriate concentration of CTAB (100 µM, 1 mM, 10 mM, or 100 mM).

The peaks for various nanoparticles are summarized in Table 11. The normalized absorbance values were obtained for all samples by using the following equation:

$$Normalized\ absorbance = (Average\ saline\ control\ absorbance\ at\ peak) - Average\ saline\ control\ absorbance\ at\ baseline) - (Sample\ absorbance\ at\ peak - Sample\ absorbance\ at\ baseline)$$

The normalized absorbance is converted to a normalized response (%) by dividing the normalized absorbance for each bacterial sample with their respective saline control. This accounts for the effect of different initial starting absorbance values for each of the nanoparticles shapes.

When testing the response of nanoparticles to saline and Millipore water, the absorbance fraction was calculated as follows:

$$Absorbance\ fraction = \frac{(Average\ absorbance\ at\ peak - average\ absorbance\ at\ baseline)\ for\ saline}{(Average\ absorbance\ at\ peak - average\ absorbance\ at\ baseline)\ for\ Millipore\ water} \times 100\%$$

Table 11: Absorption spectra characteristics of various shapes of nanoparticles used

Nanoparticle	Peak wavelength (nm)	Baseline wavelength (nm)
Nanospheres	531	800
Nanostars	579	800
Nanocubes	529	800
Nanorods	777	925

The effect of nanoparticle concentration was studied by adding gold nanostars to 1 mM CTAB solutions such that they would be diluted to 10%, 20%, 30%, 40%, 50%, 60%, 70%, 80% and 90% of the original stock concentration. The stock was used as 100% concentration. These nanostars were added to *S. aureus* and *P. aeruginosa* as mentioned above and response was measured.

7.3.6 Transmission electron microscopy of bacteria and gold nanoparticles

Gold nanospheres, nanostars, nanocubes, and nanorods were prepared for transmission electron microscopy (TEM) by adding 5 µL of the solutions to a copper grid and allowing them to dry under ambient conditions overnight. Similarly, mixtures of bacteria and gold nanoparticles (5 µL) were added to formvar-coated copper TEM grids and allowed to dry under ambient conditions overnight. Once dry, the bacteria samples were washed by placing 10 µL of Millipore water on the TEM grids for 30 seconds and then wicking the liquid using filter paper to remove excess surfactants, salts, and unbound gold nanoparticles. The samples were then imaged using Phillips (Eindhoven, The Netherlands) CM10 TEM.

7.4 Results and Discussion

7.4.1 Spectrophotometric responses of each shape to different bacteria

The UV-Visible absorption spectra—plotted as contour plots in Figure 35—show that the peak width, location, and intensity for each nanoparticle solution is different as indicated by the saline controls. The peak location is governed by the surface plasmon resonance frequency, which is unique for each shape of nanoparticle [238-240]. The peak width depends on the size and size distribution of the nanoparticles [123]. The intensity of absorption depends on the concentration and extinction coefficient of the nanoparticles [241, 242]. Each of these qualities contributes to a characteristic spectrum for the various shapes of gold nanoparticles. When combined with bacteria, a colorimetric response is obtained due to the aggregation of the nanoparticles around the bacteria, caused by electrostatic interactions between cationic CTAB and anionic cell walls [9, 15, 84, 137, 138]. Figure 35 exemplifies that the response from each bacterium is unique and distinct for different shapes of nanoparticles. While all bacteria present a concentration dependent response for each nanoparticle shape, the degree of response varies: *P. aeruginosa* provides the most change compared to saline and *E. coli* provides the least.

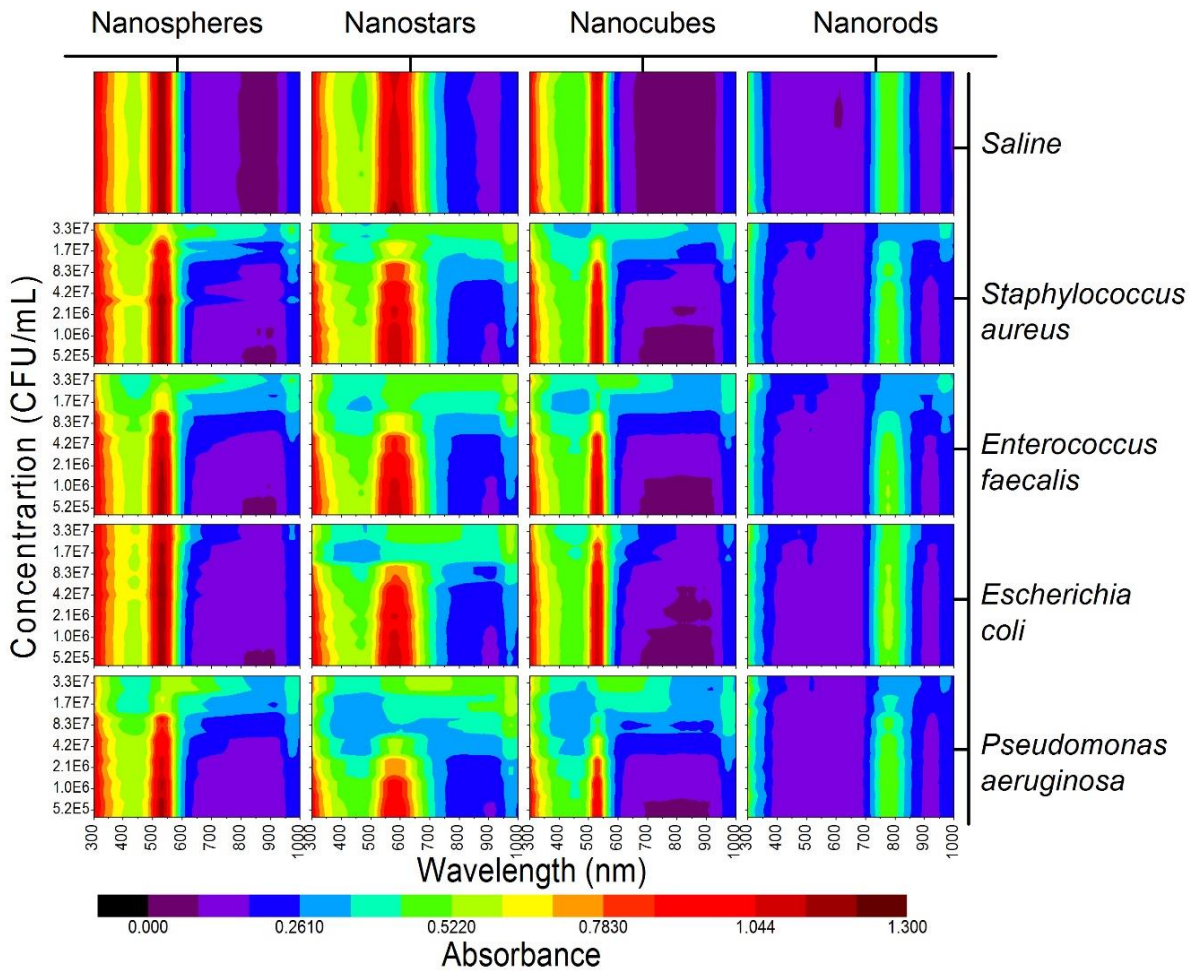

Figure 35: UV-Visible Absorption spectra of gold nanospheres, nanostars, nanocubes, and nanorods in the presence of saline (n = 12) or bacteria (n = 3 per concentration) at various concentrations ranging from approximately 5.2 x 10^5 CFU/mL to 3.3 x 10^7 CFU/mL. Each of the saline plots is made up of 12 slices (one per replicate) and bacteria plots is made of 21 slices (three per concentration).

In order to quantify the response obtained amongst different nanoparticles and bacteria, the absorbance value at the peak (Table 11) was used and normalized against saline and baseline. The normalized response demonstrates that the shape of nanoparticles has minimal effect for Gram-positive bacteria but causes a drastic difference for Gram-negative bacteria (Figure 36). Amongst all four bacteria, *P. aeruginosa* highlights the differences between nanoparticle shapes the most. Figure

36 d) also shows that the response decreases in the following order: nanostars > nanocubes > nanospheres > nanorods. Although nanorods have previously been used for sensitive detection of proteins [44] and nucleic acids [60, 61], they seem to be the least sensitive in the current experiments. As seen in the TEM images (Figure 38), this is most likely because the distance between aggregated nanorods seems to be larger than the distance between other nanoparticles and hence the particles fail to interact with each other and cause a colorimetric response.

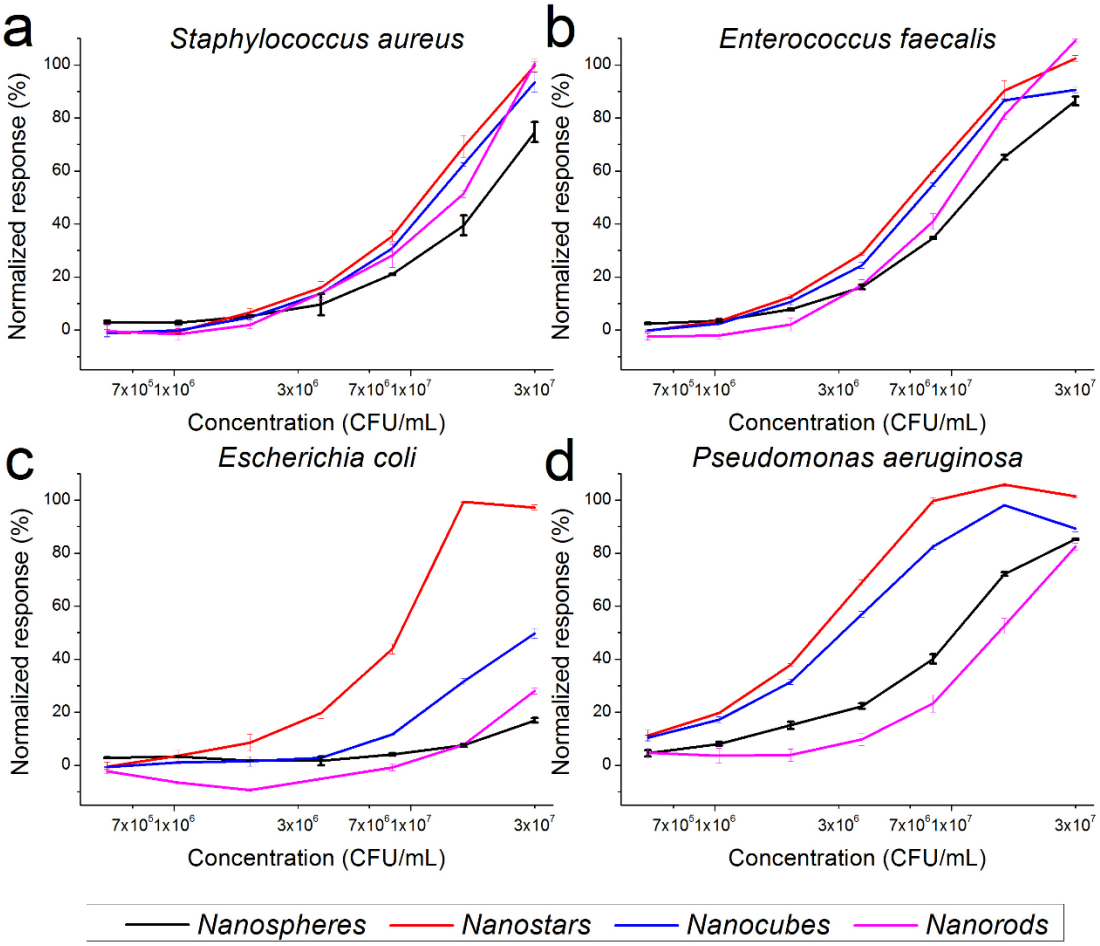

Figure 36: Concentration dependent peak response obtained from a) *Staphylococcus aureus*, b) *Enterococcus faecalis*, c) *Escherichia coli*, and d) *Pseudomonas aeruginosa* for different shapes of nanoparticles: nanospheres, nanostars, nanocubes, nanorods. Data are presented as mean ± S.D. (n = 3).

Since the concentration of CTAB could be different for each nanoparticle solution, the effect of CTAB concentration on the response needs to be tested. We used gold nanostars as the model nanoparticle and *S. aureus* as the model bacterium, while varying CTAB concentration from a range of 100 µM to 100 mM. The normalized response, reported in Figure 37, does not depend on the concentration of CTAB. The differences in response for each shape seem to be dependent on the roughness of the nanoparticles, which would provide them a higher surface area and hence a higher area for interaction with bacterial cell walls. Additionally, particles with more branching (nanostars) or edges (cubes) are expected to be more protruding into the functional groups present on the bacterial surface [84]. The concentration of salt could also influence the response of nanoparticles to bacteria, but in the current experiments the salt concentration was kept constant to obtain isotonic solutions of bacteria [140] and prevent lysis. The effect of salt concentration could be explored by changing the medium in which bacteria are suspended depending on the application of interest.

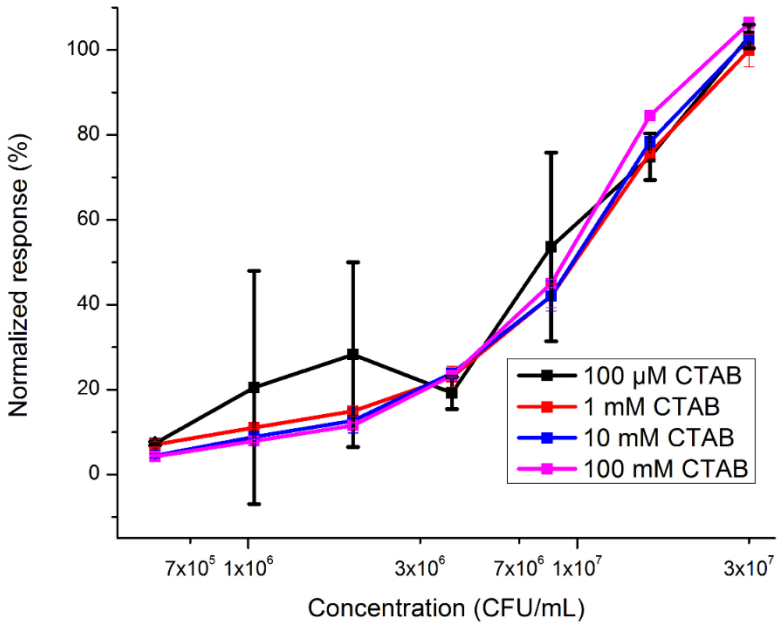

Figure 37: The effect of CTAB concentration on the response of gold nanostars to *Staphylococcus aureus*. Data is reported as mean ± S.D. (n = 3).

7.4.2 Transmission electron microscopy

In order to obtain a better understanding of the aggregation of gold nanoparticles, TEM images were obtained for all bacteria-nanoparticle combinations. The TEM images show that the sizes of nanoparticles are comparable (Figure 38). It is also observed that *S. aureus* and *E. faecalis* show complete coverage of the cell with nanospheres, nanostars, and nanocubes. In the case of nanorods, there are some areas that remain uncovered. Additionally, multilayer deposition is observed for *S. aureus*, which could be an indication of a higher extent of polyanionic teichoic acids [137, 178, 180] as compared to *E. faecalis*. In the case of Gram-negative bacteria, lipopolysaccharides and phospholipids are mostly responsible for the negative charge and hence the aggregation of cationic nanoparticles [15, 84, 101, 179]. When looking at *E. coli*, a relatively uniform but sparse distribution of nanoparticles is observed for all shapes except nanostars, which is consistent with the colorimetric response observed in Figure 36 c). The TEM images of *P. aeruginosa* highlight an important behavior: the nanoparticles aggregate in specific areas of the bacterium as observed for the nanostars and nanocubes, while other sections of the surface are completely uncovered. This observation is similar to the ones from Chapter 5 and 6. The literature suggests that this localized aggregation would be due to the formation of lipid domains around specific proteins [214] or due to the addition of cationic molecules such as CTAB [215]. Specifically, anionic lipids such as phosphatidylglycerol and diphosphatidylglycerol (cardiolipin) would attract the nanoparticles and lead to aggregation. On the other hand, gold nanorods and nanospheres show a relatively uniform adsorption on the surface of the bacterium and also a lower response. This also suggests that if the lipid domains are responsible for selective aggregation, they might only be accessible via protruding nanoparticles.

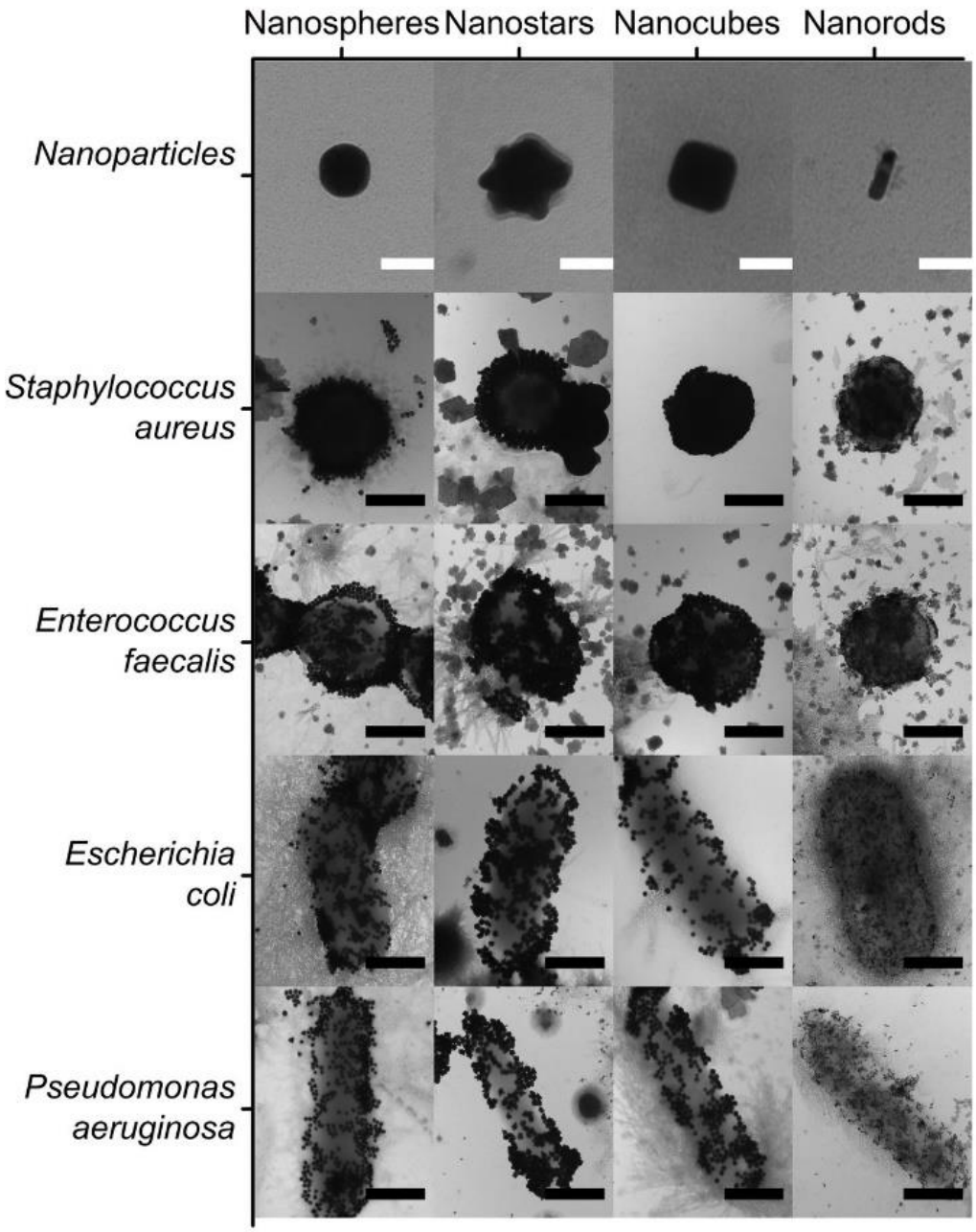

Figure 38: Transmission electron microscopy images of each of the different shapes of nanoparticles aggregating around various Gram-positive and Gram-negative bacteria. White scale bars are 50 nm and black scale bars are 500 nm.

To exclude the possibility that the differential responses observed for each type of nanoparticle were primarily due to their sizes instead of shapes, the colloidal stability of each nanoparticle solution was tested by comparing the absorbance in saline and Millipore water. The relative absorbance at peak of each nanoparticle is compared instead of the raw absorbance spectra because the absorption spectrum of each nanoparticle solution is distinct and any changes would be difficult to compare. If the response observed in the presence of bacteria was mainly a result of the size differences, it is expected that the nanoparticles would have decreasing colloidal stability and hence, lower peak absorbance values [9, 243] in the following order: nanostars < nanocubes < nanospheres < nanorods. The results from the saline experiment are presented in Figure 39 and they highlight that there is no correlation between the nanoparticle type and aggregation in saline. Thus, the bacterial response cannot be attributed to the small differences in the sizes of the various nanoparticles.

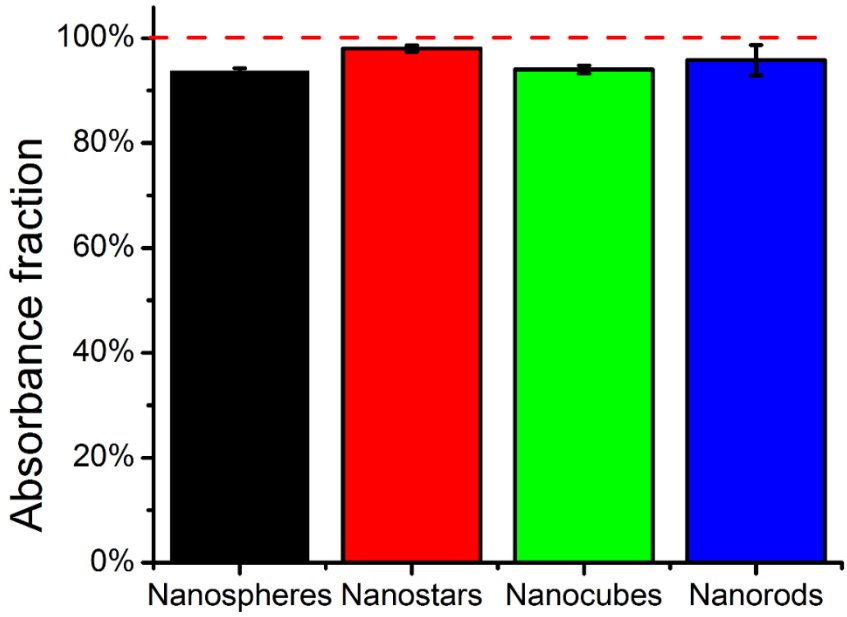

Figure 39: Peak response of the gold nanoparticles in the presence of saline. Dashed red line indicates gold nanoparticles added to Millipore water. Data is reported as mean ± S.D. (n = 3).

CTAB-coated nanoparticles can be used as a "chemical nose" by analyzing the response, developing a training set and then matching the observed response of an unknown sample to the training set as demonstrated in Chapter 4 and 5 [84]. Since each nanoparticle shape provides a unique response for different bacteria, this information can be used for increasing the specificity of the assay. This is possible if a mixture of shapes of nanoparticle is used. The mixture will have more features in the absorption spectrum as compared to a single nanoparticle solution in the form of peaks. Each of these additional peaks will respond differently to the bacteria present. When considering the shape of nanoparticles for providing drastic responses, it is observed that nanostars provide the greatest response for all bacteria tested and hence should be used for applications requiring a dramatic color change, such as in point-of-care detection.

7.4.3 The effect of nanoparticle concentration

Another strategy for altering the sensitivity and range of detection is to adjust the concentration of nanoparticles. We made linear dilutions of the stock gold nanostars in 1 mM CTAB to obtain a range of 10% - 100% fractions in increments of 10%. These fractions were then tested with various concentration of *S. aureus* and *P. aeruginosa* and the normalized peak response is presented in Figure 40. Interestingly, the concentration of nanostars has a greater impact on *S. aureus* as compared to *P. aeruginosa.* This could be because the concentrations tested for *P. aeruginosa* are already on the right side of the concentration-dependent response curve, where a saturation is observed. From the *S. aureus* samples, it is clear that the concentration of nanoparticles can be adjusted according to the bacteria concentration range of interest, where a lower fraction of nanoparticles is appropriate for a lower concentration of bacteria. This is because the colorimetric response is determined by the proportion of aggregated nanoparticles to non-aggregated nanoparticles. When there are fewer bacteria, this proportion is higher for a lower fraction of nanoparticles. In order to observe the lower end of the response from Figure 40 b and to determine the detection limit of the "chemical nose" biosensor, the experiment was repeated by using lower concentrations of *P. aeruginosa.* The linear region of normalized absorbance of *P. aeruginosa* when using 10% fraction of nanoparticles is presented in Figure 41. An R^2 value of 0.91 is obtained for the line of best fit, with the sensitivity (slope) of 1.3×10^{-7} mL/CFU, limit of linearity of 5.4×10^5 CFU/mL, and limit of detection of 4.9×10^4 CFU/mL (defined as three times the standard deviation of blank sample divided by the sensitivity).

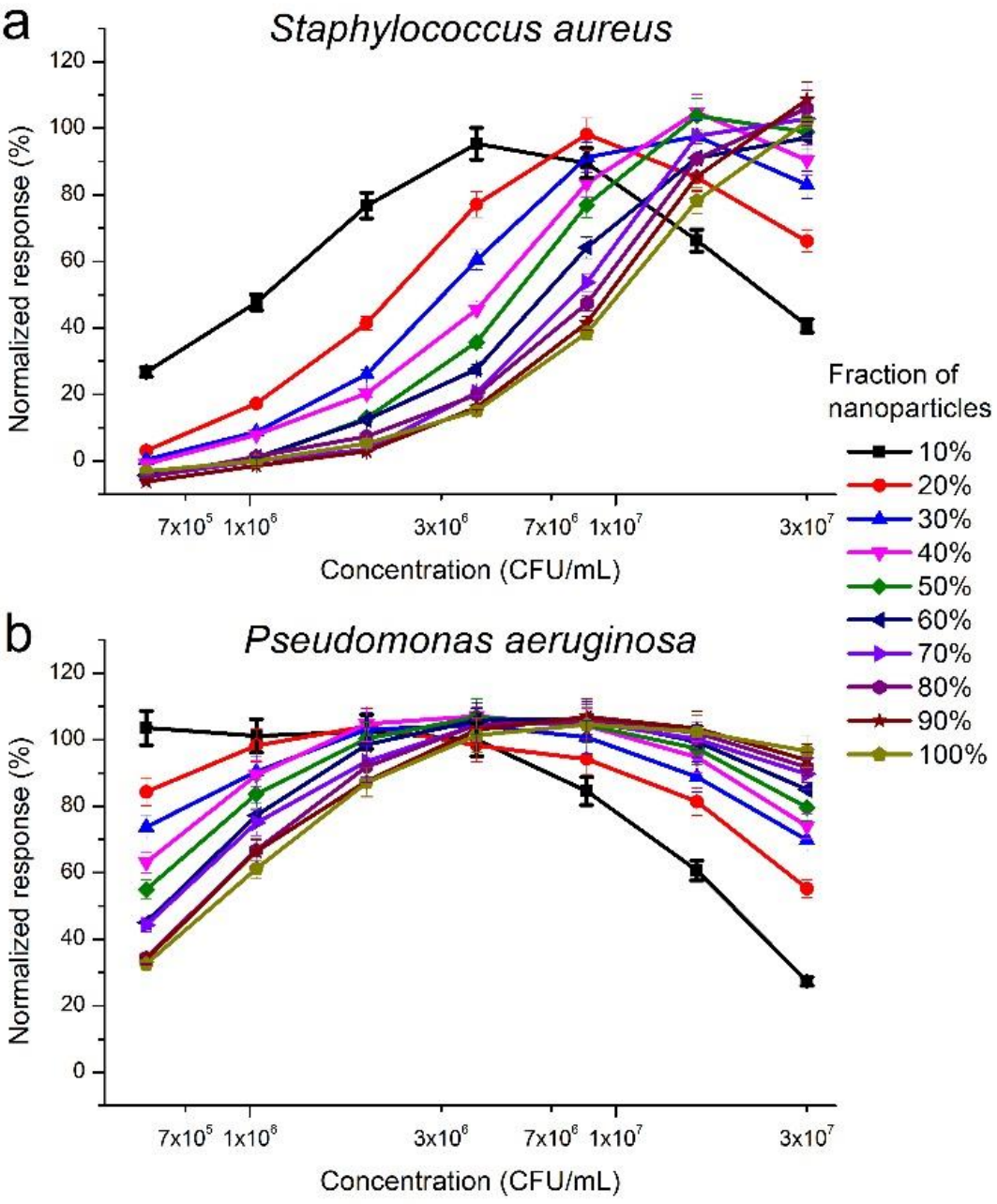

Figure 40: The effect of nanoparticle concentration on colorimetric response for a) Gram-positive *Staphyloccocus aureus* and b) Gram-negative *Pseudomonas aeruginosa.* Error bars are 5% of the normalized response values.

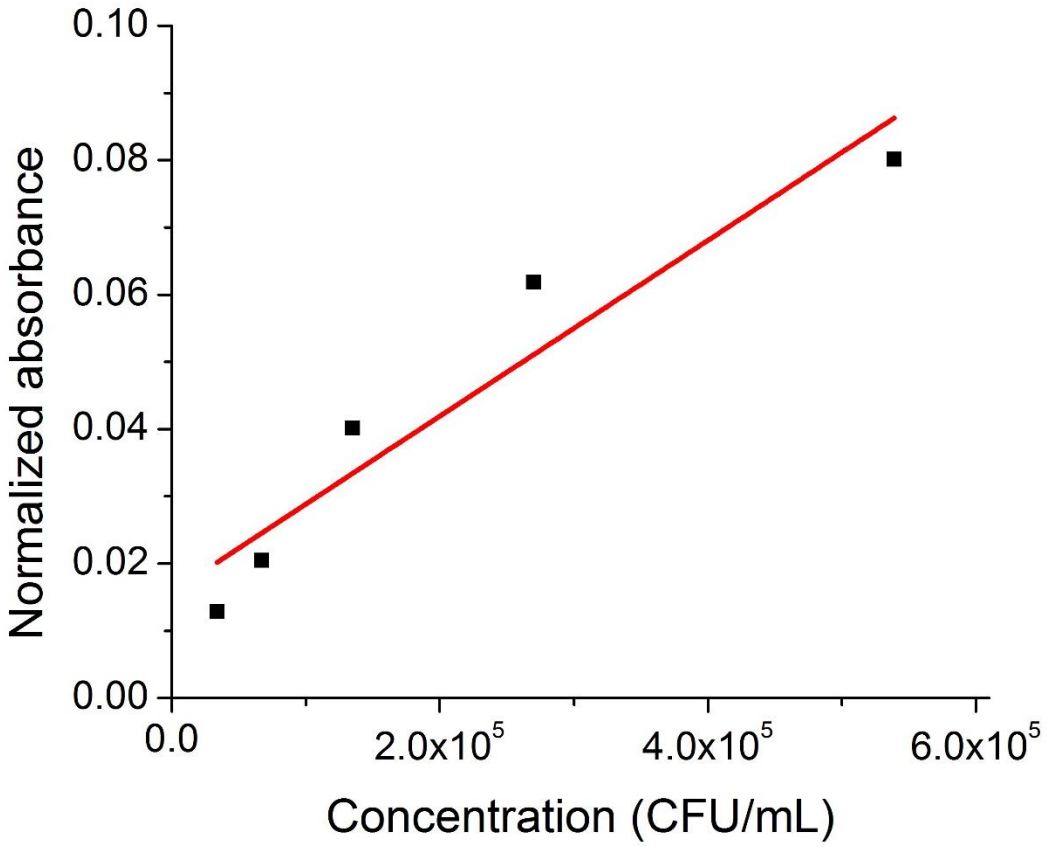

Figure 41: Linear region of saline normalized absorbance of *Pseudomonas aeruginosa* when 10% fraction of gold nanostars are used. The red line shows linear fit, which is used for determination of detection limit.

7.5 Conclusions

We have demonstrated that gold nanostars provide the most drastic response for a "chemical nose" biosensor and gold nanorods provide the least drastic. A differential response between shapes of nanoparticles can be used to improve the specificity of a "chemical nose" biosensor. The concentration of nanoparticles can tune the concentration range of bacteria that can be detected.

Chapter 8
Conclusions and Future Work

8.1 Summary

This thesis presents new findings in the fields of nanotechnology, microbiology, materials science, and chemical engineering. Gold nanoparticles hold tremendous potential as biosensors because their optical properties are extremely sensitive to their size, morphology, and aggregation state. Cationic surfactant-coated gold nanoparticles are able to detect bacteria by using electrostatic interactions with the bacterial cell wall surface. The research presented here demonstrates that the response from such a biosensor is dependent on the physical properties of the nanoparticles and the bacteria. This dependence allows the biosensor to discriminate between different bacteria when a set of responses is combined together in a "chemical nose" approach. Additionally, the kinetics of the colorimetric response are also unique for each species of bacteria, which facilitates rapid detection. Thus, this thesis provides promising results for using surfactant-coated gold nanoparticles to build "chemical nose" biosensors as an alternative to biomolecule-functionalized nanoparticles that are often expensive and limited in application.

8.2 Conclusions

Gold nanostars can be synthesized using a surfactant-assisted seed-mediated growth where the particle size and degree of branching can be directly controlled by the concentration of surfactant cetyltrimethylammonium bromide (CTAB) used and amount of gold nanoseeds added. Increasing the amount of gold nanoseeds decreases the particle size while increasing the surfactant concentration increases the degree of branching. An increasing size and branching causes a red shift in the absorption peak of the gold nanoparticle solutions and hence changes the color of the solutions from red to purple to blue. In the presence of Gram-positive bacteria, the gold nanoparticles aggregate around the bacteria and hence, the solution changes color. The rate and degree of color change are dependent on the size and branching of gold nanostars, where bigger and more branched particles show faster and greater color change.

In the presence of different species of ocular pathogens, a set of unique responses can be obtained for each bacterium by using two different types of nanoparticles: red nanostars that have a low degree of branching and blue nanostars with a high degree of branching. The nanostars aggregate around the bacteria in a unique manner because of differences in the components of the cell walls. Some bacteria show a complete coverage with nanoparticles while others show specific patterns of aggregation on the surface as observed by transmission electron microscopy (TEM).

A "chemical nose" biosensor can be developed by mixing nanoparticles with distinct sizes and morphologies, for eg. nanospheres and nanostars. The "chemical nose" provides a unique absorption spectrum for each of the eight species of bacteria tested. Using the absorption spectrum also allows for distinction between different concentrations of bacteria and mixtures of bacteria. TEM confirms that each species of bacteria shows a specific degree and pattern of aggregation of nanoparticles, which is responsible for the colorimetric response. Additionally, the difference in colorimetric response is beyond the distinction of Gram-positive and Gram-negative because some Gram-negative bacteria such as *Pseudomonas aeruginosa* and *Stenotrophomonas maltophilia* show a higher response compared to Gram-positive ones. The extracellular polymeric substances play a role in reducing the colorimetric response by shielding the lipids and proteins on the surface of certain bacterial cell walls such as *Achromobacter xylosoxidans* and *Delftia acidovorans.* Thus, a complex set of interactions is involved in governing the colorimetric response from the "chemical nose," which enables the unique responses for each bacterial species and mixtures.

The absorption spectra of the "chemical nose" can be acquired rapidly when a charge-coupled device (CCD) spectrophotometer is used because all wavelengths of light can be measured simultaneously. This design permits the use of kinetics of color change for detection whereas previous monochromator spectrophotometer could only detect temporally constant spectra. This design provided sufficient data for detection within two minutes of acquisition. Each bacterium and mixture of bacteria presented a unique rate of change suggesting that the characteristics of colorimetric response of a "chemical nose" are observed in the kinetics as well.

A broader study of shapes and concentrations of nanoparticles showed that nanoparticles with sharper features could provide a higher response for Gram-negative bacteria. Specifically, the order of response was nanostars > nanocubes > nanospheres > nanorods. Additionally, a lower concentration

of nanoparticles allowed the detection of lower concentration of bacteria. The concentration of cationic surfactant CTAB did not alter the colorimetric responses to bacteria significantly, but at a low concentration of 100 μM, the gold nanoparticles showed higher variability in the responses.

Overall, cationic gold nanoparticles are an excellent platform for providing a "chemical nose" biosensor for detecting bacteria. Mixing different shapes and sizes of nanoparticles promotes differential responses in the presence of different species of bacteria. The library of detectable bacteria can be expanded by exploring additional shapes, sizes, and surface features of gold nanoparticles.

8.3 Recommendations for future work

The following avenues are recommended based on the results from this research:

1. Synthesize additional shapes of gold nanoparticles such as prisms, hexagons, and shells to determine if the colorimetric response of these nanoparticles is different from the shapes that have already been studied. Additional shapes provide more tools to tackle the discrimination between closely related bacteria. Also, only one method was currently used for synthesizing gold nanostars. It is possible to obtain higher anisotropy of branches using other methods such as those using poly(vinylpyrrolidone). It is recommended that these methods are attempted and then the polymeric coating is replaced by CTAB to achieve the cationic nature of nanoparticles. Longer branches could provide a higher sensitivity to the biosensor.
2. Explore the incorporation of capillary electrophoresis for enhanced sensitivity and specificity. Electrophoresis could separate bacteria based on the degree of aggregation of gold nanoparticles and thus provide additional resolution between bacterial species. It could also increase sensitivity since single cell separation has been possible using electrophoresis. Additionally, a spectrophotometer with increased pathlength could be useful for higher sensitivity by using lower concentration of nanoparticles.
3. Evaluate the performance of gold nanoparticles "chemical nose" in complex biological media such as blood, serum, urine, and saliva as well as food sources to determine the effect of interferents on the detection of bacteria. It is possible that some media might cause aggregation of gold nanoparticles and thus, prevent the use of nanoparticles for those specific applications. This

could be overcome by further stabilizing the nanoparticles using surface modification such as by conjugating poly(ethylene glycol) on the surface.

4. Investigate the specific bacterial cell wall components responsible for aggregation of nanoparticles. This is possible by studying the interactions of major lipids present in the cell walls with CTAB-coated gold nanoparticles using lipid blot assays. Additionally, optical microscopy techniques might enlighten some of the aggregation processes if fluorescent dyes with affinity specific to different components of cell walls are used because gold nanoparticles would quench the fluorescence upon binding. Another approach is to use a library of single species bacterial strains with specific mutations and determine if any of the bacteria provide a change in the colorimetric response.
5. Measure the response of gold nanoparticles in the presence of antibiotic-resistant strains of pathogenic bacteria. If a differential response can be obtained for different strains of the same species, the "chemical nose" could be employed as a rapid diagnosis tool for prescribing appropriate antibiotic therapy.
6. Investigate advanced machine learning algorithms for expanding the database of bacteria. Machine learning and artificial intelligence are very active fields and are increasingly being used for carrying out scientific research. These tools will be extremely useful if a versatile "chemical nose" biosensor is to be developed.
7. Develop a portable chip along with a cellphone spectrometer for analyzing colorimetric response. Creating a kit for detection can allow rapid diagnosis in clinics. A smartphone application for analyzing the colorimetric response based on machine learning algorithms will enable the translation of this technology to the end user.

Bibliography

[1] Bertino JS,Jr. Impact of antibiotic resistance in the management of ocular infections: the role of current and future antibiotics. Clinical ophthalmology (Auckland, N.Z.) 2009;3:507-521.

[2] Tallury P, Malhotra A, Byrne LM, Santra S. Nanobioimaging and sensing of infectious diseases. Advanced Drug Delivery Reviews 2010;62(4-5):424-437.

[3] Taravati P, Lam D, Van Gelder RN. Role of molecular diagnostics in ocular microbiology. Current ophthalmology reports 2013;1(4):10.1007/s40135-013-0025-1.

[4] Kanwal A, Lakshmanan S, Bendiganavale A, Bot CT, Patlolla A, Raj R, Prodan C, Iqbal Z, Thomas GA, Farrow RC. Scalable nano-bioprobes with sub-cellular resolution for cell detection. Biosensors & bioelectronics 2013;45:267-273.

[5] Chan T, Gu F. Development of a colorimetric, superparamagnetic biosensor for the capture and detection of biomolecules. Biosensors & bioelectronics 2013;42:12-16.

[6] Verdoy D, Barrenetxea Z, Berganzo J, Agirregabiria M, Ruano-Lopez JM, Marimon JM, Olabarria G. A novel Real Time micro PCR based Point-of-Care device for Salmonella detection in human clinical samples. Biosensors & bioelectronics 2012;32(1):259-265.

[7] Upadhyayula VK. Functionalized gold nanoparticle supported sensory mechanisms applied in detection of chemical and biological threat agents: a review. Analytica Chimica Acta 2012;715:1-18.

[8] Azzazy HM, Mansour MM, Samir TM, Franco R. Gold nanoparticles in the clinical laboratory: principles of preparation and applications. Clinical chemistry and laboratory medicine : CCLM / FESCC 2012;50(2):193-209.

[9] Verma MS, Chen PZ, Jones L, Gu FX. Branching and size of CTAB-coated gold nanostars control the colorimetric detection of bacteria. RSC Advances 2014;4(21):10660-10668.

[10] Saha K, Agasti SS, Kim C, Li X, Rotello VM. Gold nanoparticles in chemical and biological sensing. Chemical reviews 2012;112(5):2739-2779.

[11] Xiao J, Qi L. Surfactant-assisted, shape-controlled synthesis of gold nanocrystals. Nanoscale 2011;3(4):1383-1396.

[12] Rotello V. Sniffing out cancer using "chemical nose" sensors. Cell cycle (Georgetown, Tex.) 2009;8(22):3615-3616.

[13] Bunz UH, Rotello VM. Gold nanoparticle-fluorophore complexes: sensitive and discerning "noses" for biosystems sensing. Angewandte Chemie (International ed.in English) 2010;49(19):3268-3279.

[14] Miranda OR, Creran B, Rotello VM. Array-based sensing with nanoparticles: 'chemical noses' for sensing biomolecules and cell surfaces. Current opinion in chemical biology 2010;14(6):728-736.

[15] Phillips RL, Miranda OR, You CC, Rotello VM, Bunz UH. Rapid and efficient identification of bacteria using gold-nanoparticle-poly(para-phenyleneethynylene) constructs. Angewandte Chemie (International ed.in English) 2008;47(14):2590-2594.

[16] Wan Y, Sun Y, Qi P, Wang P, Zhang D. Quaternized magnetic nanoparticles-fluorescent polymer system for detection and identification of bacteria. Biosensors & bioelectronics 2014;55:289-293.

[17] Boisselier E, Astruc D. Gold nanoparticles in nanomedicine: preparations, imaging, diagnostics, therapies and toxicity. Chemical Society Reviews 2009;38(6):1759-1782.

[18] Ghosh P, Han G, De M, Kim CK, Rotello VM. Gold nanoparticles in delivery applications. Advanced Drug Delivery Reviews 2008;60(11):1307-1315.

[19] Paciotti GF, Myer L, Weinreich D, Goia D, Pavel N, McLaughlin RE, Tamarkin L. Colloidal gold: a novel nanoparticle vector for tumor directed drug delivery. Drug delivery 2004;11(3):169-183.

[20] Huang X, El-Sayed IH, Qian W, El-Sayed MA. Cancer cell imaging and photothermal therapy in the near-infrared region by using gold nanorods. Journal of the American Chemical Society 2006;128(6):2115-2120.

[21] Gobin AM, Lee MH, Halas NJ, James WD, Drezek RA, West JL. Near-infrared resonant nanoshells for combined optical imaging and photothermal cancer therapy. Nano letters 2007;7(7):1929-1934.

[22] Jain PK, El-Sayed IH, El-Sayed MA. Au nanoparticles target cancer. Nano Today 2007;2(1):18-29.

[23] Murphy CJ, Gole AM, Stone JW, Sisco PN, Alkilany AM, Goldsmith EC, Baxter SC. Gold nanoparticles in biology: beyond toxicity to cellular imaging. Accounts of Chemical Research 2008;41(12):1721-1730.

[24] Popovtzer R, Agrawal A, Kotov NA, Popovtzer A, Balter J, Carey TE, Kopelman R. Targeted gold nanoparticles enable molecular CT imaging of cancer. Nano letters 2008;8(12):4593-4596.

[25] Eghtedari M, Oraevsky A, Copland JA, Kotov NA, Conjusteau A, Motamedi M. High sensitivity of in vivo detection of gold nanorods using a laser optoacoustic imaging system. Nano letters 2007;7(7):1914-1918.

[26] Hutter E, Fendler J. Exploitation of localized surface plasmon resonance. Advanced Materials 2004;16(19):1685-1706.

[27] Liu J, Lu Y. A colorimetric lead biosensor using DNAzyme-directed assembly of gold nanoparticles. Journal of the American Chemical Society 2003;125(22):6642-6643.

[28] Mayer KM, Hafner JH. Localized surface plasmon resonance sensors. Chemical reviews 2011;111(6):3828-3857.

[29] Daniel MC, Astruc D. Gold nanoparticles: assembly, supramolecular chemistry, quantum-size-related properties, and applications toward biology, catalysis, and nanotechnology. Chemical reviews 2004;104(1):293-346.

[30] Kaittanis C, Santra S, Perez JM. Emerging nanotechnology-based strategies for the identification of microbial pathogenesis. Advanced Drug Delivery Reviews 2010;62(4-5):408-423.

[31] Lazcka O, Del Campo FJ, Munoz FX. Pathogen detection: a perspective of traditional methods and biosensors. Biosensors & bioelectronics 2007;22(7):1205-1217.

[32] Skottrup PD, Nicolaisen M, Justesen AF. Towards on-site pathogen detection using antibody-based sensors. Biosensors & bioelectronics 2008;24(3):339-348.

[33] Mao X, Ma Y, Zhang A, Zhang L, Zeng L, Liu G. Disposable nucleic acid biosensors based on gold nanoparticle probes and lateral flow strip. Analytical Chemistry 2009;81(4):1660-1668.

[34] Farber JM, Peterkin PI. Listeria monocytogenes, a food-borne pathogen. Microbiological reviews 1991;55(3):476-511.

[35] Velusamy V, Arshak K, Korostynska O, Oliwa K, Adley C. An overview of foodborne pathogen detection: in the perspective of biosensors. Biotechnology Advances 2010;28(2):232-254.

[36] Khanna VK. Nanoparticle-based sensors. Defence Science Journal 2008;58(5):608-616.

[37] Agasti SS, Rana S, Park MH, Kim CK, You CC, Rotello VM. Nanoparticles for detection and diagnosis. Advanced Drug Delivery Reviews 2010;62(3):316-328.

[38] Jung YL, Jung C, Parab H, Li T, Park HG. Direct colorimetric diagnosis of pathogen infections by utilizing thiol-labeled PCR primers and unmodified gold nanoparticles. Biosensors & bioelectronics 2010;25(8):1941-1946.

[39] Saleh M, Soliman H, Schachner O, El-Matbouli M. Direct detection of unamplified spring viraemia of carp virus RNA using unmodified gold nanoparticles. Diseases of aquatic organisms 2012;100(1):3-10.

[40] Peters RP, van Agtmael MA, Danner SA, Savelkoul PH, Vandenbroucke-Grauls CM. New developments in the diagnosis of bloodstream infections. The Lancet.Infectious diseases 2004;4(12):751-760.

[41] Ahmed A, Rushworth JV, Hirst NA, Millner PA. Biosensors for whole-cell bacterial detection. Clinical microbiology reviews 2014;27(3):631-646.

[42] Renuart I, Mertens P, Leclipteux T, inventors. AnonymousOne step oligochromatographic device and method of use. . 2011 .

[43] Yaron S, Matthews KR. A reverse transcriptase-polymerase chain reaction assay for detection of viable Escherichia coli O157:H7: investigation of specific target genes. Journal of applied microbiology 2002;92(4):633-640.

[44] Wang C, Chen Y, Wang T, Ma Z, Su Z. Biorecognition-driven self-assembly of gold nanorods: A rapid and sensitive approach toward antibody sensing. Chemistry of Materials 2007;19(24):5809-5811.

[45] Nath N, Chilkoti A. A colorimetric gold nanoparticle biosensor: Effect of particle size on sensitivity. Second Joint Embs-Bmes Conference 2002, Vols 1-3, Conference Proceedings: Bioengineering - Integrative Methodologies, New Technologies 2002:574-575.

[46] Willets KA, Van Duyne RP. Localized surface plasmon resonance spectroscopy and sensing. Annual Review of Physical Chemistry 2007;58:267-297.

[47] Kim JY, Lee JS. Synthesis and thermally reversible assembly of DNA-gold nanoparticle cluster conjugates. Nano letters 2009;9(12):4564-4569.

[48] Zhao W, Brook MA, Li Y. Design of gold nanoparticle-based colorimetric biosensing assays. Chembiochem : a European journal of chemical biology 2008;9(15):2363-2371.

[49] Monis PT, Giglio S. Nucleic acid amplification-based techniques for pathogen detection and identification. Infection, genetics and evolution : journal of molecular epidemiology and evolutionary genetics in infectious diseases 2006;6(1):2-12.

[50] Lauri A, Mariani PO. Potentials and limitations of molecular diagnostic methods in food safety. Genes & nutrition 2009;4(1):1-12.

[51] Cenciarini-Borde C, Courtois S, La Scola B. Nucleic acids as viability markers for bacteria detection using molecular tools. Future microbiology 2009;4(1):45-64.

[52] Gill P, Ghaemi A. Nucleic acid isothermal amplification technologies: a review. Nucleosides, nucleotides & nucleic acids 2008;27(3):224-243.

[53] U.S. Food and Drug Administration. Fish and Fishery Products Hazards and Controls Guidance. ; 2011.

[54] Prasad D, Shankaracharya, Vidyarthi AS. Gold nanoparticles-based colorimetric assay for rapid detection of Salmonella species in food samples. World Journal of Microbiology & Biotechnology 2011;27(9):2227-2230.

[55] Deng H, Zhang X, Kumar A, Zou G, Zhang X, Liang XJ. Long genomic DNA amplicons adsorption onto unmodified gold nanoparticles for colorimetric detection of Bacillus anthracis. Chemical communications (Cambridge, England) 2013;49(1):51-53.

[56] Liu M, Yuan M, Lou X, Mao H, Zheng D, Zou R, Zou N, Tang X, Zhao J. Label-free optical detection of single-base mismatches by the combination of nuclease and gold nanoparticles. Biosensors & bioelectronics 2011;26(11):4294-4300.

[57] Xing Y, Wang P, Zang Y, Ge Y, Jin Q, Zhao J, Xu X, Zhao G, Mao H. A colorimetric method for H1N1 DNA detection using rolling circle amplification. The Analyst 2013;138(12):3457-3462.

[58] Hitchins AD, Jinneman K. Detection and Enumeration of *Listeria monocytogenes* in Foods. Bacteriological Analytical Manual: U.S. Food and Drug Administration; 1998.

[59] Fu Z, Zhou X, Xing D. Rapid colorimetric gene-sensing of food pathogenic bacteria using biomodification-free gold nanoparticle. Sensors and Actuators B-Chemical 2013;182:633-641.

[60] He W, Huang CZ, Li YF, Xie JP, Yang RG, Zhou PF, Wang J. One-step label-free optical genosensing system for sequence-specific DNA related to the human immunodeficiency virus based on the measurements of light scattering signals of gold nanorods. Analytical Chemistry 2008;80(22):8424-8430.

[61] Niazi A, Jorjani ON, Nikbakht H, Gill P. A nanodiagnostic colorimetric assay for 18S rRNA of Leishmania pathogens using nucleic acid sequence-based amplification and gold nanorods. Molecular diagnosis & therapy 2013;17(6):363-370.

[62] Taton TA, Mirkin CA, Letsinger RL. Scanometric DNA array detection with nanoparticle probes. Science (New York, N.Y.) 2000;289(5485):1757-1760.

[63] Veigas B, Machado D, Perdigao J, Portugal I, Couto I, Viveiros M, Baptista PV. Au-nanoprobes for detection of SNPs associated with antibiotic resistance in Mycobacterium tuberculosis. Nanotechnology 2010;21(41):415101-4484/21/41/415101. Epub 2010 Sep 16.

[64] Veigas B, Jacob JM, Costa MN, Santos DS, Viveiros M, Inacio J, Martins R, Barquinha P, Fortunato E, Baptista PV. Gold on paper-paper platform for Au-nanoprobe TB detection. Lab on a chip 2012;12(22):4802-4808.

[65] Costa P, Amaro A, Botelho A, Inacio J, Baptista PV. Gold nanoprobe assay for the identification of mycobacteria of the Mycobacterium tuberculosis complex. Clinical microbiology and infection : the official publication of the European Society of Clinical Microbiology and Infectious Diseases 2010;16(9):1464-1469.

[66] Chan WS, Tang BS, Boost MV, Chow C, Leung PH. Detection of methicillin-resistant Staphylococcus aureus using a gold nanoparticle-based colourimetric polymerase chain reaction assay. Biosensors & bioelectronics 2014;53:105-111.

[67] Mollasalehi H, Yazdanparast R. Non-crosslinking gold nanoprobes for detection of nucleic acid sequence-based amplification products. Analytical Biochemistry 2012;425(2):91-95.

[68] Gill P, Alvandi AH, Abdul-Tehrani H, Sadeghizadeh M. Colorimetric detection of Helicobacter pylori DNA using isothermal helicase-dependent amplification and gold nanoparticle probes. Diagnostic microbiology and infectious disease 2008;62(2):119-124.

[69] Jyoti A, Pandey P, Singh SP, Jain SK, Shanker R. Colorimetric detection of nucleic acid signature of shiga toxin producing Escherichia coli using gold nanoparticles. Journal of nanoscience and nanotechnology 2010;10(7):4154-4158.

[70] Majdinasab M, Aminlari M, Sheikhi MH, Niakousari M, Shekarforoosh S. Detection of inv A gene of Salmonella by DNA-gold nanoparticles biosensor and its comparison with PCR. Journal of Experimental Nanoscience 2013;8(2):223-239.

[71] Wang X, Li Y, Wang J, Wang Q, Xu L, Du J, Yan S, Zhou Y, Fu Q, Wang Y, Zhan L. A broad-range method to detect genomic DNA of multiple pathogenic bacteria based on the aggregation strategy of gold nanorods. The Analyst 2012;137(18):4267-4273.

[72] Chen SH, Lin KI, Tang CY, Peng SL, Chuang YC, Lin YR, Wang JP, Lin CS. Optical detection of human papillomavirus type 16 and type 18 by sequence sandwich hybridization with oligonucleotide-functionalized Au nanoparticles. IEEE transactions on nanobioscience 2009;8(2):120-131.

[73] Tang J, Zhou L, Gao W, Cao X, Wang Y. Visual DNA microarrays for simultaneous detection of human immunodeficiency virus type-1 and Treponema pallidum coupled with multiplex asymmetric polymerase chain reaction. Diagnostic microbiology and infectious disease 2009;65(4):372-378.

[74] Yeh C, Chang Y, Lin H, Chang T, Lin Y. A newly developed optical biochip for bacteria detection hybridization. Sensors and Actuators B-Chemical 2012;161(1):1168-1175.

[75] Qi H, Chen S, Hao R, Shi H, Zhang M, Wang S. Introduction of nanogold-DAB as a HRP substrate for simplifying detection in visual DNA microarrays. Analytical Methods 2012;4(4):1178-1181.

[76] Kim YT, Chen Y, Choi JY, Kim WJ, Dae HM, Jung J, Seo TS. Integrated microdevice of reverse transcription-polymerase chain reaction with colorimetric immunochromatographic detection for rapid gene expression analysis of influenza A H1N1 virus. Biosensors & bioelectronics 2012;33(1):88-94.

[77] Nagatani N, Yamanaka K, Ushijima H, Koketsu R, Sasaki T, Ikuta K, Saito M, Miyahara T, Tamiya E. Detection of influenza virus using a lateral flow immunoassay for amplified DNA by a microfluidic RT-PCR chip. The Analyst 2012;137(15):3422-3426.

[78] Shawky SM, Bald D, Azzazy HM. Direct detection of unamplified hepatitis C virus RNA using unmodified gold nanoparticles. Clinical biochemistry 2010;43(13-14):1163-1168.

[79] Wu WH, Li M, Wang Y, Ouyang HX, Wang L, Li CX, Cao YC, Meng QH, Lu JX. Aptasensors for rapid detection of Escherichia coli O157:H7 and Salmonella typhimurium. Nanoscale research letters 2012;7(1):658-276X-7-658.

[80] Liu R, Teo W, Tan S, Feng H, Padmanabhan P, Xing B. Metallic nanoparticles bioassay for Enterobacter cloacae P99 beta-lactamase activity and inhibitor screening. The Analyst 2010;135(5):1031-1036.

[81] Jiang T, Liu R, Huang X, Feng H, Teo W, Xing B. Colorimetric screening of bacterial enzyme activity and inhibition based on the aggregation of gold nanoparticles. Chemical communications (Cambridge, England) 2009;(15):1972-4. doi(15):1972-1974.

[82] Garner AL, Fullagar JL, Day JA, Cohen SM, Janda KD. Development of a high-throughput screen and its use in the discovery of Streptococcus pneumoniae immunoglobulin A1 protease inhibitors. Journal of the American Chemical Society 2013;135(27):10014-10017.

[83] Pylaev TE, Khanadeev VA, Khlebtsov BN, Dykman LA, Bogatyrev VA, Khlebtsov NG. Colorimetric and dynamic light scattering detection of DNA sequences by using positively charged gold nanospheres: a comparative study with gold nanorods. Nanotechnology 2011;22(28):285501-4484/22/28/285501. Epub 2011 May 31.

[84] Verma MS, Chen PZ, Jones L, Gu FX. "Chemical nose" for the visual identification of emerging ocular pathogens using gold nanostars. Biosensors & bioelectronics 2014;61:386-390.

[85] de la Rica R, Stevens MM. Plasmonic ELISA for the ultrasensitive detection of disease biomarkers with the naked eye. Nature nanotechnology 2012;7(12):821-824.

[86] Liandris E, Gazouli M, Andreadou M, Comor M, Abazovic N, Sechi LA, Ikonomopoulos J. Direct detection of unamplified DNA from pathogenic mycobacteria

using DNA-derivatized gold nanoparticles. Journal of microbiological methods 2009;78(3):260-264.

[87] Padmavathy B, Vinoth Kumar R, Jaffar Ali BM. A direct detection of Escherichia coli genomic DNA using gold nanoprobes. Journal of nanobiotechnology 2012;10:8-3155-10-8.

[88] Mancuso M, Jiang L, Cesarman E, Erickson D. Multiplexed colorimetric detection of Kaposi's sarcoma associated herpesvirus and Bartonella DNA using gold and silver nanoparticles. Nanoscale 2013;5(4):1678-1686.

[89] Kalidasan K, Neo JL, Uttamchandani M. Direct visual detection of Salmonella genomic DNA using gold nanoparticles. Molecular bioSystems 2013;9(4):618-621.

[90] Zagorovsky K, Chan WC. A plasmonic DNAzyme strategy for point-of-care genetic detection of infectious pathogens. Angewandte Chemie (International ed.in English) 2013;52(11):3168-3171.

[91] Carter JR, Balaraman V, Kucharski CA, Fraser TS, Fraser MJ,Jr. A novel dengue virus detection method that couples DNAzyme and gold nanoparticle approaches. Virology journal 2013;10:201-422X-10-201.

[92] Wang S, Singh AK, Senapati D, Neely A, Yu H, Ray PC. Rapid colorimetric identification and targeted photothermal lysis of Salmonella bacteria by using bioconjugated oval-shaped gold nanoparticles. Chemistry (Weinheim an der Bergstrasse, Germany) 2010;16(19):5600-5606.

[93] Khan SA, Singh AK, Senapati D, Fan Z, Ray PC. Targeted highly sensitive detection of multi-drug resistant Salmonella DT104 using gold nanoparticles. Chemical communications (Cambridge, England) 2011;47(33):9444-9446.

[94] Li XX, Cao C, Han SJ, Sim SJ. Detection of pathogen based on the catalytic growth of gold nanocrystals. Water research 2009;43(5):1425-1431.

[95] Sung YJ, Suk HJ, Sung HY, Li T, Poo H, Kim MG. Novel antibody/gold nanoparticle/magnetic nanoparticle nanocomposites for immunomagnetic separation and rapid colorimetric detection of Staphylococcus aureus in milk. Biosensors & bioelectronics 2013;43:432-439.

[96] Cao C, Gontard LC, Thuy Tram le L, Wolff A, Bang DD. Dual enlargement of gold nanoparticles: from mechanism to scanometric detection of pathogenic bacteria. Small (Weinheim an der Bergstrasse, Germany) 2011;7(12):1701-1708.

[97] Pandey SK, Suri CR, Chaudhry M, Tiwari RP, Rishi P. A gold nanoparticles based immuno-bioprobe for detection of Vi capsular polysaccharide of Salmonella enterica serovar Typhi. Molecular bioSystems 2012;8(7):1853-1860.

[98] Li CZ, Vandenberg K, Prabhulkar S, Zhu X, Schneper L, Methee K, Rosser CJ, Almeide E. Paper based point-of-care testing disc for multiplex whole cell bacteria analysis. Biosensors & bioelectronics 2011;26(11):4342-4348.

[99] Urusov AE, Kostenko SN, Sveshnikov PG, Zherdev AV, Dzantiev BB. Immunochromatographic assay for the detection of ochratoxin A. Journal of Analytical Chemistry 2011;66(8):770-776.

[100] Lim S, Koo OK, You YS, Lee YE, Kim MS, Chang PS, Kang DH, Yu JH, Choi YJ, Gunasekaran S. Enhancing nanoparticle-based visible detection by controlling the extent of aggregation. Scientific reports 2012;2:456.

[101] Sun J, Ge J, Liu W, Wang X, Fan Z, Zhao W, Zhang H, Wang P, Lee S. A facile assay for direct colorimetric visualization of lipopolysaccharides at low nanomolar level. Nano Research 2012;5(7):486-493.

[102] Su H, Ma Q, Shang K, Liu T, Yin H, Ai S. Gold nanoparticles as colorimetric sensor: A case study on E. coli O157:H7 as a model for Gram-negative bacteria. Sensors and Actuators B-Chemical 2012;161(1):298-303.

[103] Miranda OR, Li X, Garcia-Gonzalez L, Zhu ZJ, Yan B, Bunz UH, Rotello VM. Colorimetric bacteria sensing using a supramolecular enzyme-nanoparticle biosensor. Journal of the American Chemical Society 2011;133(25):9650-9653.

[104] Su H, Zhao H, Qiao F, Chen L, Duan R, Ai S. Colorimetric detection of Escherichia coli O157:H7 using functionalized Au@Pt nanoparticles as peroxidase mimetics. The Analyst 2013;138(10):3026-3031.

[105] Wang J, Gao J, Liu D, Han D, Wang Z. Phenylboronic acid functionalized gold nanoparticles for highly sensitive detection of Staphylococcus aureus. Nanoscale 2012;4(2):451-454.

[106] Marin MJ, Rashid A, Rejzek M, Fairhurst SA, Wharton SA, Martin SR, McCauley JW, Wileman T, Field RA, Russell DA. Glyconanoparticles for the plasmonic detection and discrimination between human and avian influenza virus. Organic & biomolecular chemistry 2013;11(41):7101-7107.

[107] Lee C, Gaston MA, Weiss AA, Zhang P. Colorimetric viral detection based on sialic acid stabilized gold nanoparticles. Biosensors & bioelectronics 2013;42:236-241.

[108] de Boer E, Beumer RR. Methodology for detection and typing of foodborne microorganisms. International journal of food microbiology 1999;50(1-2):119-130.

[109] Brooks BW, Devenish J, Lutze-Wallace CL, Milnes D, Robertson RH, Berlie-Surujballi G. Evaluation of a monoclonal antibody-based enzyme-linked immunosorbent assay for detection of Campylobacter fetus in bovine preputial washing and vaginal mucus samples. Veterinary microbiology 2004;103(1-2):77-84.

[110] Che Y, Li Y, Slavik M. Detection of Campylobacter jejuni in poultry samples using an enzyme-linked immunoassay coupled with an enzyme electrode. Biosensors & bioelectronics 2001;16(9-12):791-797.

[111] Ng LK, Kingombe CI, Yan W, Taylor DE, Hiratsuka K, Malik N, Garcia MM. Specific detection and confirmation of Campylobacter jejuni by DNA hybridization and PCR. Applied and Environmental Microbiology 1997;63(11):4558-4563.

[112] Drosten C, Gottig S, Schilling S, Asper M, Panning M, Schmitz H, Gunther S. Rapid detection and quantification of RNA of Ebola and Marburg viruses, Lassa virus, Crimean-Congo hemorrhagic fever virus, Rift Valley fever virus, dengue virus, and yellow fever virus by real-time reverse transcription-PCR. Journal of clinical microbiology 2002;40(7):2323-2330.

[113] Vo-Dinh T, Fales AM, Griffin GD, Khoury CG, Liu Y, Ngo H, Norton SJ, Register JK, Wang HN, Yuan H. Plasmonic nanoprobes: from chemical sensing to medical diagnostics and therapy. Nanoscale 2013;5(21):10127-10140.

[114] Dondapati SK, Sau TK, Hrelescu C, Klar TA, Stefani FD, Feldmann J. Label-free biosensing based on single gold nanostars as plasmonic transducers. ACS nano 2010;4(11):6318-6322.

[115] He Sha, Liu DingBin, Wang Zhuo, Cai KaiYong, Jiang XingYu. Utilization of unmodified gold nanoparticles in colorimetric detection. Science China-Physics Mechanics & Astronomy 2011;54(10):1757-1765.

[116] Khoury CG, Vo-Dinh T. Gold Nanostars For Surface-Enhanced Raman Scattering: Synthesis, Characterization and Optimization. Journal of Physical Chemistry C 2008;112(48):18849-18859.

[117] Yuan H, Fales AM, Khoury CG, Liu J, Vo-Dinh T. Spectral characterization and intracellular detection of Surface-Enhanced Raman Scattering (SERS)-encoded plasmonic gold nanostars. Journal of Raman Spectroscopy 2013;44(2):234-239.

[118] Vigderman L, Zubarev ER. Starfruit-Shaped Gold Nanorods and Nanowires: Synthesis and SERS Characterization. Langmuir 2012;28(24):9034-9040.

[119] Rodriguez-Lorenzo L, Alvarez-Puebla RA, Javier Garcia de Abajo F, Liz-Marzan LM. Surface Enhanced Raman Scattering Using Star-Shaped Gold Colloidal Nanoparticles. Journal of Physical Chemistry C 2010;114(16):7336-7340.

[120] Giannini V, Rodriguez-Oliveros R, Sanchez-Gil JA. Surface Plasmon Resonances of Metallic Nanostars/Nanoflowers for Surface-Enhanced Raman Scattering. Plasmonics 2010;5(1):99-104.

[121] Esenturk EN, Walker ARH. Surface-enhanced Raman scattering spectroscopy via gold nanostars. Journal of Raman Spectroscopy 2009;40(1):86-91.

[122] Senthil Kumar P, Pastoriza-Santos I, Rodriguez-Gonzalez B, Javier Garcia de Abajo F, Liz-Marzan LM. High-yield synthesis and optical response of gold nanostars. Nanotechnology 2008;19(1):015606-4484/19/01/015606. Epub 2007 Nov 29.

[123] Yuan H, Khoury CG, Hwang H, Wilson CM, Grant GA, Vo-Dinh T. Gold nanostars: surfactant-free synthesis, 3D modelling, and two-photon photoluminescence imaging. Nanotechnology 2012;23(7):075102-4484/23/7/075102. Epub 2012 Jan 20.

[124] Lu W, Singh AK, Khan SA, Senapati D, Yu H, Ray PC. Gold nano-popcorn-based targeted diagnosis, nanotherapy treatment, and in situ monitoring of photothermal therapy response of prostate cancer cells using surface-enhanced Raman spectroscopy. Journal of the American Chemical Society 2010;132(51):18103-18114.

[125] Kozanoglu D, Apaydin DH, Cirpan A, Esenturk EN. Power conversion efficiency enhancement of organic solar cells by addition of gold nanostars, nanorods, and nanospheres. Organic Electronics 2013;14(7):1720-1727.

[126] Shao L, Susha AS, Cheung LS, Sau TK, Rogach AL, Wang J. Plasmonic Properties of Single Multispiked Gold Nanostars: Correlating Modeling with Experiments. Langmuir 2012;28(24):8979-8984.

[127] Sau TK, Rogach AL, Doblinger M, Feldmann J. One-step high-yield aqueous synthesis of size-tunable multispiked gold nanoparticles. Small (Weinheim an der Bergstrasse, Germany) 2011;7(15):2188-2194.

[128] Trigari S, Rindi A, Margheri G, Sottini S, Dellepiane G, Giorgetti E. Synthesis and modelling of gold nanostars with tunable morphology and extinction spectrum. Journal of Materials Chemistry 2011;21(18):6531-6540.

[129] Barbosa S, Agrawal A, Rodriguez-Lorenzo L, Pastoriza-Santos I, Alvarez-Puebla RA, Kornowski A, Weller H, Liz-Marzan LM. Tuning size and sensing properties in colloidal gold nanostars. Langmuir : the ACS journal of surfaces and colloids 2010;26(18):14943-14950.

[130] El-Boubbou K, Gruden C, Huang X. Magnetic glyco-nanoparticles: a unique tool for rapid pathogen detection, decontamination, and strain differentiation. Journal of the American Chemical Society 2007;129(44):13392-13393.

[131] Chen L, Razavi FS, Mumin A, Guo X, Sham T, Zhang J. Multifunctional nanoparticles for rapid bacterial capture, detection, and decontamination. Rsc Advances 2013;3(7):2390-2397.

[132] Laurino P, Kikkeri R, Azzouz N, Seeberger PH. Detection of bacteria using glyco-dendronized polylysine prepared by continuous flow photofunctionalization. Nano letters 2011;11(1):73-78.

[133] Wang Y, Ye Z, Ying Y. New trends in impedimetric biosensors for the detection of foodborne pathogenic bacteria. Sensors (Basel, Switzerland) 2012;12(3):3449-3471.

[134] Karoonuthaisiri N, Charlermroj R, Uawisetwathana U, Luxananil P, Kirtikara K, Gajanandana O. Development of antibody array for simultaneous detection of foodborne pathogens. Biosensors & bioelectronics 2009;24(6):1641-1648.

[135] Schmid-Hempel P, Frank SA. Pathogenesis, virulence, and infective dose. PLoS pathogens 2007;3(10):1372-1373.

[136] Chang YC, Yang CY, Sun RL, Cheng YF, Kao WC, Yang PC. Rapid single cell detection of Staphylococcus aureus by aptamer-conjugated gold nanoparticles. Scientific reports 2013;3:1863.

[137] Berry V, Gole A, Kundu S, Murphy CJ, Saraf RF. Deposition of CTAB-terminated nanorods on bacteria to form highly conducting hybrid systems. Journal of the American Chemical Society 2005;127(50):17600-17601.

[138] Hayden SC, Zhao G, Saha K, Phillips RL, Li X, Miranda OR, Rotello VM, El-Sayed MA, Schmidt-Krey I, Bunz UH. Aggregation and interaction of cationic nanoparticles on bacterial surfaces. Journal of the American Chemical Society 2012;134(16):6920-6923.

[139] Parfentjev IA, Catelli AR. Tolerance of Staphylococcus aureus to Sodium Chloride. Journal of Bacteriology 1964;88:1-3.

[140] Clinical and Laboratory Standards Institute. Performance Standards for Antimicrobial Disk Susceptibility Tests; Approved Standard—Eleventh Edition. Eleventh ed. Pennsylvania, USA: Clinical and Laboratory Standards Institute; 2012.

[141] Chen HM, Peng HC, Liu RS, Asakura K, Lee CL, Lee JF, Hu SF. Controlling the length and shape of gold nanorods. The journal of physical chemistry.B 2005;109(42):19553-19555.

[142] Grzelczak M, Perez-Juste J, Mulvaney P, Liz-Marzan LM. Shape control in gold nanoparticle synthesis. Chemical Society Reviews 2008;37(9):1783-1791.

[143] Nehl CL, Liao H, Hafner JH. Optical properties of star-shaped gold nanoparticles. Nano letters 2006;6(4):683-688.

[144] Sau TK, Rogach AL. Nonspherical noble metal nanoparticles: colloid-chemical synthesis and morphology control. Advanced materials (Deerfield Beach, Fla.) 2010;22(16):1781-1804.

[145] Wu H, Chen C, Huang MH. Seed-Mediated Synthesis of Branched Gold Nanocrystals Derived from the Side Growth of Pentagonal Bipyramids and the Formation of Gold Nanostars. Chemistry of Materials 2009;21(1):110-114.

[146] Min-Chen H, Liu R, Tsai DP. A Versatile Route to the Controlled Synthesis of Gold Nanostructures. Crystal Growth & Design 2009;9(5):2079-2087.

[147] Li W, Han Y, Zhang J, Wang L, Song J. Thermodynamic modeling of CTAB aggregation in water-ethanol mixed solvents. Colloid Journal 2006;68(3):304-310.

[148] Ha TH, Koo H, Chung BH. Shape-controlled syntheses of gold nanoprisms and nanorods influenced by specific adsorption of halide ions. Journal of Physical Chemistry C 2007;111(3):1123-1130.

[149] Auvray X, Petipas C, Anthore R, Rico I, Lattes A. X-Ray-Diffraction Study of Mesophases of Cetyltrimethylammonium Bromide in Water, Formamide, and Glycerol. Journal of Physical Chemistry 1989;93(21):7458-7464.

[150] Xia F, Zuo X, Yang R, Xiao Y, Kang D, Vallee-Belisle A, Gong X, Yuen JD, Hsu BB, Heeger AJ, Plaxco KW. Colorimetric detection of DNA, small molecules, proteins, and ions using unmodified gold nanoparticles and conjugated polyelectrolytes. Proceedings of the National Academy of Sciences of the United States of America 2010;107(24):10837-10841.

[151] Link S, El-Sayed MA. Shape and size dependence of radiative, non-radiative and photothermal properties of gold nanocrystals. International Reviews in Physical Chemistry 2000;19(3):409-453.

[152] Hao F, Nehl CL, Hafner JH, Nordlander P. Plasmon resonances of a gold nanostar. Nano letters 2007;7(3):729-732.

[153] Green M, Apel A, Stapleton F. A longitudinal study of trends in keratitis in Australia. Cornea 2008;27(1):33-39.

[154] Stapleton F, Carnt N. Contact lens-related microbial keratitis: how have epidemiology and genetics helped us with pathogenesis and prophylaxis. Eye (London, England) 2012;26(2):185-193.

[155] Keay L, Edwards K, Naduvilath T, Taylor HR, Snibson GR, Forde K, Stapleton F. Microbial keratitis predisposing factors and morbidity. Ophthalmology 2006;113(1):109-116.

[156] Bui TH, Cavanagh HD, Robertson DM. Patient compliance during contact lens wear: perceptions, awareness, and behavior. Eye & contact lens 2010;36(6):334-339.

[157] de Oliveira PR, Temporini-Nastari ER, Ruiz Alves M, Kara-Jose N. Self-evaluation of contact lens wearing and care by college students and health care workers. Eye & contact lens 2003;29(3):164-167.

[158] Hall BJ, Jones L. Contact lens cases: the missing link in contact lens safety? Eye & contact lens 2010;36(2):101-105.

[159] Tilia D, Lazon de la Jara P, Zhu H, Naduvilath TJ, Holden BA. The Effect of Compliance on Contact Lens Case Contamination. Optometry and vision science : official publication of the American Academy of Optometry 2014.

[160] Hau SC, Dart JK, Vesaluoma M, Parmar DN, Claerhout I, Bibi K, Larkin DF. Diagnostic accuracy of microbial keratitis with in vivo scanning laser confocal microscopy. The British journal of ophthalmology 2010;94(8):982-987.

[161] Mascarenhas J, Lalitha P, Prajna NV, Srinivasan M, Das M, D'Silva SS, Oldenburg CE, Borkar DS, Esterberg EJ, Lietman TM, Keenan JD. Acanthamoeba, fungal, and bacterial keratitis: a comparison of risk factors and clinical features. American Journal of Ophthalmology 2014;157(1):56-62.

[162] Inoue T, Ohashi Y. Utility of real-time PCR analysis for appropriate diagnosis for keratitis. Cornea 2013;32 Suppl 1:S71-6.

[163] Safavieh M, Ahmed MU, Sokullu E, Ng A, Braescu L, Zourob M. A simple cassette as point-of-care diagnostic device for naked-eye colorimetric bacteria detection. The Analyst 2014;139(2):482-487.

[164] Oh S, Jadhav M, Lim J, Reddy V, Kim C. An organic substrate based magnetoresistive sensor for rapid bacteria detection. Biosensors & bioelectronics 2013;41:758-763.

[165] Siddiqui S, Dai Z, Stavis CJ, Zeng H, Moldovan N, Hamers RJ, Carlisle JA, Arumugam PU. A quantitative study of detection mechanism of a label-free impedance biosensor using ultrananocrystalline diamond microelectrode array. Biosensors & bioelectronics 2012;35(1):284-290.

[166] Safavieh M, Ahmed MU, Tolba M, Zourob M. Microfluidic electrochemical assay for rapid detection and quantification of Escherichia coli. Biosensors & bioelectronics 2012;31(1):523-528.

[167] Pohlmann C, Wang Y, Humenik M, Heidenreich B, Gareis M, Sprinzl M. Rapid, specific and sensitive electrochemical detection of foodborne bacteria. Biosensors & bioelectronics 2009;24(9):2766-2771.

[168] Jacquier H, Le Monnier A, Carbonnelle E, Corvec S, Illiaquer M, Bille E, Zahar JR, Jaureguy F, Fihman V, Tankovic J, Cattoir V, Gmc Study Group. In vitro antimicrobial

activity of "last-resort" antibiotics against unusual nonfermenting Gram-negative bacilli clinical isolates. Microbial drug resistance (Larchmont, N.Y.) 2012;18(4):396-401.

[169] Kiernan DF, Chin EK, Sclafani LA, Saidel MA. Multiple drug-resistant Alcaligenes xylosoxidans keratitis in a sanitation worker. Eye & contact lens 2009;35(4):212-214.

[170] Park JH, Song NH, Koh JW. Achromobacter xylosoxidans keratitis after contact lens usage. Korean journal of ophthalmology : KJO 2012;26(1):49-53.

[171] Ahmed AA, Pineda R. Alcaligenes xylosoxidans contact lens-related keratitis--a case report and literature review. Eye & contact lens 2011;37(6):386-389.

[172] Dantam J, Zhu H, Stapleton F. Biocidal efficacy of silver-impregnated contact lens storage cases in vitro. Investigative ophthalmology & visual science 2011;52(1):51-57.

[173] Ray M, Lim DK. A rare polymicrobial keratitis involving Chryseobacterium meningosepticum and Delftia acidovorans in a cosmetic contact lens wearer. Eye & contact lens 2013;39(2):192-193.

[174] Wiley L, Bridge DR, Wiley LA, Odom JV, Elliott T, Olson JC. Bacterial biofilm diversity in contact lens-related disease: emerging role of Achromobacter, Stenotrophomonas, and Delftia. Investigative ophthalmology & visual science 2012;53(7):3896-3905.

[175] Li W, Feng L, Ren J, Wu L, Qu X. Visual detection of glucose using conformational switch of i-Motif DNA and non-crosslinking gold nanoparticles. Chemistry (Weinheim an der Bergstrasse, Germany) 2012;18(40):12637-12642.

[176] Chen C, Zhao C, Yang X, Ren J, Qu X. Enzymatic manipulation of DNA-modified gold nanoparticles for screening G-quadruplex ligands and evaluating selectivities. Advanced materials (Deerfield Beach, Fla.) 2010;22(3):389-393.

[177] Kilvington S, Shovlin J, Nikolic M. Identification and susceptibility to multipurpose disinfectant solutions of bacteria isolated from contact lens storage cases of patients with corneal infiltrative events. Contact lens & anterior eye : the journal of the British Contact Lens Association 2013;36(6):294-298.

[178] Berry V, Saraf RF. Self-assembly of nanoparticles on live bacterium: an avenue to fabricate electronic devices. Angewandte Chemie (International ed.in English) 2005;44(41):6668-6673.

[179] Hong Y, Brown DG. Cell surface acid-base properties of Escherichia coli and Bacillus brevis and variation as a function of growth phase, nitrogen source and C:N ratio. Colloids and surfaces.B, Biointerfaces 2006;50(2):112-119.

[180] Navarre WW, Schneewind O. Surface proteins of gram-positive bacteria and mechanisms of their targeting to the cell wall envelope. Microbiology and molecular biology reviews : MMBR 1999;63(1):174-229.

[181] DiRienzo JM, Nakamura K, Inouye M. The outer membrane proteins of Gram-negative bacteria: biosynthesis, assembly, and functions. Annual Review of Biochemistry 1978;47:481-532.

[182] Boonaert CJ, Rouxhet PG. Surface of lactic acid bacteria: relationships between chemical composition and physicochemical properties. Applied and Environmental Microbiology 2000;66(6):2548-2554.

[183] Hong Y, Brown DG. Electrostatic behavior of the charge-regulated bacterial cell surface. Langmuir : the ACS journal of surfaces and colloids 2008;24(9):5003-5009.

[184] Scott JR, Barnett TC. Surface proteins of gram-positive bacteria and how they get there. Annual Review of Microbiology 2006;60:397-423.

[185] Ho KC, Tsai PJ, Lin YS, Chen YC. Using biofunctionalized nanoparticles to probe pathogenic bacteria. Analytical Chemistry 2004;76(24):7162-7168.

[186] Wang C, Irudayaraj J. Gold nanorod probes for the detection of multiple pathogens. Small (Weinheim an der Bergstrasse, Germany) 2008;4(12):2204-2208.

[187] Torres-Chavolla E, Alocilja EC. Aptasensors for detection of microbial and viral pathogens. Biosensors & bioelectronics 2009;24(11):3175-3182.

[188] Chung HJ, Castro CM, Im H, Lee H, Weissleder R. A magneto-DNA nanoparticle system for rapid detection and phenotyping of bacteria. Nature nanotechnology 2013;8(5):369-375.

[189] Jung JH, Cheon DS, Liu F, Lee KB, Seo TS. A Graphene Oxide Based Immuno-biosensor for Pathogen Detection. Angewandte Chemie-International Edition 2010;49(33):5708-5711.

[190] Verma MS, Rogowski JL, Jones L, Gu FX. Colorimetric biosensing of pathogens using gold nanoparticles. Biotechnology Advances 2015(0).

[191] Folmer-Andersen JF, Kitamura M, Anslyn EV. Pattern-based discrimination of enantiomeric and structurally similar amino acids: an optical mimic of the mammalian taste response. Journal of the American Chemical Society 2006;128(17):5652-5653.

[192] De M, Rana S, Akpinar H, Miranda OR, Arvizo RR, Bunz UH, Rotello VM. Sensing of proteins in human serum using conjugates of nanoparticles and green fluorescent protein. Nature chemistry 2009;1(6):461-465.

[193] Wright AT, Zhong Z, Anslyn EV. A functional assay for heparin in serum using a designed synthetic receptor. Angewandte Chemie (International ed.in English) 2005;44(35):5679-5682.

[194] Peng G, Tisch U, Adams O, Hakim M, Shehada N, Broza YY, Billan S, Abdah-Bortnyak R, Kuten A, Haick H. Diagnosing lung cancer in exhaled breath using gold nanoparticles. Nature nanotechnology 2009;4(10):669-673.

[195] Li X, Kong H, Mout R, Saha K, Moyano DF, Robinson SM, Rana S, Zhang X, Riley MA, Rotello VM. Rapid identification of bacterial biofilms and biofilm wound models using a multichannel nanosensor. ACS nano 2014;8(12):12014-12019.

[196] Bajaj A, Miranda OR, Kim IB, Phillips RL, Jerry DJ, Bunz UH, Rotello VM. Detection and differentiation of normal, cancerous, and metastatic cells using nanoparticle-polymer sensor arrays. Proceedings of the National Academy of Sciences of the United States of America 2009;106(27):10912-10916.

[197] Bajaj A, Rana S, Miranda OR, Yawe JC, Jerry DJ, Bunz UHF, Rotello VM. Cell surface-based differentiation of cell types and cancer states using a gold nanoparticle-GFP based sensing array. Chemical Science 2010;1(1):134-138.

[198] Rana S, Le ND, Mout R, Saha K, Tonga GY, Bain RE, Miranda OR, Rotello CM, Rotello VM. A multichannel nanosensor for instantaneous readout of cancer drug mechanisms. Nature nanotechnology 2015;10(1):65-69.

[199] Verma MS, Chen PZ, Jones L, Gu FX. Controlling “chemical nose” biosensor characteristics by modulating gold nanoparticle shape and concentration. Sensing and Bio-Sensing Research 2015(0).

[200] Liu J, Lu Y. Preparation of aptamer-linked gold nanoparticle purple aggregates for colorimetric sensing of analytes. Nature protocols 2006;1(1):246-252.

[201] Liu H, Fang HH. Extraction of extracellular polymeric substances (EPS) of sludges. Journal of Biotechnology 2002;95(3):249-256.

[202] Ghosh SK, Pal T. Interparticle coupling effect on the surface plasmon resonance of gold nanoparticles: from theory to applications. Chemical reviews 2007;107(11):4797-4862.

[203] Rakic A, Djurisic A, Elazar J, Majewski M. Optical properties of metallic films for vertical-cavity optoelectronic devices. Applied Optics 1998;37(22):5271-5283.

[204] Wang DS, Lin CW. Density-dependent optical response of gold nanoparticle monolayers on silicon substrates. Optics Letters 2007;32(15):2128-2130.

[205] Bohren CF, Huffman DR. Absorption and scattering of light by small particles. : John Wiley & Sons; 2008.

[206] Swinehart DF. The Beer-Lambert Law. Journal of chemical education 1962;39(7):333.

[207] Ricci RW, Ditzler M, Nestor LP. Discovering the Beer-Lambert Law. Journal of chemical education 1994;71(11):983.

[208] Niklasson GA, Granqvist CG, Hunderi O. Effective medium models for the optical properties of inhomogeneous materials. Applied Optics 1981;20(1):26-30.

[209] Lim SH, Feng L, Kemling JW, Musto CJ, Suslick KS. An optoelectronic nose for the detection of toxic gases. Nature chemistry 2009;1(7):562-567.

[210] Zhanel GG, Adam HJ, Baxter MR, Fuller J, Nichol KA, Denisuik AJ, Lagace-Wiens PR, Walkty A, Karlowsky JA, Schweizer F, Hoban DJ, Canadian Antimicrobial Resistance Alliance. Antimicrobial susceptibility of 22746 pathogens from Canadian hospitals: results of the CANWARD 2007-11 study. The Journal of antimicrobial chemotherapy 2013;68 Suppl 1:i7-22.

[211] Lockhart SR, Abramson MA, Beekmann SE, Gallagher G, Riedel S, Diekema DJ, Quinn JP, Doern GV. Antimicrobial resistance among Gram-negative bacilli causing infections in intensive care unit patients in the United States between 1993 and 2004. Journal of clinical microbiology 2007;45(10):3352-3359.

[212] Joshi S. Hospital antibiogram: a necessity. Indian journal of medical microbiology 2010;28(4):277-280.

[213] Korgaonkar A, Trivedi U, Rumbaugh KP, Whiteley M. Community surveillance enhances Pseudomonas aeruginosa virulence during polymicrobial infection. Proceedings of the National Academy of Sciences of the United States of America 2013;110(3):1059-1064.

[214] Matsumoto K, Kusaka J, Nishibori A, Hara H. Lipid domains in bacterial membranes. Molecular microbiology 2006;61(5):1110-1117.

[215] Epand RM, Epand RF. Lipid domains in bacterial membranes and the action of antimicrobial agents. Biochimica et biophysica acta 2009;1788(1):289-294.

[216] Dowler S, Kular G, Alessi DR. Protein lipid overlay assay. Science's STKE : signal transduction knowledge environment 2002;2002(129):pl6.

[217] Zambre A, Chanda N, Prayaga S, Almudhafar R, Afrasiabi Z, Upendran A, Kannan R. Design and development of a field applicable gold nanosensor for the detection of luteinizing hormone. Analytical Chemistry 2012;84(21):9478-9484.

[218] Vierck JL, Bryne KM, Dodson MV. Evaluating dot and Western blots using image analysis and pixel quantification of electronic images. Methods in cell science : an official journal of the Society for In Vitro Biology 2000;22(4):313-318.

[219] Ung T, Liz-Marzan L, Mulvaney P. Gold nanoparticle thin films. Colloids and Surfaces A-Physicochemical and Engineering Aspects 2002;202(2-3):119-126.

[220] Donnelly T, Doggett B, Lunney J. Pulsed laser deposition of nanostructured Ag films. Applied Surface Science 2006;252(13):4445-4448.

[221] Dumont E, Dugnoille B. In situ characterization of chemically deposited nickel thin films on float glass by ellipsometry. Journal of Non-Crystalline Solids 1997;218:307-311.

[222] Moskovits M, Hulse J. Ultraviolet-Visible Spectra of Diatomic, Triatomic, and Higher Nickel Clusters. Journal of Chemical Physics 1977;66(9):3988-3994.

[223] Shinde SB, Fernandes CB, Patravale VB. Recent trends in in-vitro nanodiagnostics for detection of pathogens. Journal of controlled release : official journal of the Controlled Release Society 2012;159(2):164-180.

[224] Niemz A, Ferguson TM, Boyle DS. Point-of-care nucleic acid testing for infectious diseases. Trends in biotechnology 2011;29(5):240-250.

[225] Martinez AW, Phillips ST, Carrilho E, Thomas SW,3rd, Sindi H, Whitesides GM. Simple telemedicine for developing regions: camera phones and paper-based microfluidic devices for real-time, off-site diagnosis. Analytical Chemistry 2008;80(10):3699-3707.

[226] Gallegos D, Long KD, Yu H, Clark PP, Lin Y, George S, Nath P, Cunningham BT. Label-free biodetection using a smartphone. Lab on a chip 2013;13(11):2124-2132.

[227] Mudanyali O, Dimitrov S, Sikora U, Padmanabhan S, Navruz I, Ozcan A. Integrated rapid-diagnostic-test reader platform on a cellphone. Lab on a chip 2012;12(15):2678-2686.

[228] Zhu H, Sikora U, Ozcan A. Quantum dot enabled detection of Escherichia coli using a cell-phone. The Analyst 2012;137(11):2541-2544.

[229] Smith ZJ, Chu K, Espenson AR, Rahimzadeh M, Gryshuk A, Molinaro M, Dwyre DM, Lane S, Matthews D, Wachsmann-Hogiu S. Cell-phone-based platform for biomedical device development and education applications. PloS one 2011;6(3):e17150.

[230] Teichroeb JH, McVeigh PZ, Forrest JA. Influence of nanoparticle size on the pH-dependent structure of adsorbed proteins studied with quantitative localized surface plasmon spectroscopy. The European physical journal.E, Soft matter 2009;30(2):157-164.

[231] Giljohann DA, Mirkin CA. Drivers of biodiagnostic development. Nature 2009;462(7272):461-464.

[232] Vu B, Chen M, Crawford RJ, Ivanova EP. Bacterial extracellular polysaccharides involved in biofilm formation. Molecules (Basel, Switzerland) 2009;14(7):2535-2554.

[233] Joshi N, Ngwenya BT, French CE. Enhanced resistance to nanoparticle toxicity is conferred by overproduction of extracellular polymeric substances. Journal of hazardous materials 2012;241-242:363-370.

[234] You CC, Miranda OR, Gider B, Ghosh PS, Kim IB, Erdogan B, Krovi SA, Bunz UH, Rotello VM. Detection and identification of proteins using nanoparticle-fluorescent polymer 'chemical nose' sensors. Nature nanotechnology 2007;2(5):318-323.

[235] Kusolkamabot K, Sae-ung P, Niamnont N, Wongravee K, Sukwattanasinitt M, Hoven VP. Poly(N-isopropylacrylamide)-stabilized gold nanoparticles in combination with

tricationic branched phenylene-ethynylene fluorophore for protein identification. Langmuir : the ACS journal of surfaces and colloids 2013;29(39):12317-12327.

[236] Boucher HW, Talbot GH, Bradley JS, Edwards JE, Gilbert D, Rice LB, Scheld M, Spellberg B, Bartlett J. Bad bugs, no drugs: no ESKAPE! An update from the Infectious Diseases Society of America. Clinical infectious diseases : an official publication of the Infectious Diseases Society of America 2009;48(1):1-12.

[237] Ahn H, Lee H, Jin K, Nam KT. Extended gold nano-morphology diagram: synthesis of rhombic dodecahedra using CTAB and ascorbic acid. Journal of Materials Chemistry C 2013;1(41):6861-6868.

[238] Kelly K, Coronado E, Zhao L, Schatz G. The optical properties of metal nanoparticles: The influence of size, shape, and dielectric environment. Journal of Physical Chemistry B 2003;107(3):668-677.

[239] El-Sayed MA. Some interesting properties of metals confined in time and nanometer space of different shapes. Accounts of Chemical Research 2001;34(4):257-264.

[240] Xia Y, Xiong Y, Lim B, Skrabalak SE. Shape-controlled synthesis of metal nanocrystals: simple chemistry meets complex physics? Angewandte Chemie (International ed.in English) 2009;48(1):60-103.

[241] Jain PK, Lee KS, El-Sayed IH, El-Sayed MA. Calculated absorption and scattering properties of gold nanoparticles of different size, shape, and composition: applications in biological imaging and biomedicine. The journal of physical chemistry.B 2006;110(14):7238-7248.

[242] Liu X, Atwater M, Wang J, Huo Q. Extinction coefficient of gold nanoparticles with different sizes and different capping ligands. Colloids and surfaces.B, Biointerfaces 2007;58(1):3-7.

[243] Zhang G, Yang Z, Lu W, Zhang R, Huang Q, Tian M, Li L, Liang D, Li C. Influence of anchoring ligands and particle size on the colloidal stability and in vivo biodistribution of polyethylene glycol-coated gold nanoparticles in tumor-xenografted mice. Biomaterials 2009;30(10):1928-1936.